海産ラン藻 Okeania hirsuta 由来の低分子化合物群に関する研究

Doctoral Dissertation

SECONDARY METABOLITES FROM THE MARINE CYANOBACTERIUM *Okeania hirsuta:* CHEMICAL AND BIOLOGICAL ASPECTS

March 2024

Graduate School of Marine Science and Technology

Tokyo University of Marine Science and Technology

Doctoral Course of Applied Marine Environmental Studies

Zhang Botao

Doctoral Dissertation

SECONDARY METABOLITES FROM THE MARINE CYANOBACTERIUM *Okeania hirsuta:* CHEMICAL AND BIOLOGICAL ASPECTS

March 2024

Graduate School of Marine Science and Technology

Tokyo University of Marine Science and Technology

Doctoral Course of Applied Marine Environmental Studies

Zhang Botao

List of abbreviations

List of abbreviations

^{13}C	carbon thirteen
^{1}H	proton
BuOH	butanol
$CDCl_3$	deuterated chloroform
COSY	correlation spectroscopy
EtOAc	ethyl acetate
HMBC	heteronuclear multiple bond coherence spectroscopy
HPLC	high performance liquid chromatography
HSQC	heteronuclear multiple quantum coherence spectroscopy
HRESIMS	high resolution electrospray ionization mass spectrometry
MeCN	acetonitrile
MeOH	methanol
NMR	nuclear magnetic resolution
NOESY	nuclear overhauser effect spectroscopy
ODS	octadecylsilyl
TOCSY	total correlation spectroscopy

Chapter 1. General Introduction

1.1 The natural products chemistry of marine cyanobacteria

Cyanobacteria are known botanically as Cyanophyta or "blue-green algae", thought to be the most ancient group of oxygenic photosynthetic organisms. For over 3 billion years, this bacterial phylum has evolved to thrive in most of the planet's environments, making it one of the most abundant and widely distributed groups of prokaryotes in the world.[1]

Cyanobacteria are well-known to play important ecological roles in marine environments around the world, contributing significantly to global oxygen production, nitrogen fixation, and the global carbon cycle.[2] In addition, cyanobacteria, particularly filamentous benthic marine types from tropical and subtropical regions, are known to produce structurally diverse and highly bioactive secondary metabolites.[3] Some of these compounds are potent toxins and are implicated in harmful cyanobacterial blooms that can be hazardous to human health as well as natural environments.[4-5] And, more importantly, a wide range of cyanobacterial metabolites have shown various biological activities such as antitumor, antimalarial, and antibacterial effects, which makes cyanobacteria a great source for drug discovery (Figure 1.1-1).[6-7]

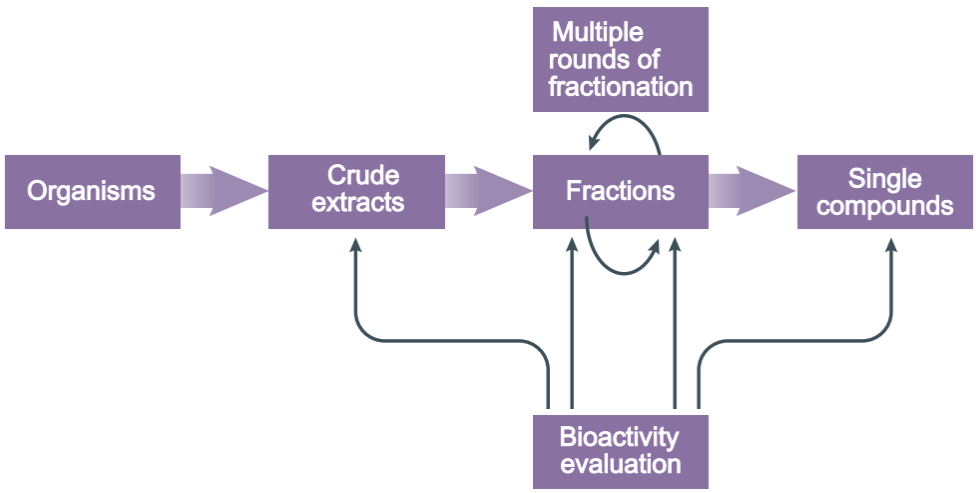

Figure 1.1-1 Outline of traditional bioactivity-guided isolation steps in natural product drug discovery [8]

Much of the recognition of this biosynthetic ability of marine cyanobacteria owes to the effort of Richard E. Moore who pioneered the investigation of anticancer agents from field-collected marine cyanobacteria from Hawaii and Enewetok beginning in mid-1970s. This work notably led to characterizing debromoaplysiatoxin, oscillatoxins, and lyngbyatoxin as the potent inflammatory agents and tumor-promoting factors in *Lyngbya majuscula*.[9] Furthermore, these findings pointed that aplysiatoxins, which had been thought to be the toxic constituents of marine mollusk,[10] actually originated from marine cyanobacteria and accumulated in marine mollusks through the food chain.[11] Since then, marine cyanobacteria have attracted great attention as producer of bioactive compounds. With the increasing interest in marine cyanobacterial secondary metabolites, many novel compounds with potent antiproliferative effects on cancer cells have been discovered in the last 30 years, including dolastatin 10(1987),[12-13] curacin A (1994),[14] apratoxin A (2001),[15] largazole (2008),[16] biselyngbyaside (2015),[17] and iezoside (2022)[18].

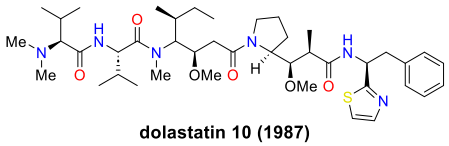

dolastatin 10 (1987)

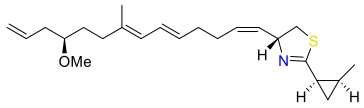

curacin A (1994)

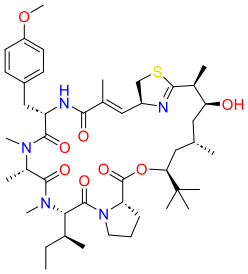

apratoxin A (2001)

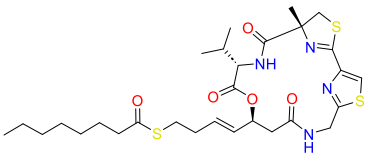

largazole (2008)

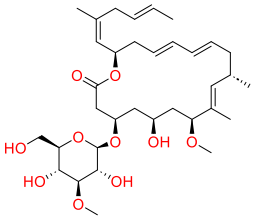

biselyngbyaside (2015)

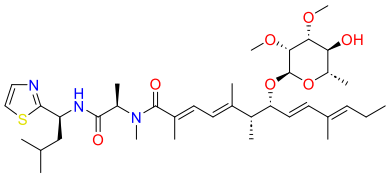

iezoside (2022)

Figure 1.1-2 Structures of 6 representative cyanobacterial metabolites with anticancer potential.

In terms of chronological order, the discovery of potent bioactive substances derived from cyanobacteria has shown a tendency to persist, indicating ongoing findings in this area. Furthermore, it is worth to note that these compounds, all of which exhibit potent cytotoxicity against cancer cells, possess very different chemical structures and modes of action on cancer cells (Table 1.1-1). [6-7]

Overall, the study of marine cyanobacterial metabolites has the potential to identify new lead compounds with unique chemical structures and mechanisms of action.

Table 1.1-1 Summary of 6 representative anticancer cyanobacterial metabolites and their mode of action

Compound	Analogs	Class/type	Source	Mode of action
dolastatin 10	dolastatin 15	Linear pentapeptide/ peptide	*Dolabella auricularia Symploca* sp. *VP642*	Tubulin polymerization Inhibition
curacin A		Thiazoline-containing polyketide/ polyketide	*Lyngbya majuscula*	Tubulin polymerization inhibition
apratoxin A	apratoxin B-D apratoxin S10	cyclic depsipeptide/ peptide-polyketide hybrid	*Lyngbya* sp.	preventing protein translocation by directly targeting Sec61α
largazole		thioester-containing cyclic depsipeptide/ peptide-polyketide hybrid	*Symploca* sp.	stimulation of histone hyperacetylation in the tumor
biselyngbyaside	Biselyngbyaside A Biselyngbyolide B, C, and E	Glicomacrolide/ polyketide hybrid glycoside	*Lyngbya* sp.	induce endoplasmic reticulum (ER) stress via inhibition of Ca^{2+}-ATPase
iezoside		lipopeptide /peptide−polyketide hybrid glycoside	*Leptochromothrix valpauliae*	induces ER stress via inhibition of Ca^{2+}-ATPase

1.2 Taxonomy of marine cyanobacteria

From the perspective of taxonomy, the order Oscillatoriales accounts for 58% of all isolated secondary metabolites from marine cyanobacterial sources while the Nostocales accounts for 24%, Chroococcales 10%, Stigonematales 8%.[3] Hence, a majority of the unique natural products of cyanobacteria are derived from filamentous forms with generally larger genome sizes (6.0-10 Mbp) than the unicellular forms (1.7-4.0 Mbp), and this matches the deduced capacity to produce natural products from genome sequence information (Figure 1.2-1).

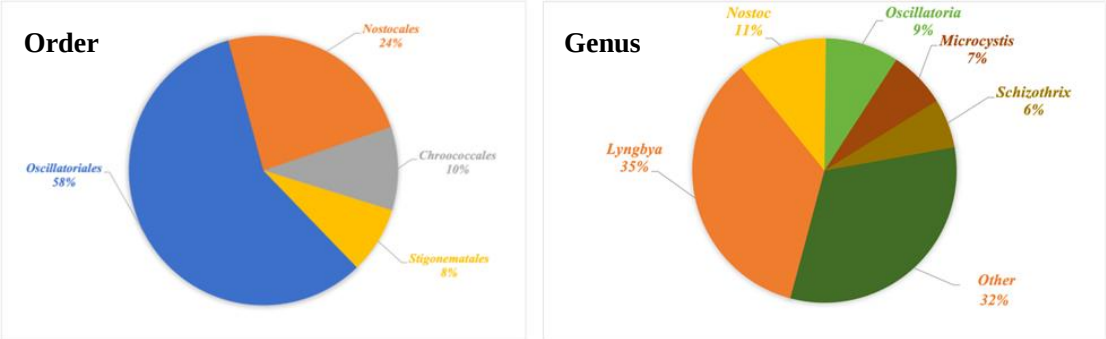

Figure 1.2-1. Percentage of isolated marine cyanobacterial natural products by order and genus. [3]

(n = 678)

The genus that has yielded the most reported structures is *Lyngbya*, accounting for 35% of all cyanobacterial secondary metabolites. Other genera with significant contributions are *Nostoc* (11%), *Oscillatoria* (9%), *Microcystis* (7%), and *Schizothrix* (6%). Within the genus *Lyngbya*, it is worth to note that the majority of natural products have been ascribed as being produced by one single species *Lyngbya majuscula*.[3] However, the fact is that most of these studies have utilized morphological observation to identify cyanobacterial species and lack a molecular phylogenetic analysis for the samples.[19]

Historically, the taxonomic classification of cyanobacteria has been based primarily upon morphological features. However, there are few distinct morphological features among taxa, and many of the morphological characters are highly variable and influenced by environmental factors. Recent molecular phylogenetic investigations have also revealed that morphological-based taxonomic systems are insufficient to accurately identify distinct genetic strains with phenotypic similarities.[20] As a result, many marine cyanobacterial specimens, particularly those collected from

unexplored environments or geographic locations, have been incorrectly classified. Instead of being recognized as new taxa, cyanobacterial specimens have often been classified within existing classification systems based on morphological resemblances and thus resulted in a significant underestimation of natural biodiversity.[21]

The genus of *Lyngbya*

A representative example of such morphologically based taxonomic confusion is that of the genus *Lyngbya* (C. Agardh ex Gomont 1892) and unrelated filamentous cyanobacteria that resemble this group. The genus *Lyngbya* is among the most abundant and broadly distributed in the tropical marine benthos and has, to date, yielded the greatest number of bioactive secondary metabolites among marine cyanobacteria. Specimens characterized by relatively large filaments of discoid cells within a distinct sheath and lacking nitrogen-fixing heterocyst cells have routinely been assigned to the genus *Lyngbya*.[22] However, phylogenetic investigations have shown that *Lyngbya* is composed of multiple, evolutionarily distantly related groups with morphological similarities. As a result of recent genetic analyses, several new genera were erected from this genus, such as *Moorena*, Okeania, *Limnoraphis*, *Microseira*, and *Dapis*.[22] Furthermore, the misidentification of *Okeania* or *Moorena* as *Lyngbya* has been a source of considerable taxonomic confusion as well as the major reason for the perceived chemical richness of the genus *Lyngbya*.

The genus of *Okeania*

The genus *Okeania* was established as a novel generic entity with five new species, *O. hirsuta*, *O. plumata*, *O. lorea*, *O. erythroflocculosa*, and *O. comitata* by Niclas Engene and coworkers in 2013.[23] *Okeania* is a filamentous cyanobacterium that thrives in tropical and seasonally in subtropical marine oceans. It is commonly found in many coral reef environments, at depths ranging from 0.5 to 30 meters and sometimes even deeper. The filaments are unbranched, extending up to several centimeters in length, with filament diameters varying between 9–52 µm. Members of the genus *Okeania* are of considerable ecological and biomedical importance, as they produce biologically active secondary metabolites and are known to form blooms in coastal benthic environments. This group is typically rich in bioactive secondary metabolites that are primarily biosynthesized by polyketide synthases (PKS), non-ribosomal peptide synthetases (NRPS), or mixed PKS/NRPS pathways.[23]

With respect to the species *Okeania hirsuta* , the representative secondary metabolites of this group are shown to be (–)-*trans*-7(*S*)-methoxytetradec-4-enoic acid[24] (commonly known as lyngbic acid) and malyngamide derivatives. Although lyngbic acid, an oxygenated derivative of myristic acid, possesses low micromolar antifungal and cancer cell cytotoxic properties in free form, it is a frequent component of a number of more complex and bioactive cyanobacterial natural products, including the malyngamides[25] and the hermitamides.[26]

Chapter 2. Okinawan Cyanobacterium *Okeania hirsuta*

2.1 Cyanobacterial bloom on Kuba Beach, Okinawa

In July 2010, a massive outbreak of toxic filamentous cyanobacteria occurred on Kuba Beach, Nakagusuku, Okinawa, Japan. The entire area of Kuba Beach, which has a sandy beach of approximately 1.3 km, was covered with black thread-like algae. The collected algae were observed under a microscope at the Okinawa Institute of Public Health, confirming the characteristics of *Lyngbya*. Later, this cyanobacterium was presumed to be *Lyngbya majuscula* based on the morphological analysis by Professor Shoichiro Suda (University of the Ryukyu).

Lyngbya sp. is a toxic cyanobacterium that has led to health issues including dermatitis and food poisoning globally. In July 1968, a significant health incident occurred where 242 swimmers at Gushigawa Beach in Okinawa Prefecture reported developing dermatitis, marking a considerable public health concern. Consequently, concerning the toxicity of the cyanobacterial bloom, Kuba Beach was set off-limits to the public to prevent health hazards at that time (Figure 2.1-1).

Figure 2.1-1 The cyanobacterial bloom occurred on Kuba Beach, Okinawa, Japan in July 2010.

The preliminary investigation of the toxicity of these cyanobacteria was carried out by a mouse skin contact test. As a result, the skin surface of the mice treated with the extracts of cyanobacteria was inflamed, and showed symptoms such as redness, swelling and bleeding. Further analysis of causative compounds in the cyanobacteria was performed using LC/MS/MS. The toxic components were confirmed as aplysiatoxin and debromoaplysiatoxin by comparing the standards provided by Professor Hiroshi Nagai.[27]

This cyanobacterial bloom lasted for approximately a month, and we were able to collect a substantial amount of samples with the cooperation of the Okinawa Prefectural Institute of Public Health. The collected samples were stored at −30 ℃ until the experiments were performed. A voucher specimen of this sample (20100713-a) was deposited at the Tokyo University of Marine Science and Technology.

2.2 Identification of the Okinawan cyanobacterial bloom samples

The sample was initially identified as *Moorea producens* (formerly *Lyngbya majuscula*) based on morphological observations. However, a recent analysis of the 16S rRNA sequence revealed that the predominant species in this sample was *Okeania hirsuta*.[28]

Morphological characterization

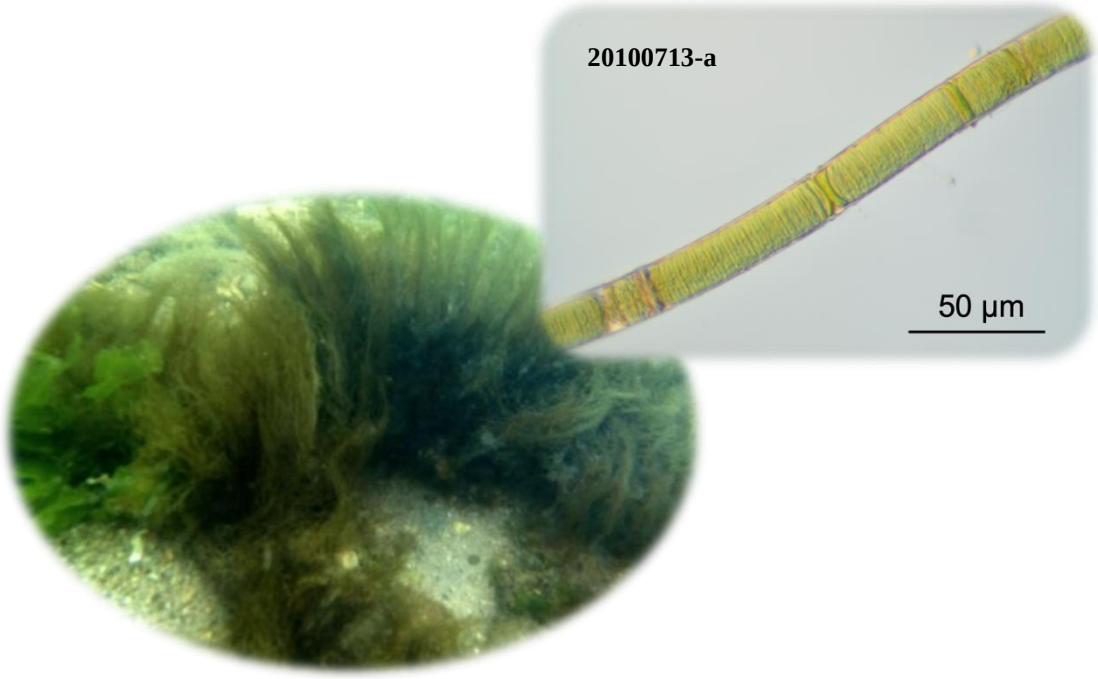

Characteristics	**20100713-a (this study)**	*Okeania comitata*	*Okeania erythroflocculosa*	*Okeania lorea*	*Okeania plumata*	*Okeania hirsuta*
Color	**Dark brown**	Black	Dark red	Copper-brown	Black	Black to dark brown
Filament width (µm)	**36.1-71.3 54.4 (mean)**	11-13	32-42	14-16	20-25	25-47
Cell width (µm)	**31.5-57.5 41.5 (mean)**	10-12	32-35	13-15	20-23	24-45
Cell length (µm)	**2-5 3.0 (mean)**	1.5-2.5	2-3	1.5-2.5	1.5-2	2-3
Epiphytes	**Diatoms**	Not reported	Not reported	Not reported	Not reported	Diatoms

Figure 2.2-1 Morphological characteristics of 20100713-a and other *Okeania* species.[28]

Phylogenetic analysis

The nucleotide sequence of the 16S ribosomal RNA (rRNA) gene obtained in this study was used for phylogenetic analysis with the dataset of related cyanobacterial genes. The sequence of the 16S region gene was aligned using the MAFFT multiple sequence alignment program. As a result, the collected cyanobacterium (20100713-a) was classified as *Okeania hirsuta*.

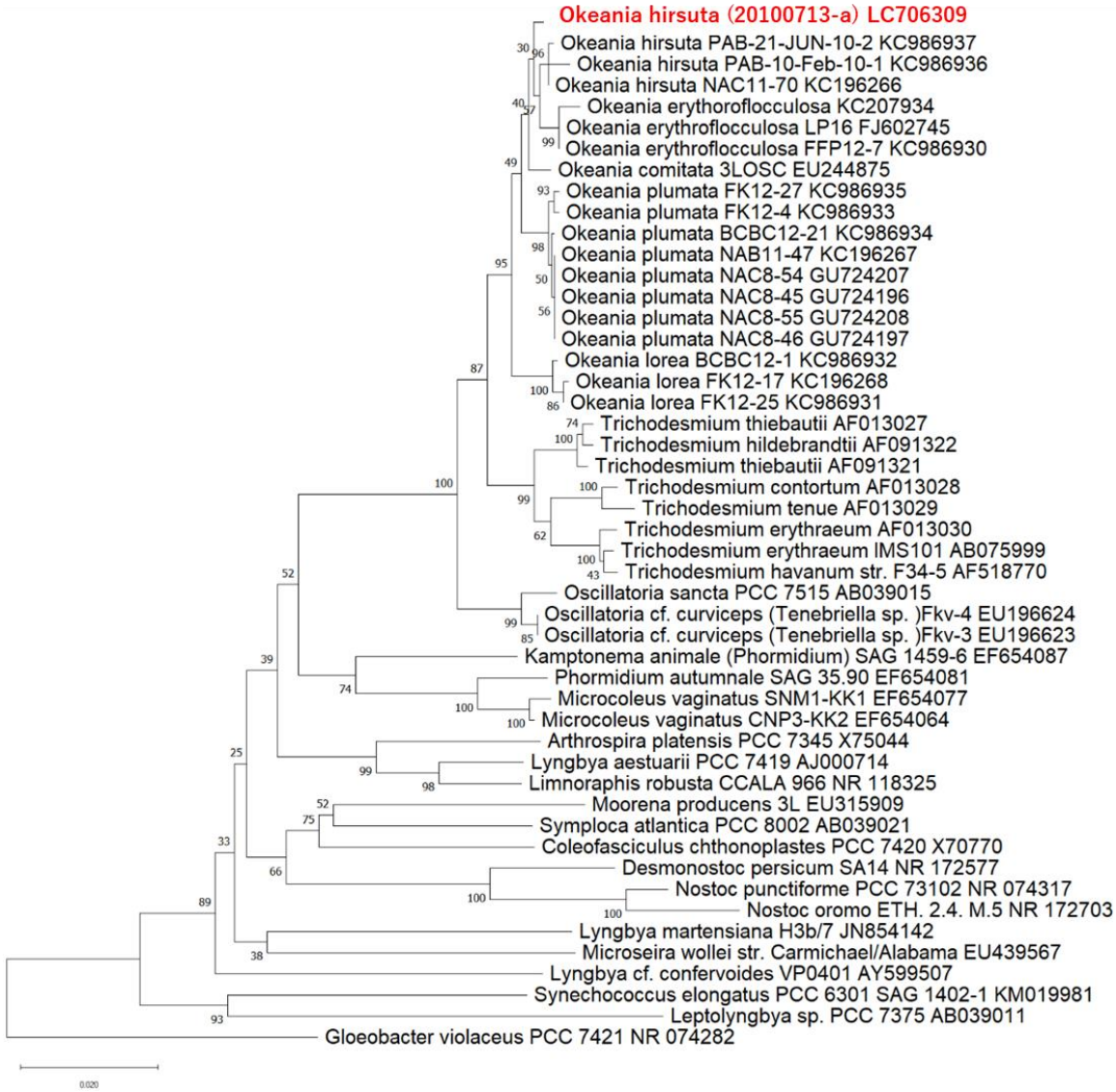

Figure 2.2-2 Phylogenetic tree inferred from 16S rDNA sequence. The phylogeny is rooted with *Gloeobacter violaceus* PCC 7421. [28]

This figure was reprinted from "7-Epi-30-methyloscillatoxin D from an Okinawan cyanobacterium *Okeania hirsuta*" by Kanda, N et al., *Natural Product Communication* 2023.

2.3 Research objectives

Prior to this study, more than 30 compounds, including different types of secondary metabolites have been characterized from this *O. hirsuta* sample. Impressively, over half of these were novel compounds (Figure 2.3-1), which revealed that this *O. hirsuta* sample is an important source of biochemicals.[29–34] Therefore, in this study we are mainly centered on exploring natural organic compounds continuously from the Okinawan cyanobacterium *Okeania hirsuta*, focusing on their isolation and structural elucidation through comprehensive chromatographic techniques and spectroscopic analyses.

Our previous exploratory studies have shown a high rate of discovery of new compounds in this cyanobacterium. Therefore, we thought a thorough investigation of the components of this cyanobacterium would lead to further discoveries. Since a large number of samples have been obtained, we are able to conduct an investigation of trace compounds in this cyanobacterium and anticipate isolating novel bioactive compounds. Furthermore, this cyanobacterium has shown to produce a series of ATX-related compounds, so we are aim at discovering more new natural analogs and related compounds to approach the biosynthetic pathway of ATXs.

aplysiatoxin-related compounds (polyketide)

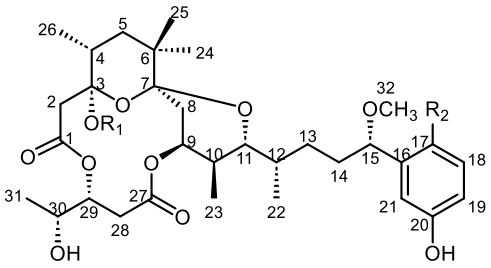

aplysiatoxin : R_1=H, R_2=Br
debromoaplysiatoxin : R_1=H, R_2=H
3-methoxyaplysiatoxin : R_1=CH_3, R_2=Br

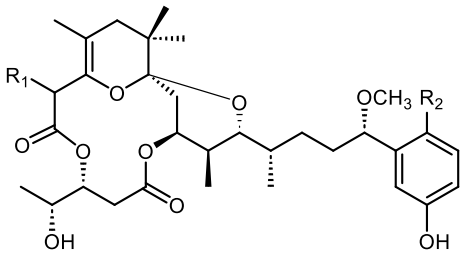

anhydroaplysiatoxin : R_1=H, R_2=Br
anhydrodebromoaplysiatoxin : R_1=H, R_2=H
★ 2-hydroxyanhydroaplysiatoxin : R_1=OH, R_2=Br

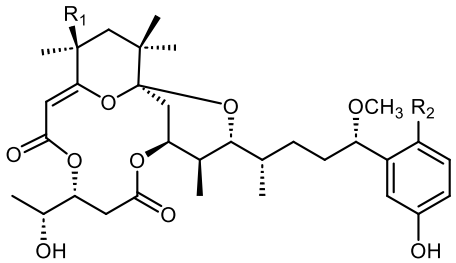

oscillatoxin B2 : R_1=OH, R_2=H
★ 17-bromooscillatoxin B2 : R_1=OH, R_2=Br
★ 17-bromo-4-hydroperoxyoscillatoxin B2 : R_1=OOH, R_2=Br
★ 4-hydroperoxyoscillatoxin B2 : R_1=OOH, R_2=H

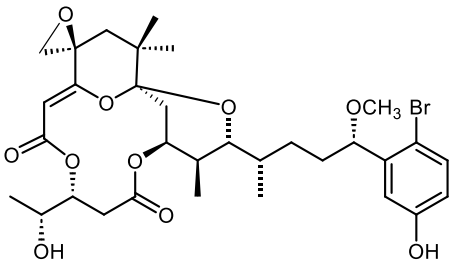

★ 17-bromo-4,26-epoxyoscillatoxin B2

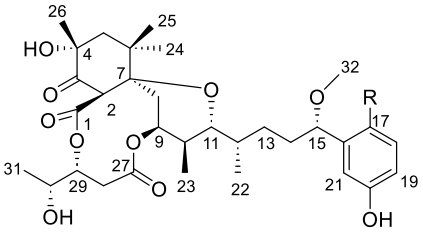

★ neo-aplysiatoxin A: R=Br
neo-debromoaplysiatoxin A: R=H

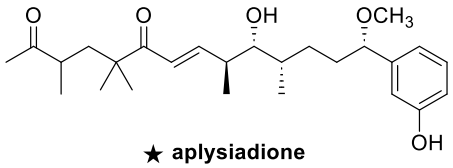

★ aplysiadione

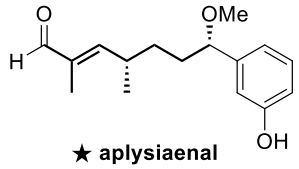

★ aplysiaenal

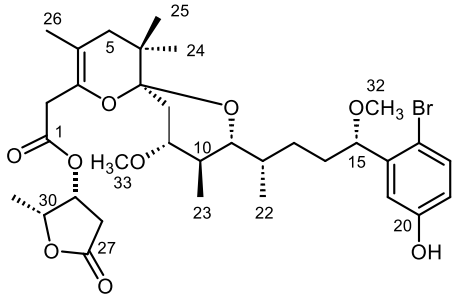

★ oscillatoxin H

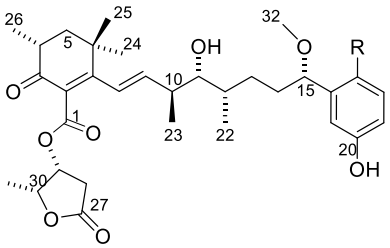

★ oscillatoxin I: R=Br
★ debromooscillatoxin I: R=H

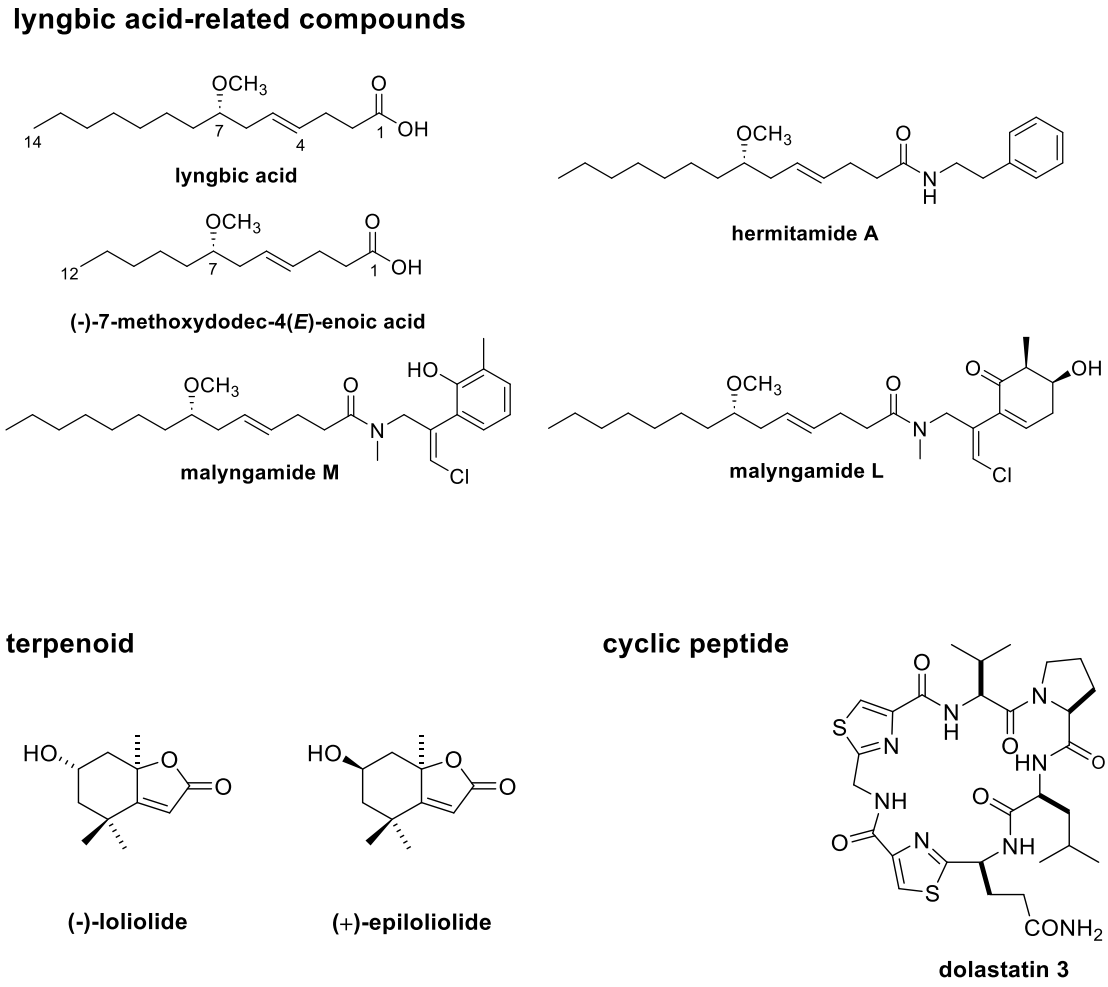

Figure 2.3-1 Summary of isolated compounds from the Okinawan cyanobacterium *O. hirsuta* before this study (★: new compounds)

Chapter 3. Aplysiatoxin-related Compounds (ATXs) from the Okinawan Cyanobacterium *Okeania hirsuta*

3.1 Introduction

At the third UPAC (International Union of Pure and Applied Chemistry) International Conference held in Kyoto in 1964, the structure of tetrodotoxin was determined simultaneously by Robert B. Woodward, Yoshimasa Hirata, and Kyosuke Tsuda' groups, which was an important milestone in the development of natural product chemistry field.[35] In the same year, its mechanism of action, selective blocking of the sodium channel, was also unraveled by Toshio Narahashi and John W. Moore, using the sucrose gap voltage clamp technique.[36] Since then, the attention of many natural product chemists has been directed towards marine-oriented research and we have witnessed many magnificent achievements in the structure determination of marine toxins in the ensuing years. These achievements include the structural elucidation of aplysiatoxin[10] in 1974, saxitoxin in 1975,[37] palytoxin in 1981,[38] ciguatoxin in 1989.[39]

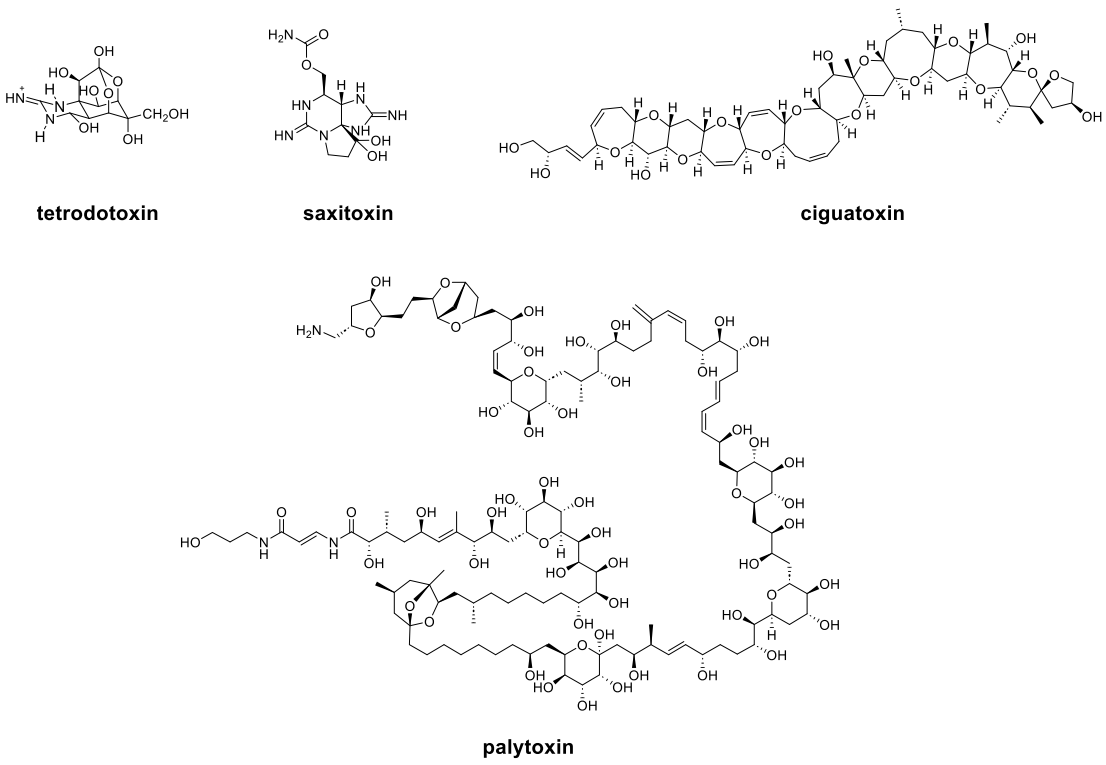

Figure 3.1-1 Structures of representative marine toxins

In the present study, a variety of ATX-related compounds have been isolated from the Okinawan cyanobacterium *O. hirsuta*, so we would like to have a brief introduction on the discovery of ATXs before discussing these findings.

Aplysiatoxins (ATXs), a class of polyketides dermatotoxins, were first discovered from the digestive gland of the *Stylocheilus longicauda*.[10] Subsequent research revealed that these toxins actually came from cyanobacteria and accumulated in marine mollusks through the food chain. The molecular architecture of the aplysiatoxin are bislactones of 3,4-dihydroxyvaleric acid and of 4,6,6,10,12-pentamethyl-3,7,9,11,15-tetraoxy-15-phenylpentadecanoic-acid, encompassing a symmetrical trioxacyclododecane (Figure 3.1-2). This unique skeletal structure was revealed by major chemical degradations in various conditions and spectral data by Y. Kato and P. J. Scheuer in 1974.[10] In toto, 12 g of toxin, which was extracted from 50 kg of *S. longicauda*, about 5000 animals were used to determine the planar structure of aplysiatoxin. Scheme 3-1 illustrate how these complex chemical degradation steps were conducted.[40]

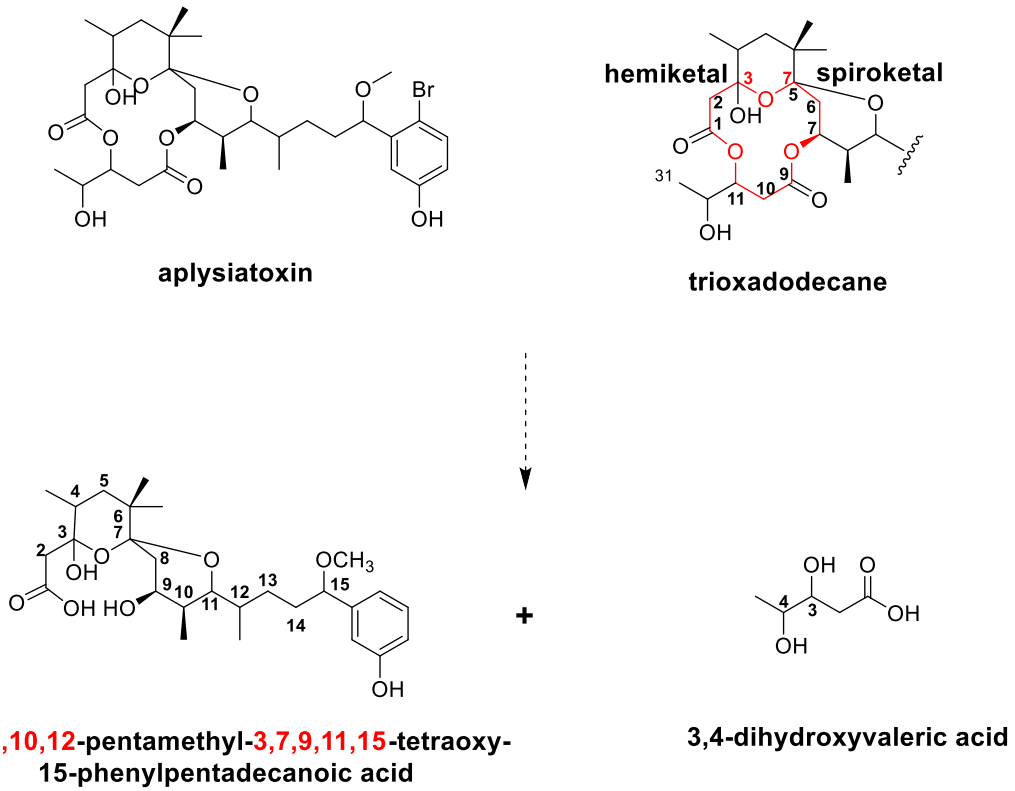

Figure 3.1-2 Molecular architecture of the ATX

Step1: ^{1}H NMR, IR, MS fragment

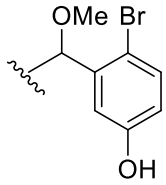

part stucture. 1

Step2: mild base treatment at room temperature

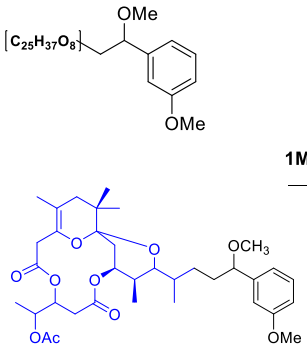

$C_{25}H_{37}O_8$

part structure. 2 $C_7H_{10}O_4$
4-acetoxy-trans-2-pentenoic acid

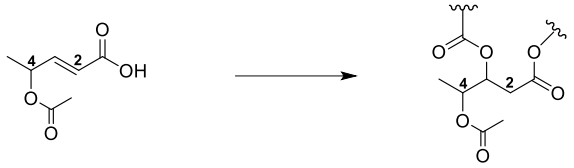

part structure. 2 $C_7H_{10}O_4$
4-acetoxy-trans-2-pentenoic acid

part structure. 3
bis-lactone

Step3: metal hydride reductive treatment

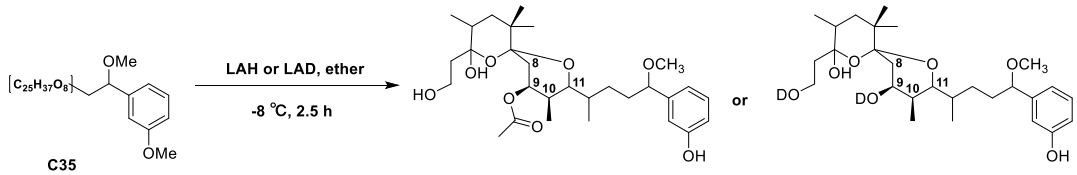

C35

C28 diols

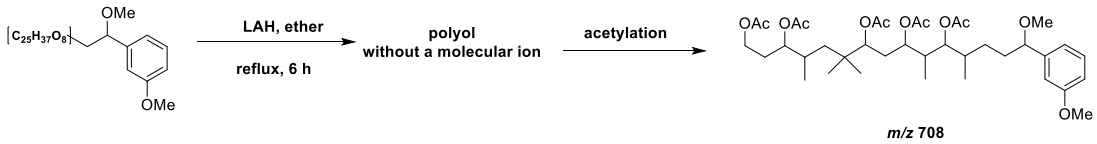

***m/z* 708**

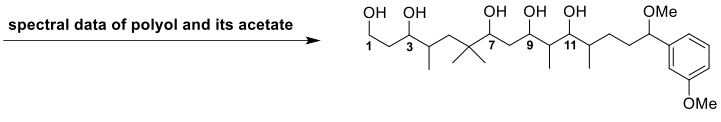

pentanol (*m/z* 498)

Step 4 :Base degradation

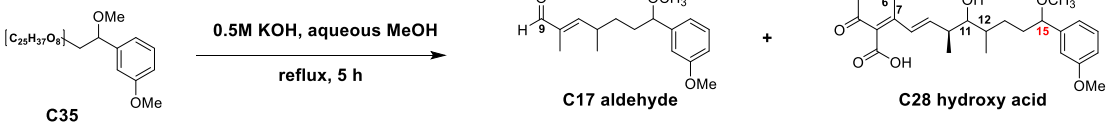

C35

C17 aldehyde

C28 hydroxy acid

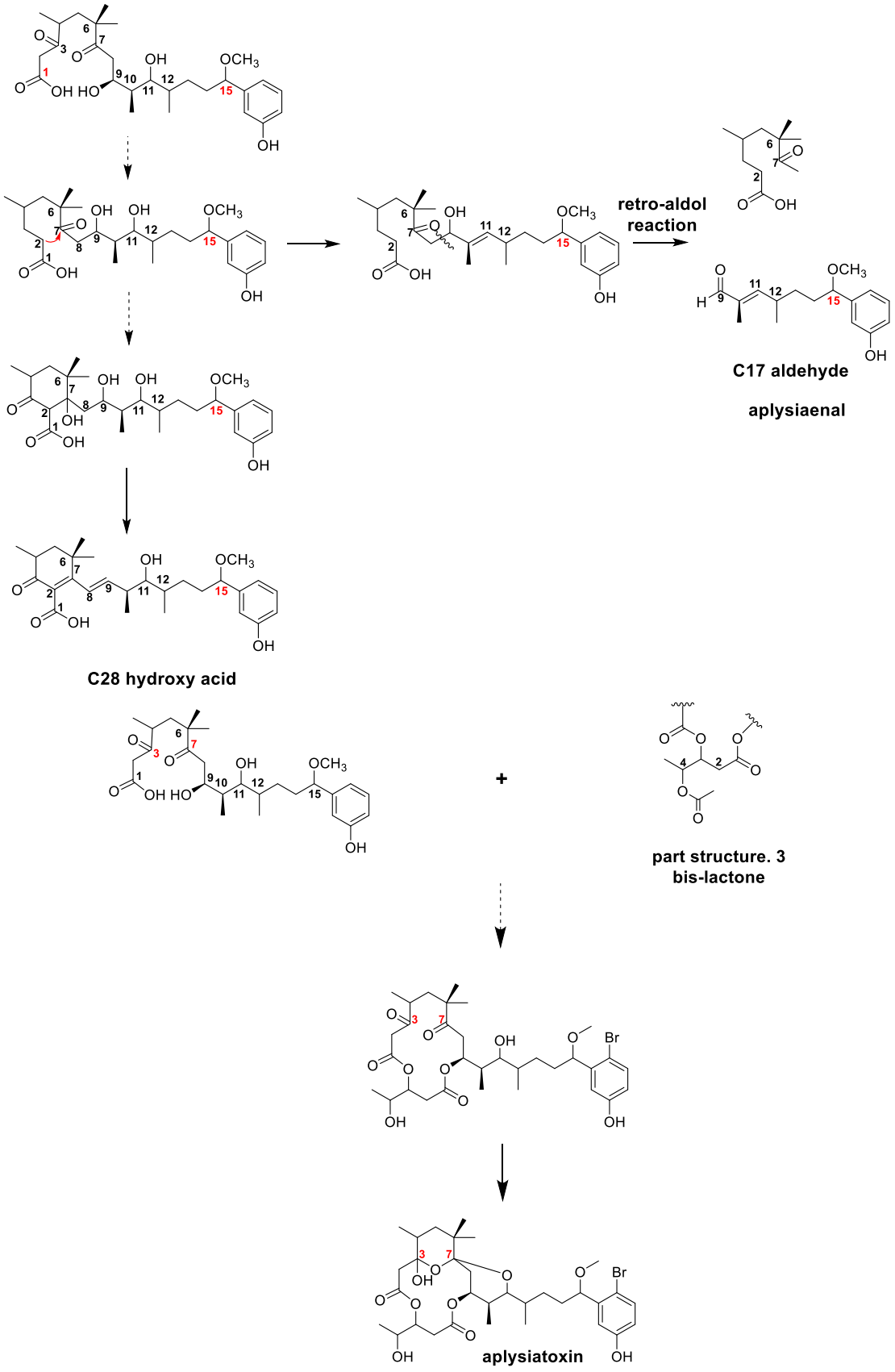

Scheme 3-1. The steps of chemical degradations performed for ATXs by Y. Kato and P. J. Scheuer.[40]

In the early 1970s, prior to the advent of two-dimensional NMR spectroscopy, the structure of ATX was determined accurately by majorly performing a series of chemical degradations. The wisdom and perseverance of chemists at that time deeply impressed me and I hold tremendous admiration for their works.

As outlined, the limitation of isolation and structural characterization techniques at the time, made the structural elucidation of natural products require extensive time and a high level of knowledge. However, these challenges ignited researchers' curiosity in unknown natural components and motivated continued exploration and study of their structures, thereby driving the development and progress of marine natural product chemistry.

In the present study, a variety of ATX derivatives were isolated including a novel compound debromooscillatoxin G with our ongoing efforts in discovering natural products from the Okinawan cyanobacterium *O. hirusuta*.

The frozen *O. hirsuta* sample was soaked in MeOH for several days at room temperature. After filtration, the sample was extracted five times with methanol and once with acetone. These extracts were then combined and concentrated *in vacuo* to obtain a residue, which was subsequently partitioned between 80% aqueous MeOH and hexane. The 80% aqueous MeOH layer was then evaporated and partitioned between EtOAc and H_2O to obtain an EtOAc layer. The H_2O layer was further extracted with BuOH to afford BuOH layer and H_2O layer.

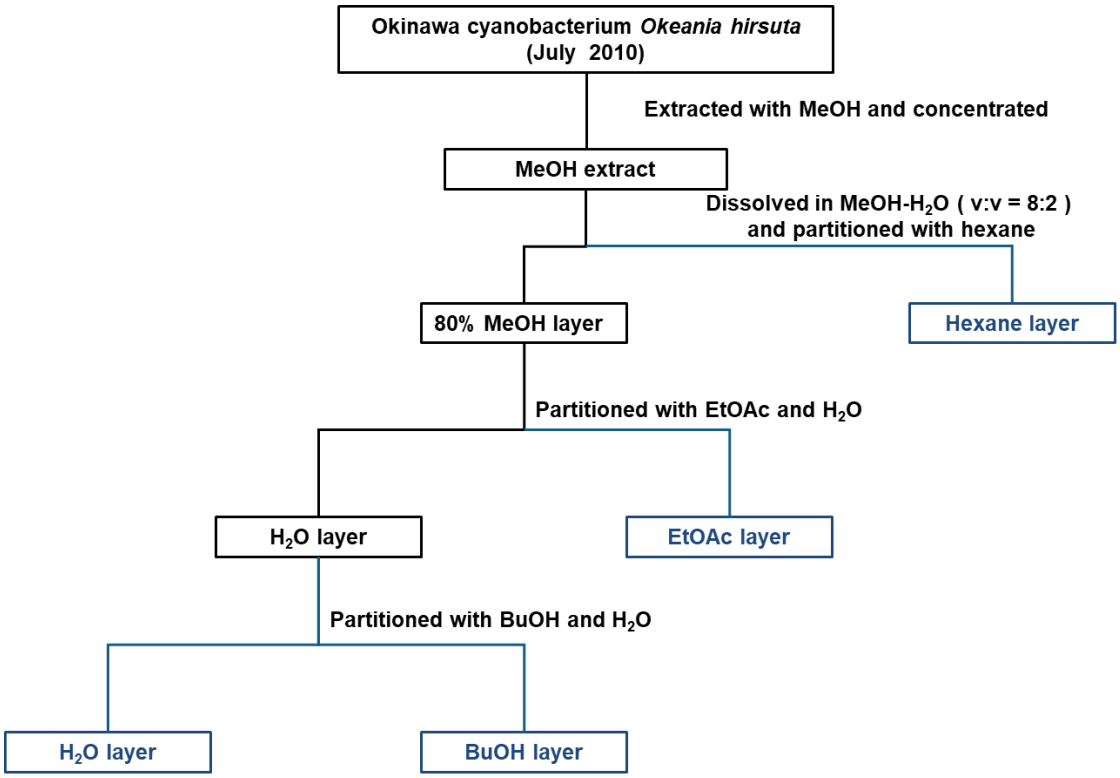

Scheme 3-2 Extraction of secondary metabolites from cyanobacterium *O. hirsuta*.

3.2 Reisolation and identification of ATXs from the 90% MeOH fraction

Isolation

The EtOAc extract, which showed the most potent cytotoxicity against mouse L1210 leukemia cells was separated on an open glass column (Cosmosil 75C18-OPN resin, φ40 × 400 mm) through stepwise elution with 50%, 70%, 90%, and 100% MeOH (Scheme 3-3).

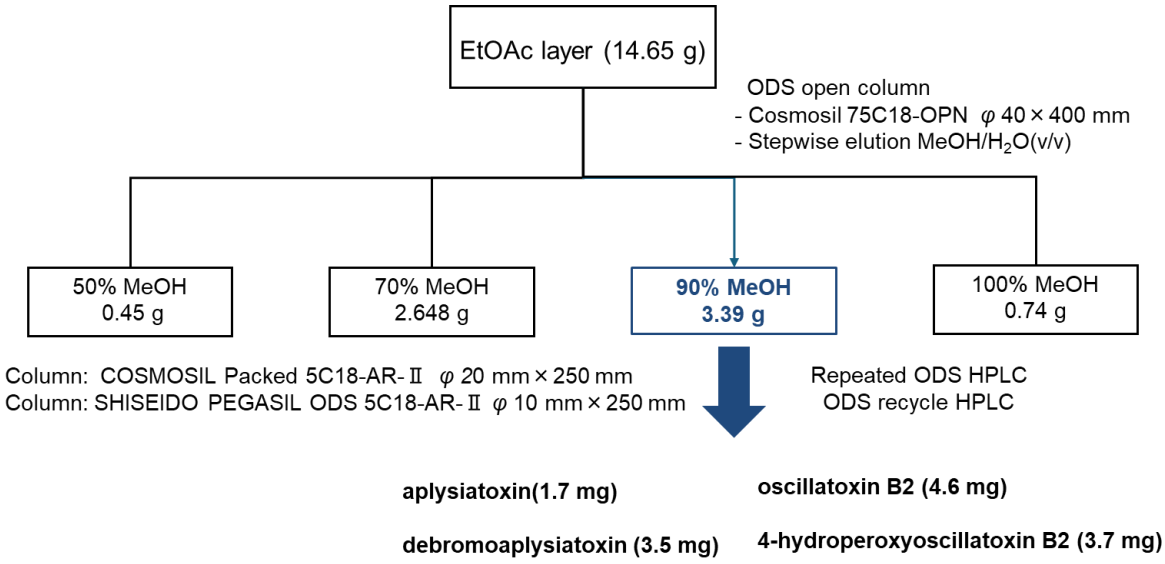

Scheme 3-3. Isolation of known ATXs from 90% MeOH fraction of EtOAc layer.

The 90% MeOH fraction with the highest quantity was subjected to fractionation using repeated semi-preparative reversed-phase HPLC to yield aplysiatoxin (ATX) (1.7 mg), debromoaplysiatoxin (DATX) (3.5 mg), oscillatoxin B2 (OTX B2) (4.6 mg), and 4-hydroperoxyoscillatoxin B2 (4-hydroperoxyOTX B2) (3.7 mg) (Figure 3.2-1).

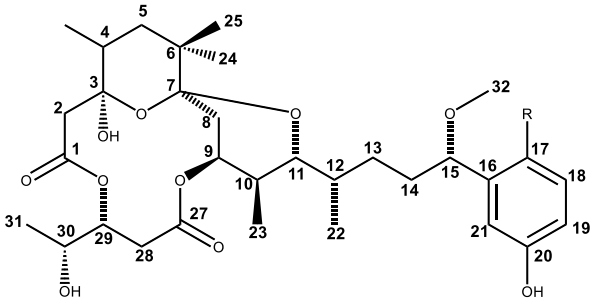

aplysiatoxin (1.7 mg): R = Br

debromoaplysiatoxin (3.5 mg): R = H

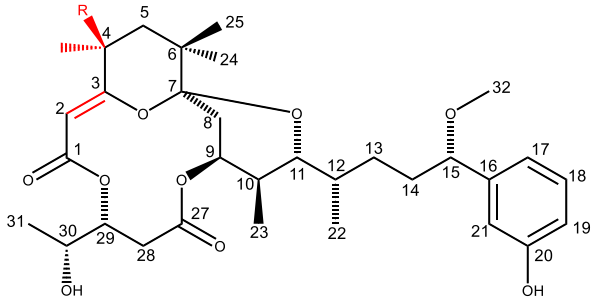

oscillatoxin B2 (4.6 mg): R = OH

4-hydroperoxyoscillatoxin B2 (3.7 mg): R = OOH

Figure 3.2-1 Structures of isolated known ATXs from 90% MeOH fraction.

Structure elucidation

Aplysiatoxin ($C_{32}H_{47}BrO_{10}$)

HRESIMS

$[M-H]^-$ peak at *m/z* 669.2246 and 671.2232 (calcd. for $C_{32}H_{46}BrO_{10}$: *m/z* 669.2269 and 671.2255)

^{1}H NMR (600 MHz, acetone)

δ 8.57 (s, 1H), 7.32 (d, *J* = 8.6 Hz, 1H), 7.10 (d, *J* = 3.1 Hz, 1H), 6.69 (dd, *J* = 8.6, 3.1 Hz, 1H), 5.23 (dt, *J* = 3.2, 3.2 Hz, 1H), 5.20 (dt, *J* = 10.3, 3.8 Hz, 1H), 4.48 (dd, *J* = 6.9, 5.5 Hz, 1H), 4.28 (d, *J* = 1.9 Hz, 1H), 4.20 (d, *J* = 5.3 Hz, 1H), 4.03 – 3.97 (m, 1H), 3.93 (dd, *J* = 10.8, 2.3 Hz, 1H), 3.19 (s, 3H), 2.90 – 2.88 (m, 2H), 2.74 (d, *J* = 12.6 Hz, 1H), 2.69 (dd, *J* = 14.6, 3.0 Hz, 1H), 2.61 (d, *J* = 12.5 Hz, 1H), 2.01 – 1.96 (m, 1H), 1.92 – 1.85 (m, 1H), 1.75 – 1.71 (m, 1H) 1.72 (dd, *J* = 14.7, 3.6 Hz, 1H), 1.62 (t, *J* = 13.1 Hz, 1H), 1.57 – 1.54 (m, 1H), 1.54 – 1.50 (m, 1H), 1.49 – 1.45 (m, 1H), 1.44 – 1.39 (m, 1H), 1.10 (d, *J* = 6.5 Hz, 3H), 1.06 (dd, *J* = 13.4, 3.6 Hz, 1H), 0.85 (s, 3H), 0.85 (d, *J* = 6.7 Hz, 3H) 0.84 (s, 3H), 0.82 (d, *J* = 6.7 Hz, 3H), 0.73 (d, *J* = 6.9 Hz, 3H).

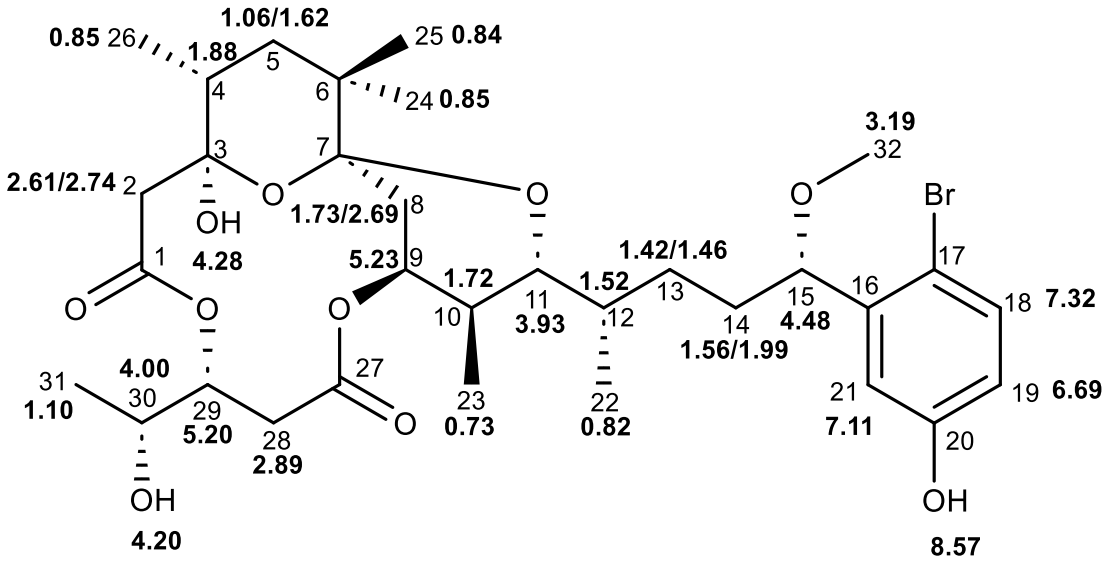

Figure 3.2-2 Proton chemical shifts of ATX.

Debromoaplysiatoxin($C_{32}H_{48}O_{10}$)

HRESIMS

$[M+H]^+$ peak at *m/z* 593.3342 (calcd. for $C_{32}H_{49}O_{10}$: *m/z* 593.3320)

^{1}H NMR (600 MHz, acetone)

δ 7.13 (t, *J* = 7.8 Hz, 1H), 6.92 (dd, *J* = 2.6, 1.4 Hz, 1H), 6.84 (d, *J* = 7.8 Hz, 1H), 6.71 (ddd, *J* = 8.1, 2.5, 1.0 Hz, 1H), 5.29 – 5.13 (m, 2H), 4.29 (d, *J* = 1.8 Hz, 1H), 4.07 – 4.02 (m, 1H), 3.99 (t, *J* = 6.5 Hz, 1H), 3.93 (dd, *J* = 10.8, 2.3 Hz, 1H), 3.17 (s, 3H), 2.89 (dd, *J* = 3.9, 2.3 Hz, 1H), 2.76 (d, *J* = 12.5 Hz, 1H), 2.68 (dd, *J* = 14.7, 2.9 Hz, 1H), 2.52 (d, *J* = 12.6 Hz, 1H), 1.97 (tt, *J* = 12.1, 5.6 Hz, 1H), 1.85 (q, *J* = 6.4 Hz, 1H), 1.71 (dd, *J* = 14.8, 3.8 Hz, 2H), 1.62 (t, *J* = 12.8 Hz, 1H), 1.52 (q, *J* = 6.9 Hz, 1H), 1.45 – 1.35 (m, 1H), 1.33 – 1.28 (m, 1H), 1.12 (d, *J* = 6.5 Hz, 3H), 1.05 (dd, *J* = 13.4, 3.6 Hz, 1H), 0.86 (d, *J* = 6.9 Hz, 2H), 0.83 (s, 3H), 0.80 (s, 3H), 0.79 (d, *J* = 7.5 Hz, 3H), 0.71 (d, *J* = 6.9 Hz, 3H).

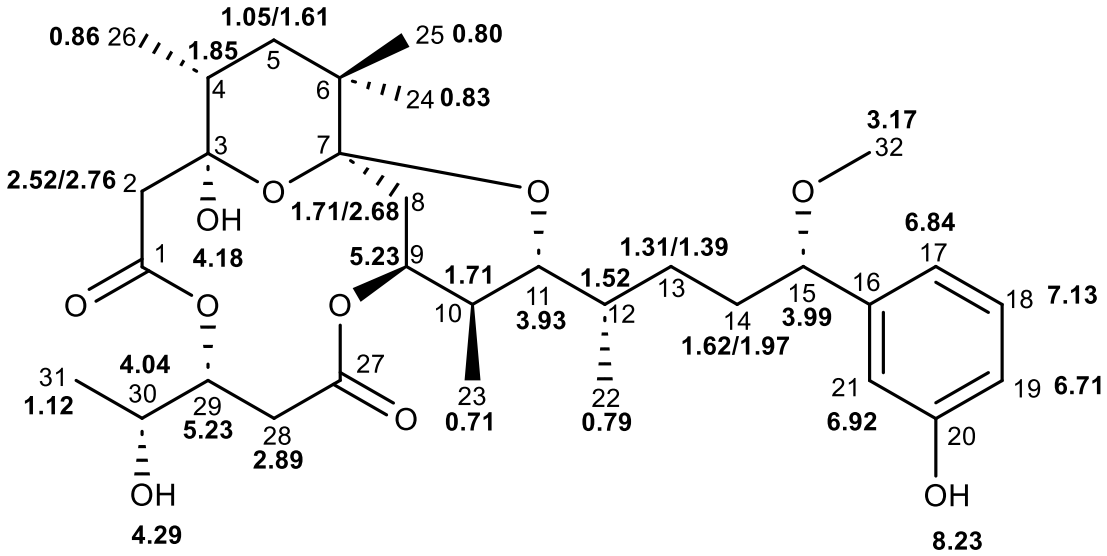

Figure 3.2-3 Proton chemical shifts of DATX.

Aplysiatoxin and debromoaplysiatoxin

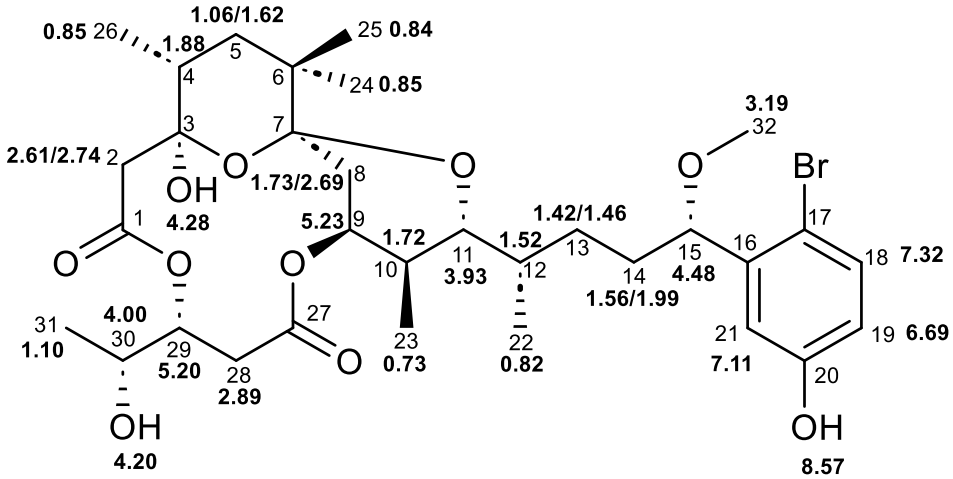

ATX

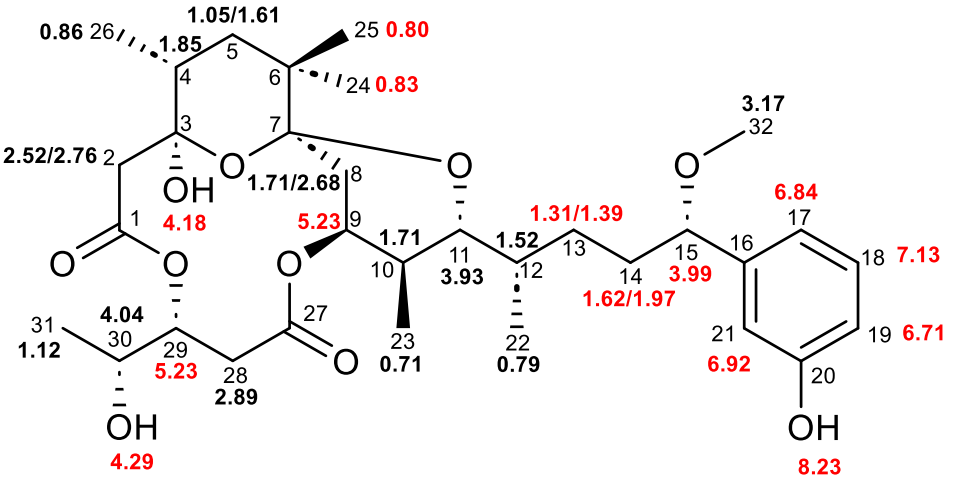

DATX

Figure 3.2-4 Comparison of proton chemical shifts for ATX and DATX.

Oscillatoxin B2 ($C_{32}H_{46}O_{10}$) and 4-hydroperoxyoscillatoxin B2 ($C_{32}H_{46}O_{11}$)

HRESIMS

OTX B2: $[M-H]^-$ peak at *m/z* 589.3035 (calcd. for $C_{32}H_{45}O_{10}$: *m/z* 589.3007)

4-hydroperoxyOTX B2: $[M-H]^-$ peak at *m/z* 605.2983 (calcd. for $C_{32}H_{45}O_{11}$: *m/z* 605.2956)

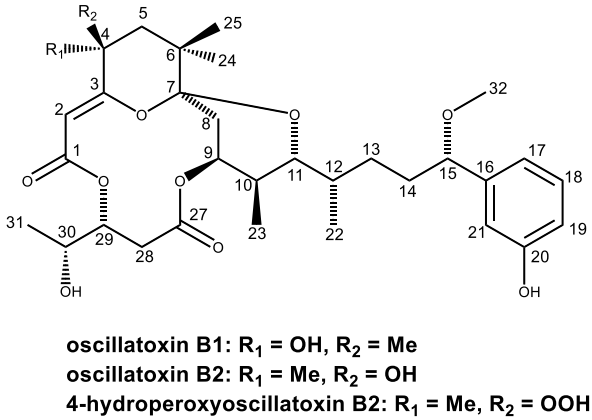

oscillatoxin B1: R_1 = OH, R_2 = Me
oscillatoxin B2: R_1 = Me, R_2 = OH
4-hydroperoxyoscillatoxin B2: R_1 = Me, R_2 = OOH

Figure 3.2-5 Structures of OTX B.

The structural elucidation of OTX B2 and 4-hydroperoxyOTX B2 was carried out by comparing the ^{1}H NMR spectra with those of standards that were previously isolated in our laboratory.[30]

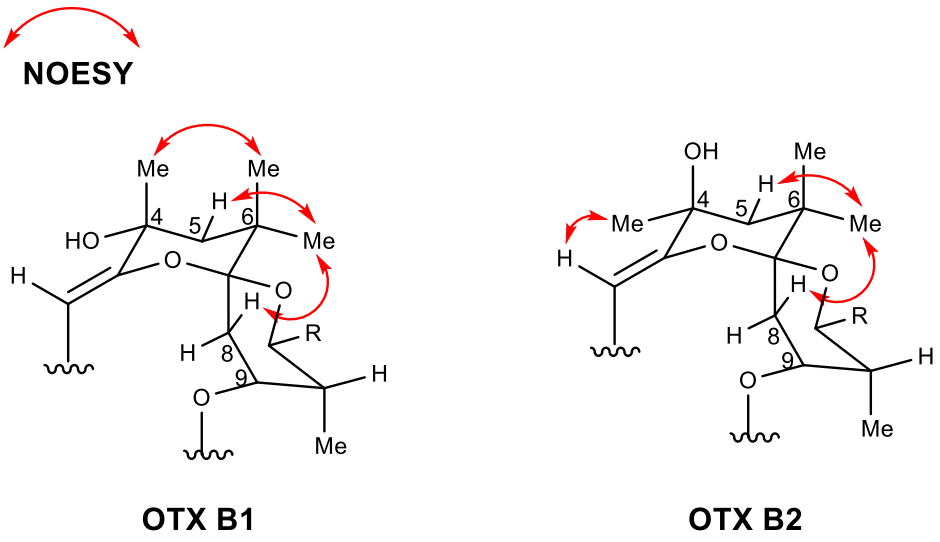

Figure 3.2-6 Key NOESY correlations of OTX B1 and OTX B2 in spiro ring moiety.

According to the configuration of C-4, OTX B had two isomers, OTX B1 and OTX B2 (Figure3.2-6).[41] These two isomers were distinguished by NOESY experiments. In the NOESY spectra of these two isolated compounds, the correlation for H-2/Me-26 was observed while Me-26/M-24 and Me-26/Me-25 were not observed, suggesting that Me-26 was oriented equatorially. Therefore, these two compounds were identified as OTX B2 and 4-hydroperoxy OTX B2 respectively.

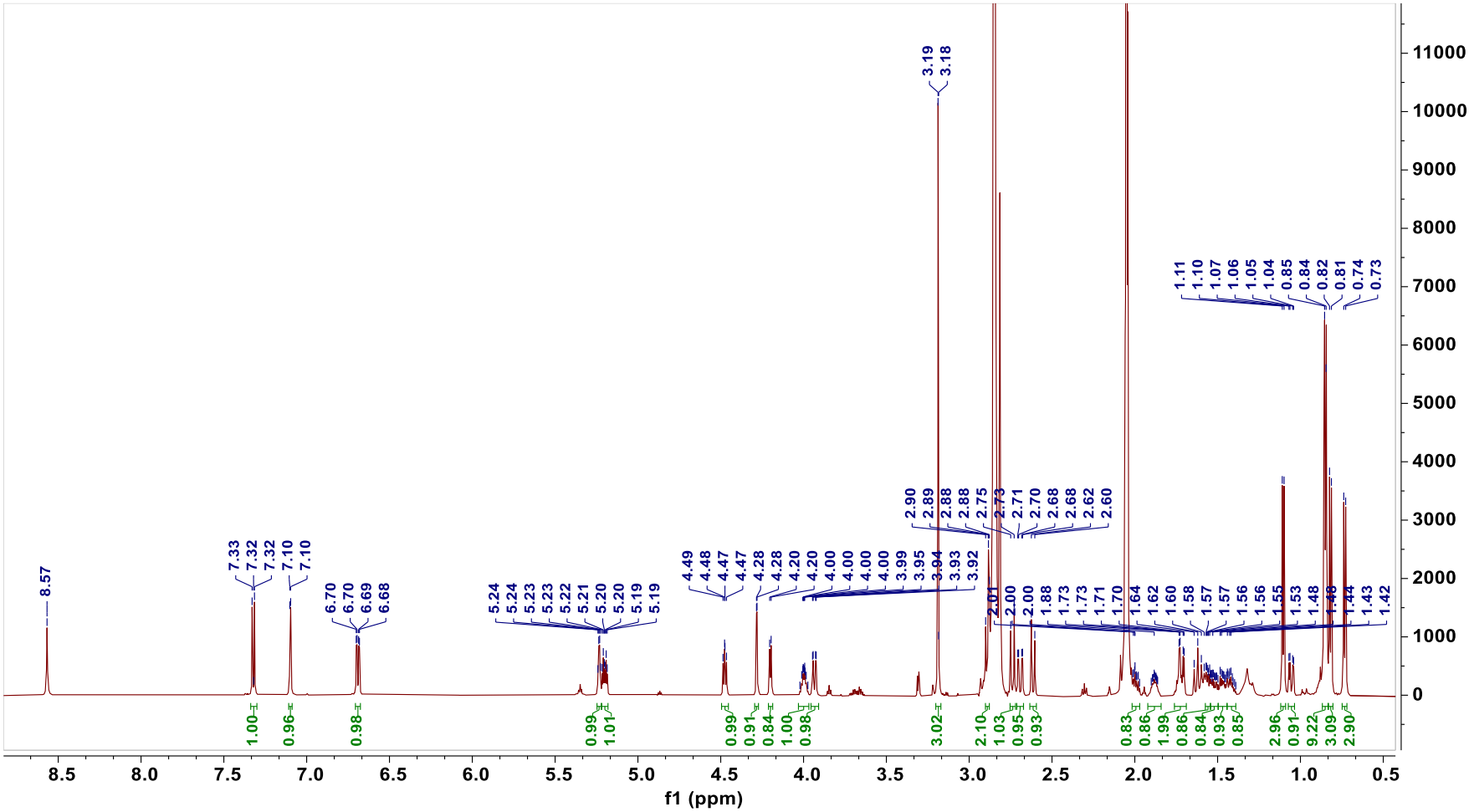

Figure 3.2-7 ^{1}H NMR spectrum of ATX.

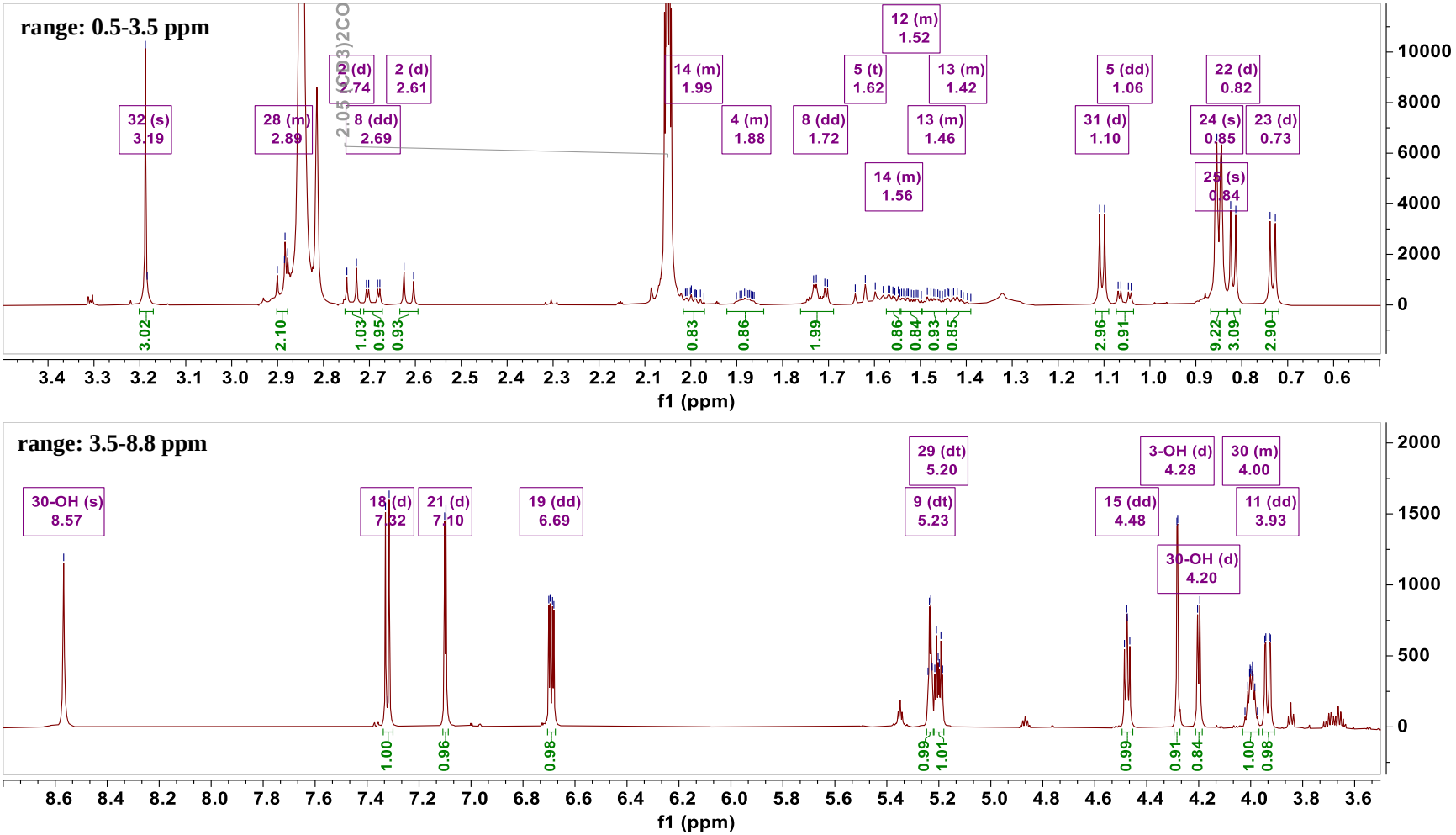

Figure 3.2-8 ^{1}H NMR assignments of ATX (top: 0.5-3.5 ppm; bottom: 3.5-8.8 ppm).

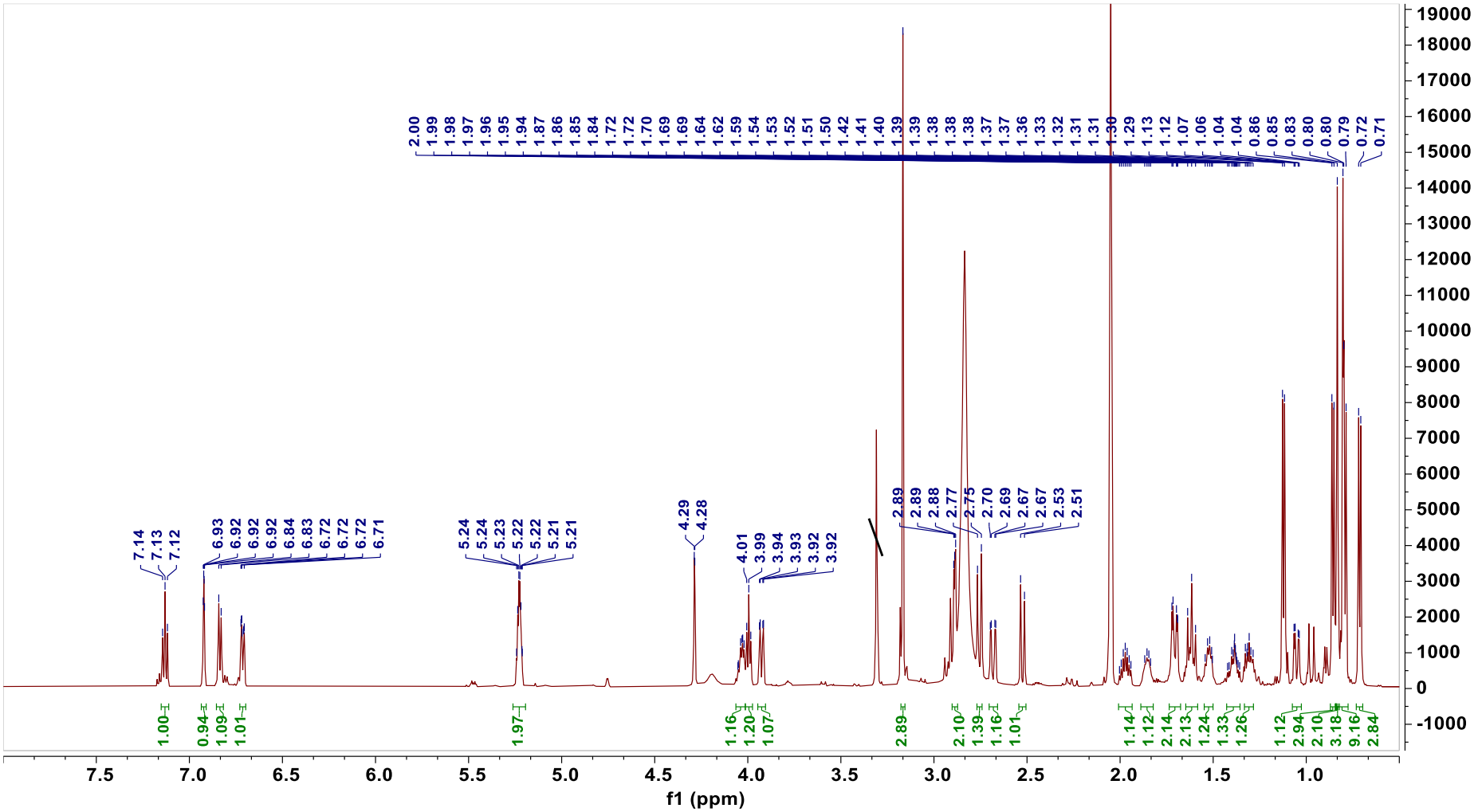

Figure 3.2-9 ^{1}H NMR spectrum of DATX.

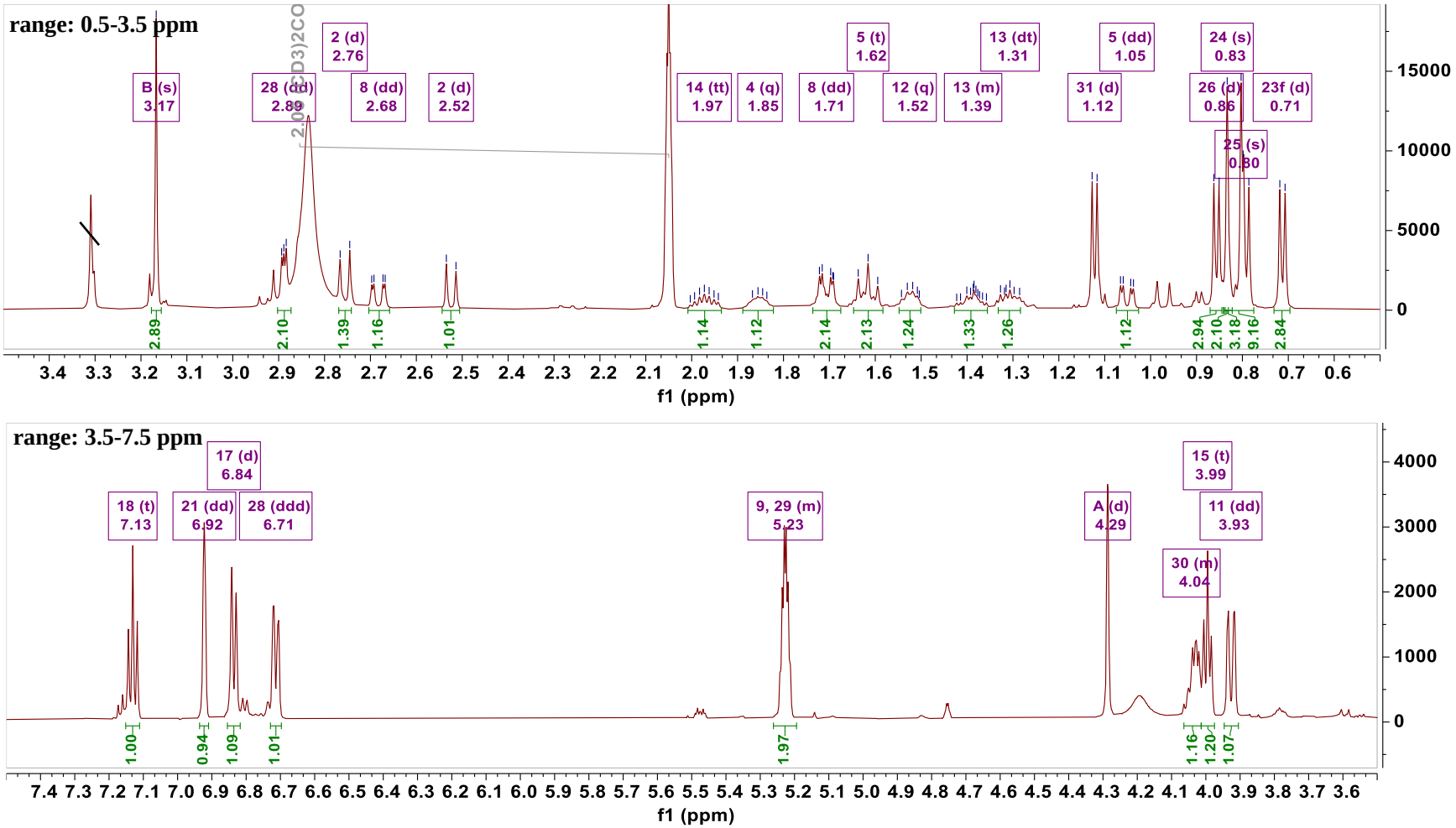

Figure 3.2-10 [1]H NMR assignment of DATX (top: 0.5-3.5 ppm; bottom: 3.5-7.5 ppm).

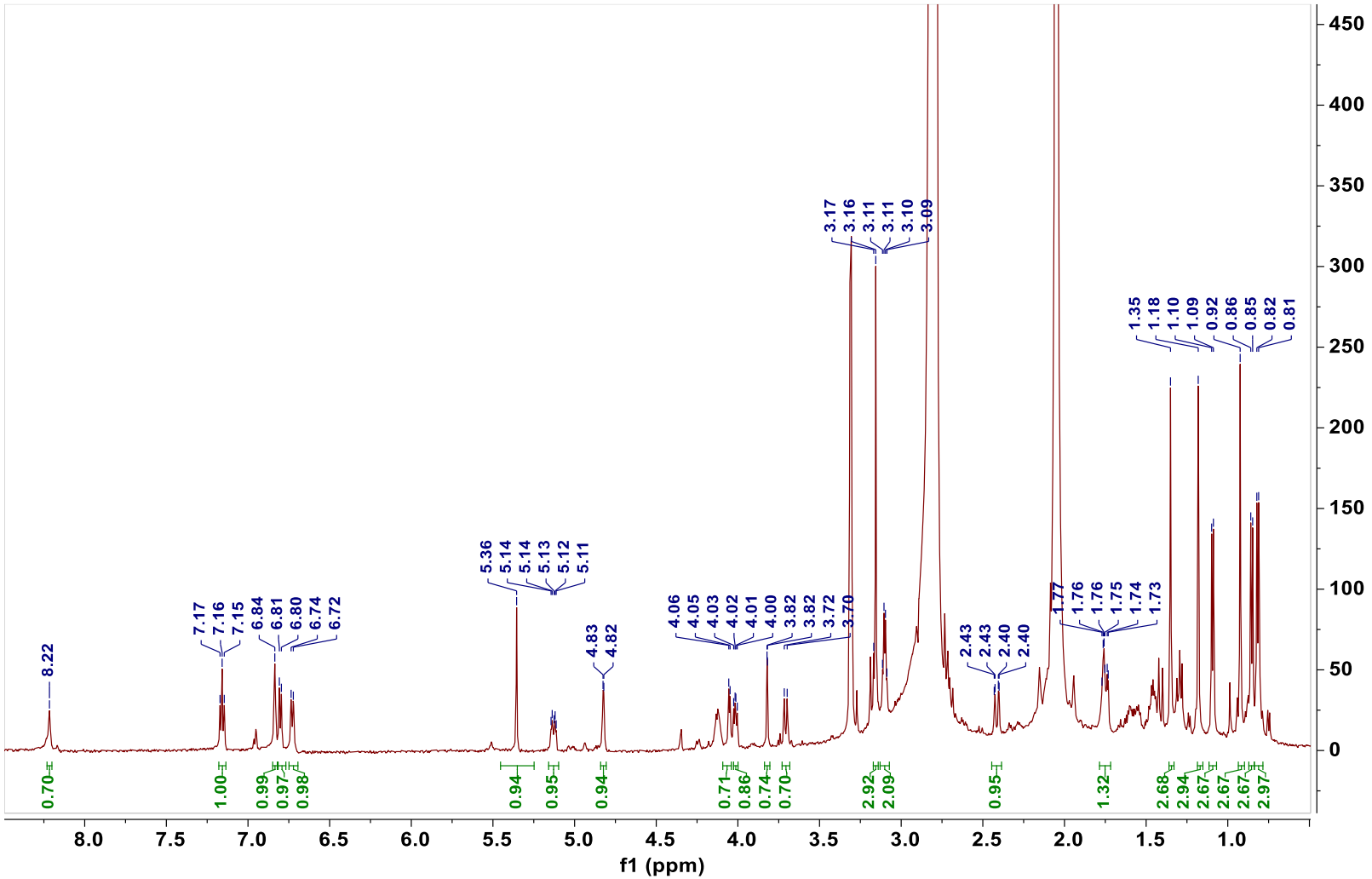

Figure 3.2-11 ^{1}H NMR spectrum of OTX B2.

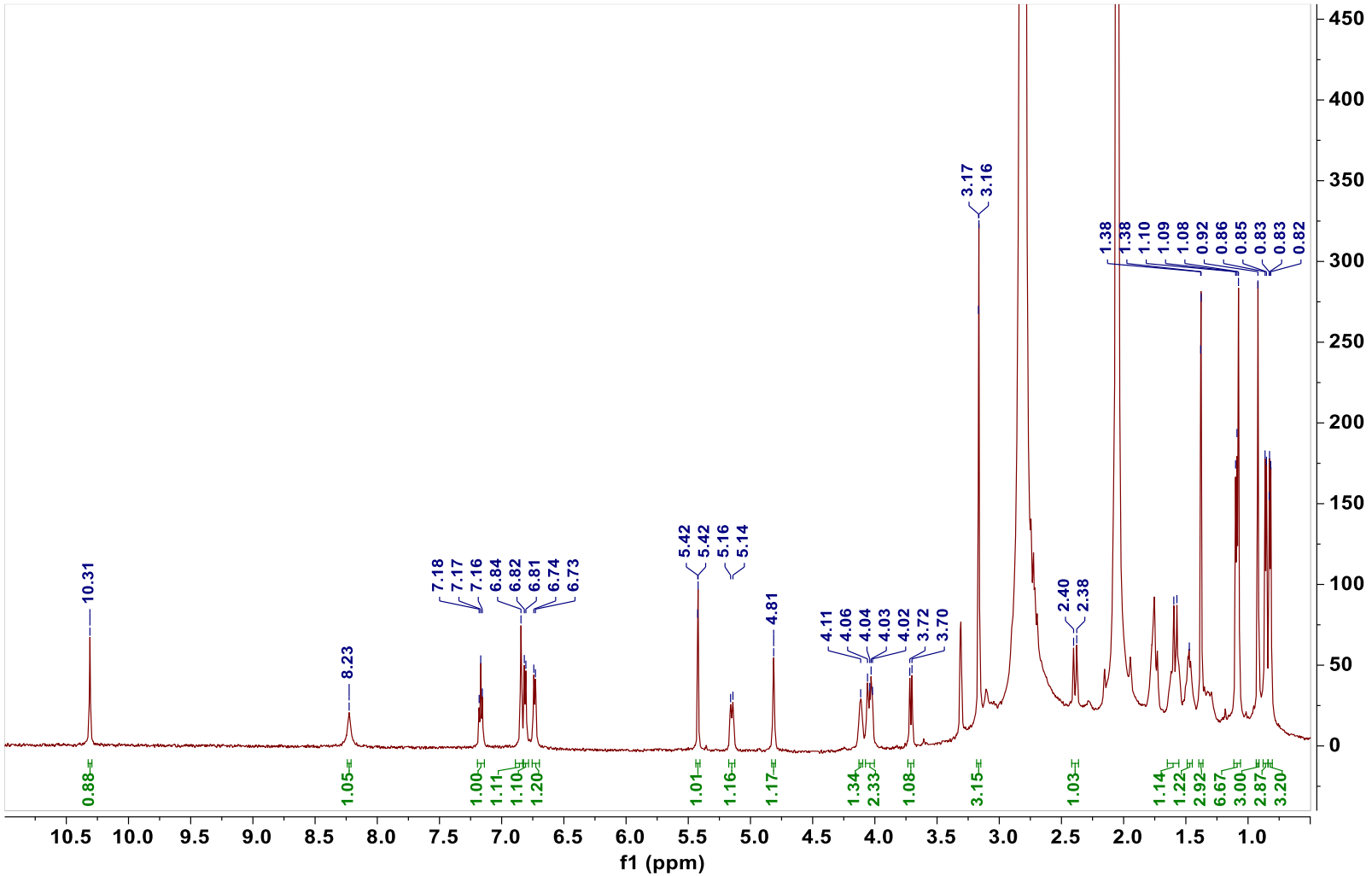

Figure 3.2-12 ^{1}H NMR spectrum of 4-hydroperoxyOTX B2.

3.3 Isolation and structure elucidation of ATXs from 70% MeOH fraction

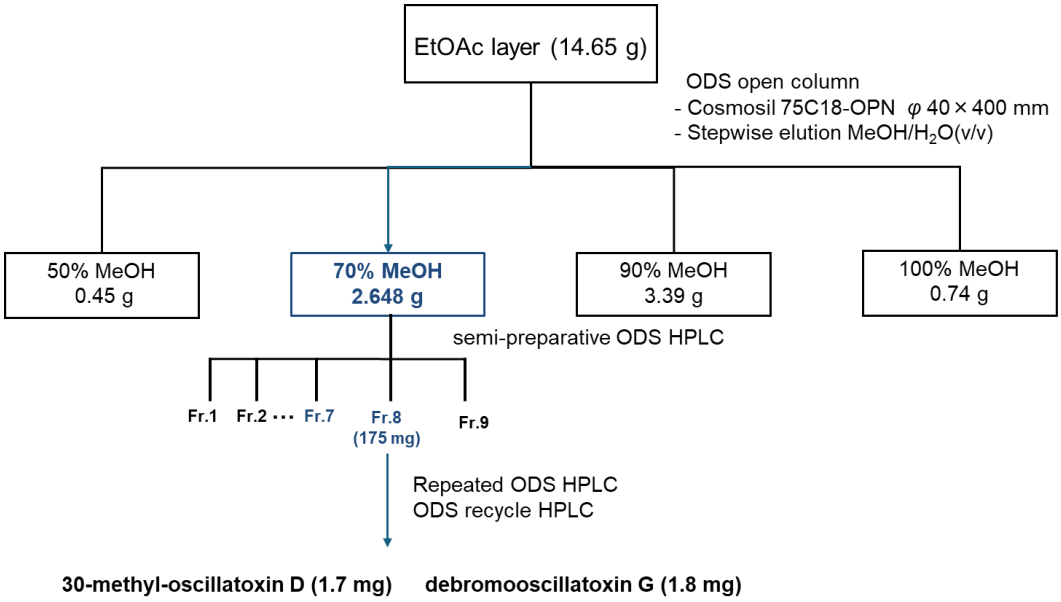

Scheme 3-4. Isolation of ATXs from 70% MeOH fraction of EtOAc layer.

3.3.1 Isolation and structural elucidation of 30-methyl-oscillatoxin D with its natural degradation product OTX F

Isolation

Fraction 8 (175 mg) was subject to a semi-preparative HPLC [column, Cosmosil 5C_{18}-AR-II (10 × 250 mm); flow rate, 2.0 mL/min; detection at 210 nm; solvent MeOH/H_2O gradient condition, 45-min linear gradient elution from 65% to 100% MeOH, after which the 100% MeOH extract was held for an additional 15 min] to produce 5 subfractions (Fr. 1-5). Subfraction 4 (18.8 mg) was further separated using recycle HPLC [column, Cosmosil 5C_{18}-AR-II (φ 10 × 250 mm); flow rate, 3.0 mL/min; detection at 210 nm; solvent 70% MeOH] to yield oscillatoxin B (OTX B), 4-hydroperoxy oscillatoxin B (4-hydroperoxyOTX B), and 30-methyl-oscillatoxin D (**1**) (30-Me-OTX D), together with anhydroDATX.

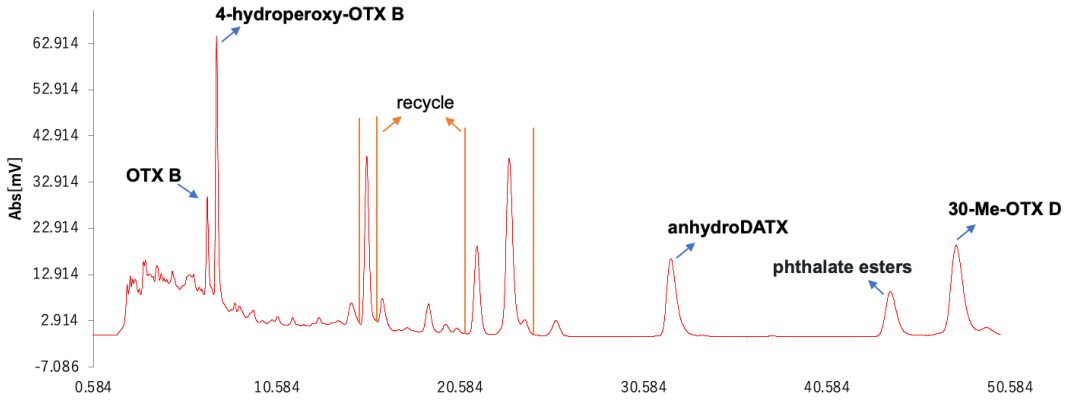

compound	retention time (min)	Weight (mg)
OTX B	**7.6**	0.6
4-hydroperoxyOTX B	**8.3**	0.8
anhydroDATX	**17.8**	1.2
30-Me-OTX D (**1**)	**27.3**	1.7

Figure 3.3-1 Recycle HPLC chromatogram of subfraction 4 containing 30-Me-OTX D.

Structure elucidation

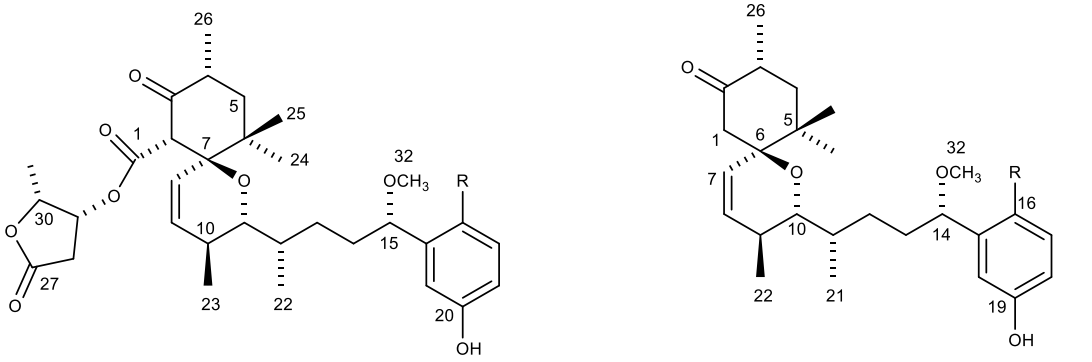

Figure 3.3-2 Structures of 30-Me-OTX D-related compounds.

30-Me-OTX D (**1**) was obtained as a colorless oil. The structural elucidation of **1** was carried out by comparing the ^{1}H and ^{13}C NMR data with those of synthetic 30-Me-OTX D. [42] However, when the ^{1}H NMR spectrum was remeasured for **1** after an overnight 2D NMR measurement, some discernible changes were observed. Thus, we conducted a detailed spectroscopic analysis for the resulting material and found that the rapid conversion of **1** to OTX F (**3**) occurred during measurement by β-elimination from the lactone moiety followed by decarboxylation of the products (Scheme 3-5).

Considering the transformation occurred in 30-Me-OTX D (**1**), we turned our attention to 17-Br-30-Me-OTX D (**2**) to investigate whether it would undergo similar changes as **1**. 17-Br-30-Me-OTX D, which had been isolated from the same *O. hirsuta* sample, was observed to present some unidentified peaks during the NMR analysis, as reported by Watanabe in 2017. Thus, a comprehensive spectroscopic analysis was performed for **2**. As a result, the conversion of **2** to 16-Br-OTX F (**4**) was also confirmed. It is worth to note that 16-Br-OTX F has not been obtained as a natural product, while the isolation of OTX F from the marine cyanobacterium *Lyngbya* sp. was reported in 2019.[43] Moreover, Araki et al demonstrated that β-elimination followed by decarboxylation also occurred during the synthesis of OTX-D and 30-Me-OTX D from OTX E, resulting reduced yields of OTX D (26%) and 30-Me-OTX D (40%).[42] On the other hand, 7-*epi*-30-Me-OTX D, which possesses inversion of configuration at the C-7 spiro atom compared to **1** was

stable for over two years under the dry, dark, and refrigerated conditions after isolation.[28] However, the mechanism of this difference was still under investigation.

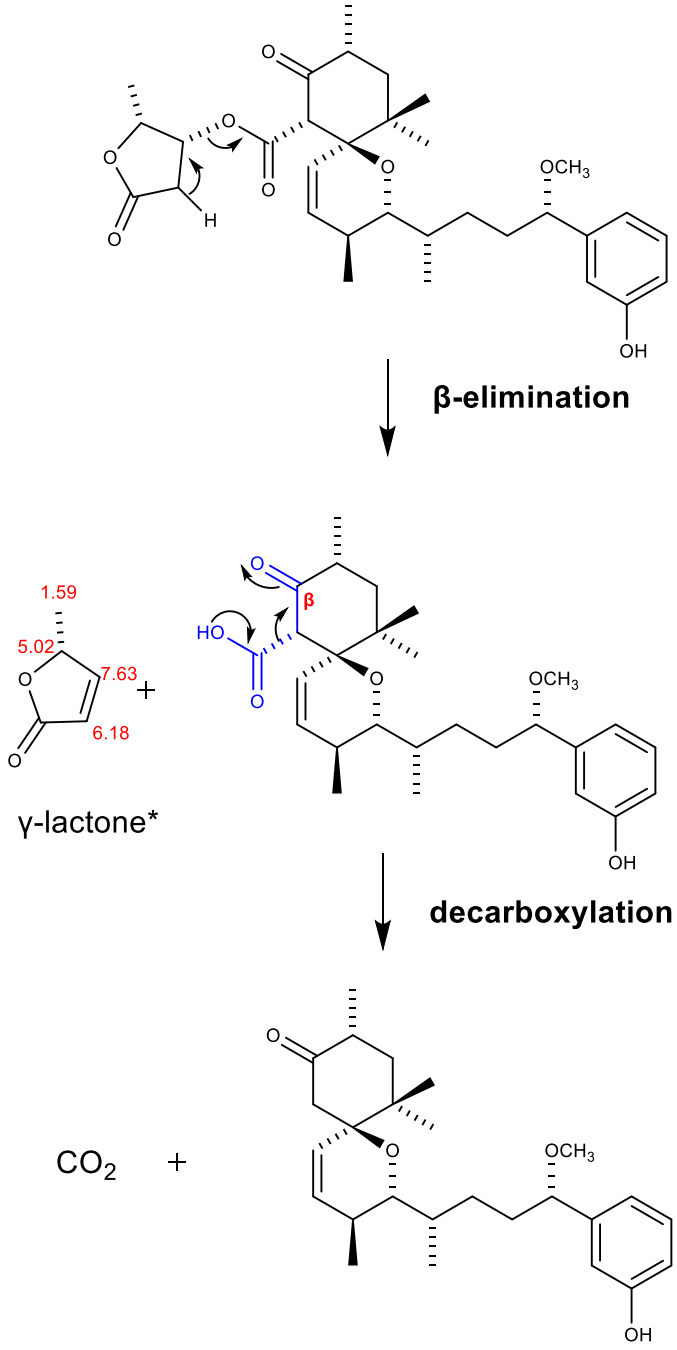

*The ^{1}H NMR chemical shifts of γ-lactone in $CDCl_3$ were predicted by ChemDraw

Scheme 3-5. β-elimination followed by decarboxylation on the lactone moiety of 30-Me-OTX D

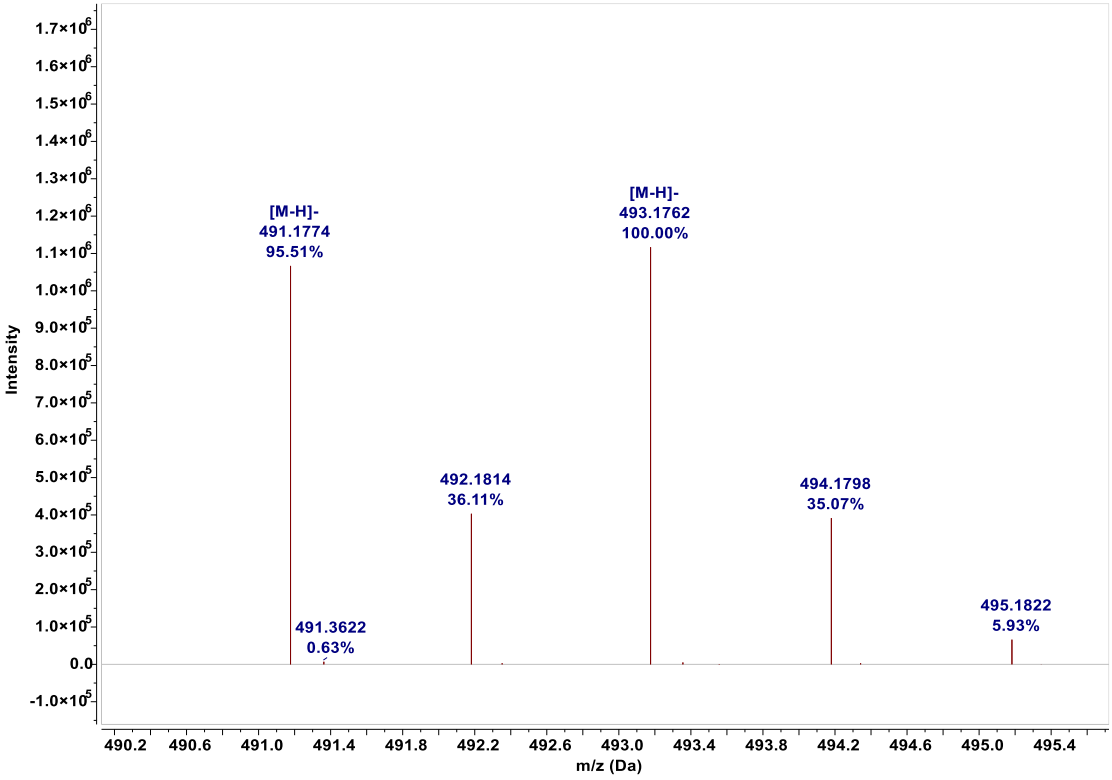

Figure 3.3-3 MS spectrum of 16-Br-OTX F.

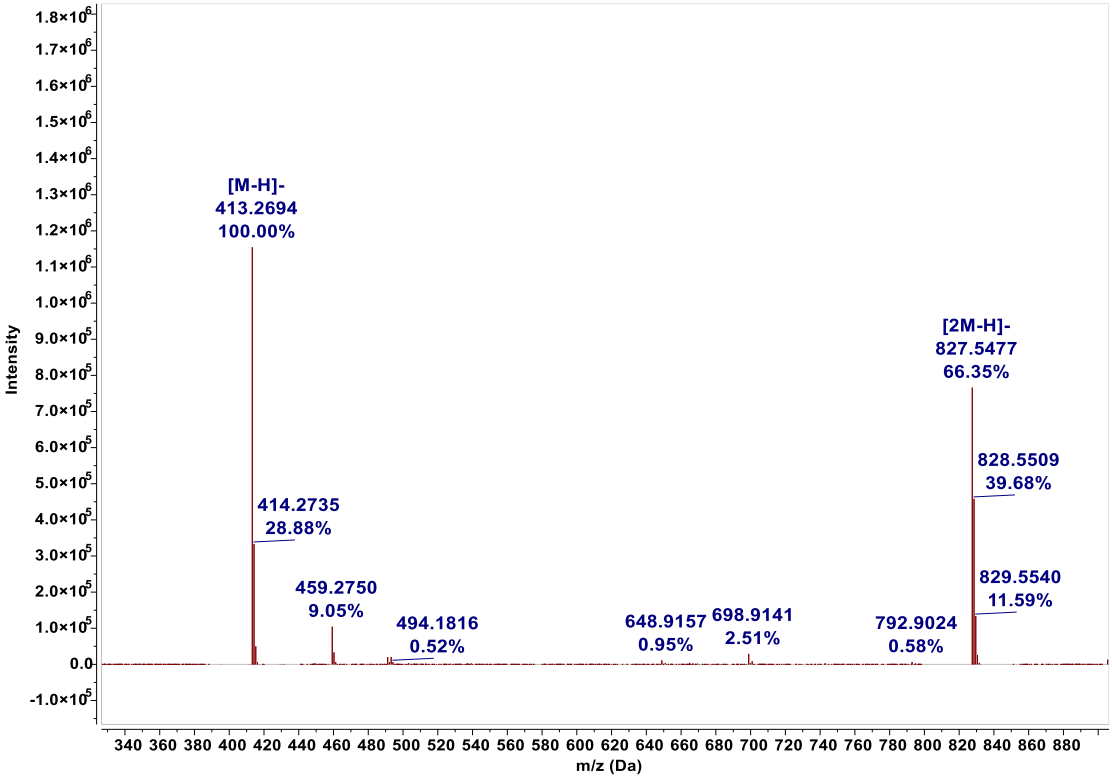

Figure 3.3-4 MS spectrum of OTX F.

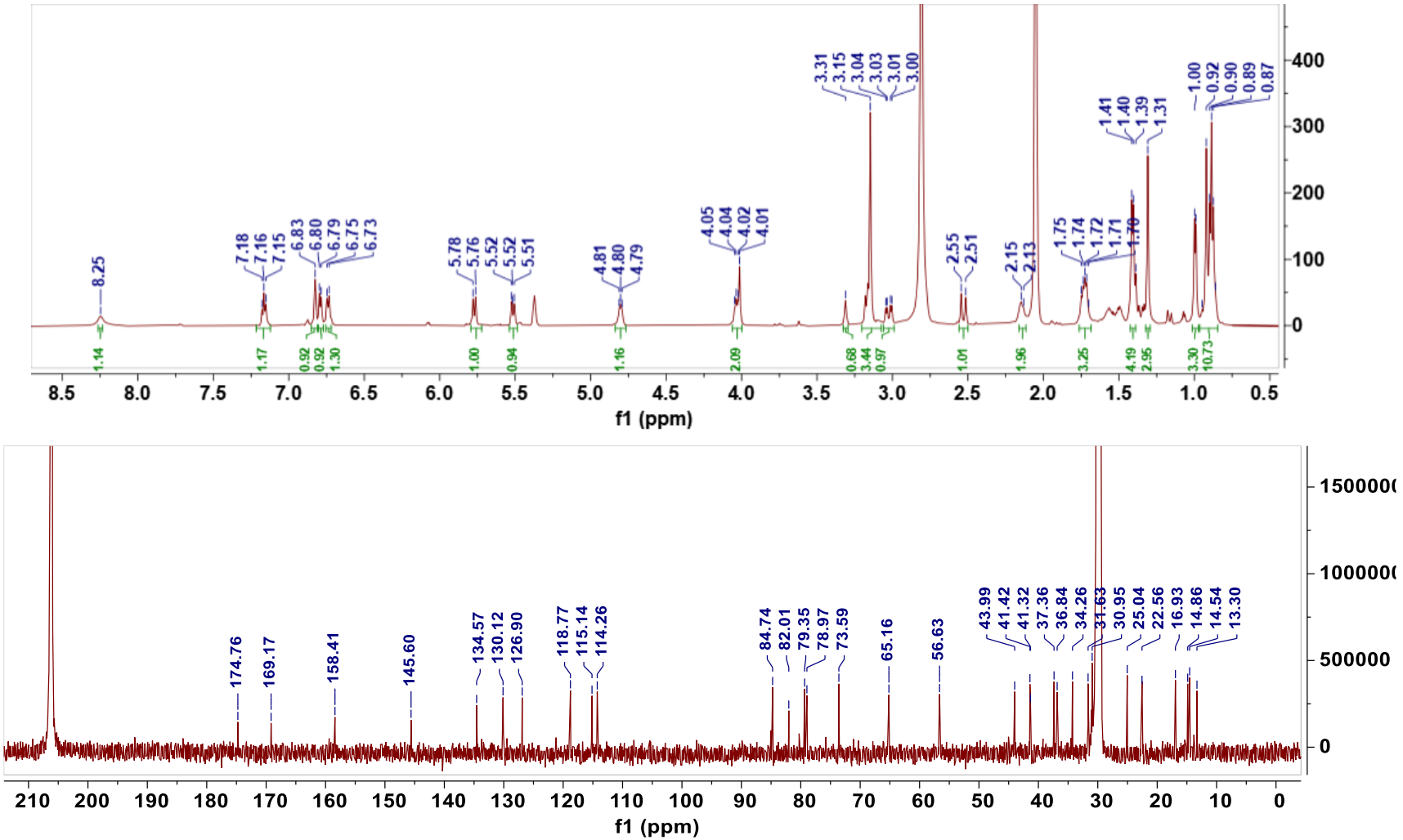

Figure 3.3-5 ^{1}H and ^{13}C NMR spectra of 30-Me-OTX D.

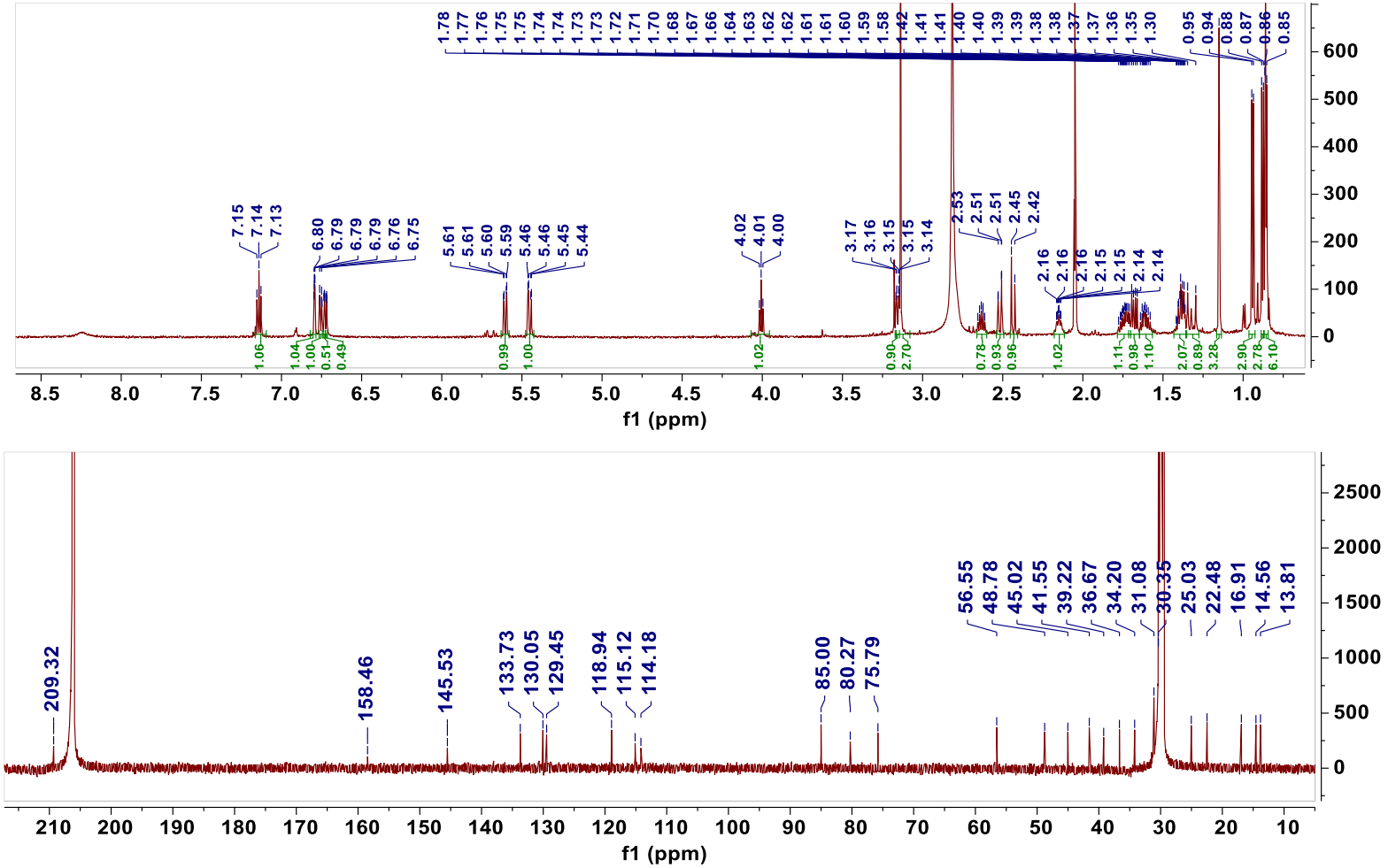

Figure 3.3-6 ^{1}H and ^{13}C NMR spectra of OTX F, a natural degradation product of 30-Me-OTX D.

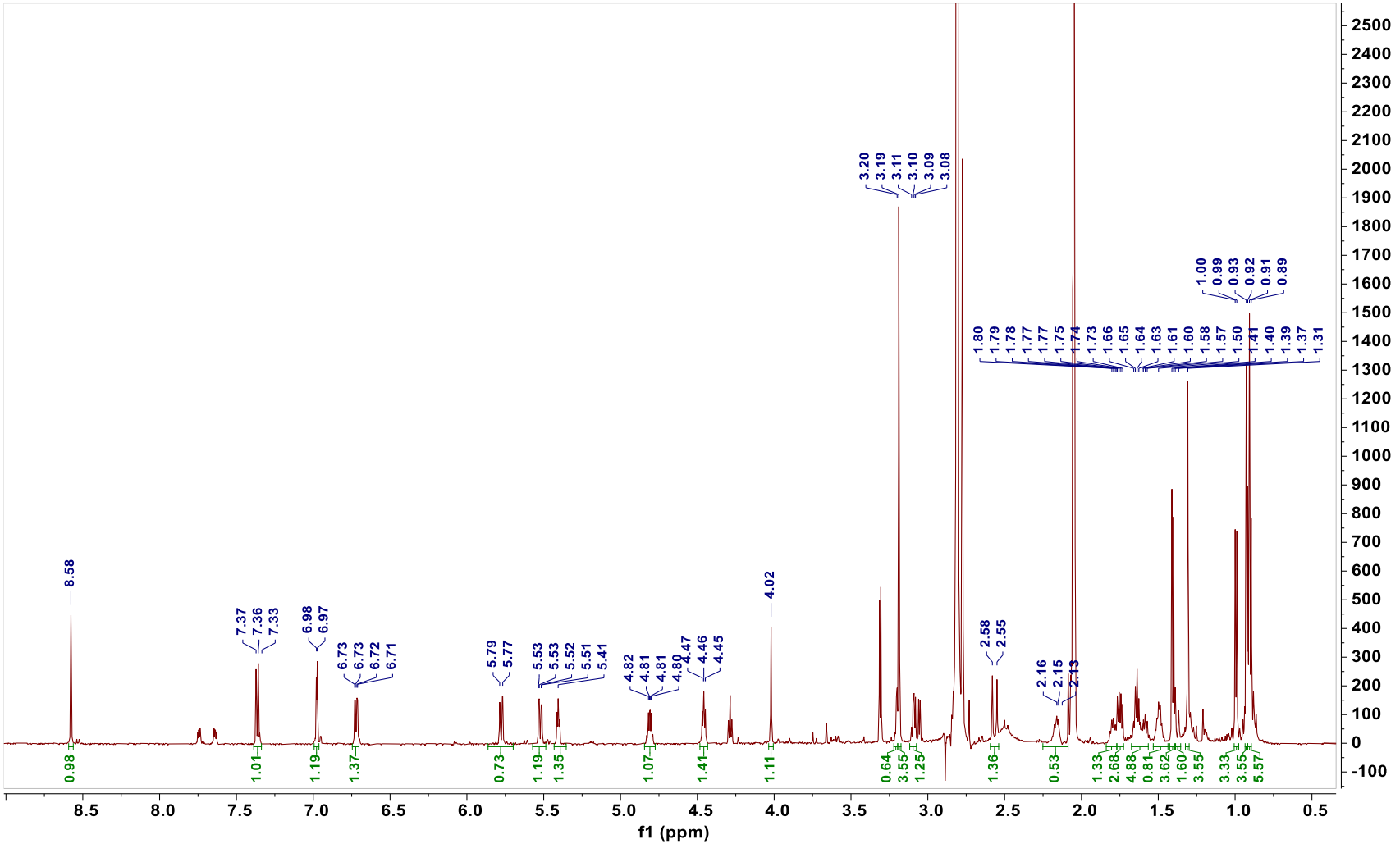

Figure 3.3-7 ^{1}H NMR of 17-Br-30-Me-OTX D, isolated by our group in 2017.

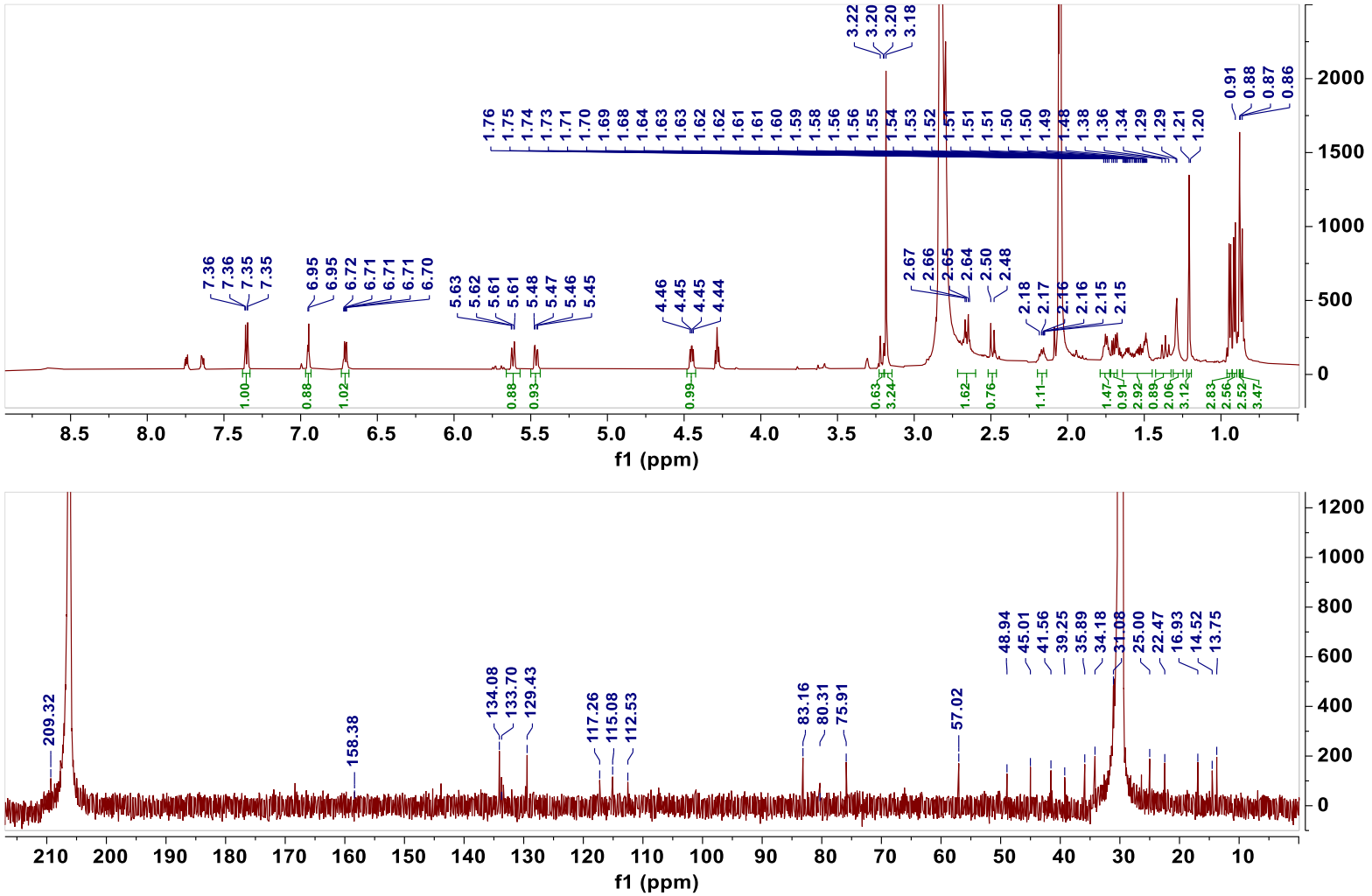

Figure 3.3-8 ^{1}H and ^{13}C NMR spectra of 16-Br-OTX F, a natural degradation product of 17-Br-30-Me-OTX D.

Table 3.3-1 Detailed NMR data for 16-Br-OTX F in Acetone-d_6 and $CDCl_3$

16-Br-OTX F Acetone-d6			16-Br-OTX F $CDCl_3$			OTX F $CDCl_3$ [a]		
^{1}H (600 MHz) and ^{13}C NMR (150 MHz) Acetone-d6 (δ in ppm, J in Hz)			^{1}H (600 MHz) and ^{13}C NMR (150 MHz) $CDCl_3$ (δ in ppm, J in Hz)			^{1}H (600 MHz) and ^{13}C NMR (150 MHz) $CDCl_3$ (δ in ppm, J in Hz)		
No	δ H (J in Hz)	δC, type	No	δ H (J in Hz)	δC, type	No	δ H (J in Hz)	δC, type
1α	2.49, d (12.8)	49.0, CH_2	1α	2.56, d (13.6)	47.3,CH_2	1α	2.50, d (13.5)	47.8,CH_2
1β	2.65, d (12.8)		1β	2.51, d (13.6)		1β	2.38, d (13.5)	
2		209.4,qC	2		213.2,qC	2		212.4,qC
3	2.66 overlap	41.7,CH	3	2.53 overlap	41.4,CH	3	2.56 m	41.4,CH
4α	1.38, dd (13.4, 13.4)	45.1,CH_2	4α	1.31, dd (14.0, 10.6)	44.0,CH_2	4α	1.31, dd (14.2, 11.5)	44.3,CH_2
4β	1.71, dd (13.4, 6.4)		4β	1.77, dd (14.0, 7.0)		4β	1.71, dd (14.0, 6.8)	
5		39.4,qC	5		38.6,qC	5		38.6,qC
6		80.4,qC	6		79.8,qC	6		79.7,qC
7	5.47, dd (10.3, 2.8)	129.5,CH	7	5.42, dd (10.3, 2.8)	128.1,CH	7	5.39, dd (10.3, 2.8)	128.1,CH
8	5.62, dd (10.3, 1.8)	133.8,CH	8	5.60, dd (10.3, 1.8)	133.8,CH	8	5.58, dd (10.3, 1.7)	133.6,CH
9	2.16, m	30.2,CH	9	2.14, m	30.3,CH	9	2.12, m	30.3,CH
10	3.21,overlap	76.0,CH	10	3.09, m	76.0,CH	10	3.05, dd(9.5, 1.8)	75.5,CH
11	1.75,m	34.3,CH	11	1.65,m	33.9,CH	11	1.61,overlap	33.7,CH
12α	1.53,m	31.2,CH_2	12α	1.25,m	29.6,CH_2	12α	1.27,m	30.2,CH_2
12β	1.29,m		12β	1.39,m		12β	1.33,m	
13α	1.70, m	36.0,CH_2	13α	1.66, m	35.1,CH_2	13α	1.78, m	36.1,CH_2
13β	1.63, m		13β	1.66, m		13β	1.61, m	
14	4.45, dd (7.6, 4.9)	83.3,CH	14	4.53, dd (6.0, 6.0)	82.1,CH	14	3.99, t (6.6)	84.4,CH
15		143.9,qC	15		142.6,qC	15		144.3,qC
16		112.5,qC	16		113.6,qC	16	6.79, overlap	119.5,CH
17	7.35, d (8.6)	134.2,CH	17	7.34, d (8.6)	133.5,CH	17	7.17, t (8.0)	129.5,CH
18	6.71, dd (8.6, 3.0)	117.3.,CH	18	6.65, dd (8.6, 3.1)	116.7.,CH	18	6.74, dd (8.6, 2.5)	114.9.,CH
19		158.4,qC	19		155.9,qC	19		156.4,qC
20	6.95, d (3.0)	115.1,CH	20	6.90, d (3.1)	115.0,CH	20	6.79, overlap	113.5,CH
21	0.91, d (6.7)	13.9,CH_3	21	0.84, d (6.9)	13.1,CH_3	21α	0.84, d (6.8)	13.4,CH_3
22	0.87, d (7.3)	17.0,CH_3	22	0.83, d (7.2)	16.8,CH_3	22β	0.80, d (7.2)	16.7,CH_3
23α	0.88, s	25.1,CH3	23α	0.92, s	25.0,CH3	23α	0.87, s	24.9,CH3
24β	1.21, s	22.6,CH3	24β	1.08, s	22.9,CH3	24β	1.07, s	22.6,CH3
25	0.94, d (6.5)	14.6,CH3	25	1.05, d (6.8)	15.6,CH3	25	1.03, d (6.6)	14.9,CH3
26	3.18, s	57.1,CH3	26	3.22, s	57.1,CH3	26	3.20, s	56.7,CH3

[a]Yang-Hua Tang, Bing-Nan Han. et al. (2019). *RSC Advances*, *9* (14), 7594–7600.　上の赤字はどういう意味ですか？

3.3.2 Isolation and structural elucidation of debromooscillatoxin G

Isolation

Subfraction 5 (15.2 mg) was further separated using recycle HPLC [column, Cosmosil 5C_{18}-AR-II (φ 10 × 250 mm); flow rate, 3.0 mL/min; detection at 210 nm; solvent 75% MeOH] to yield debromooscillatoxin G (**5**) (DOTX G) and DATX.

【HPLC condition】

column: Cosmosil 5C_{18}-AR-II (φ 10 × 250 mm)

flow rate: 3.0 mL/min detection wavelength: 210 nm

solvent: 75% MeOH (MeOH/H_2O)

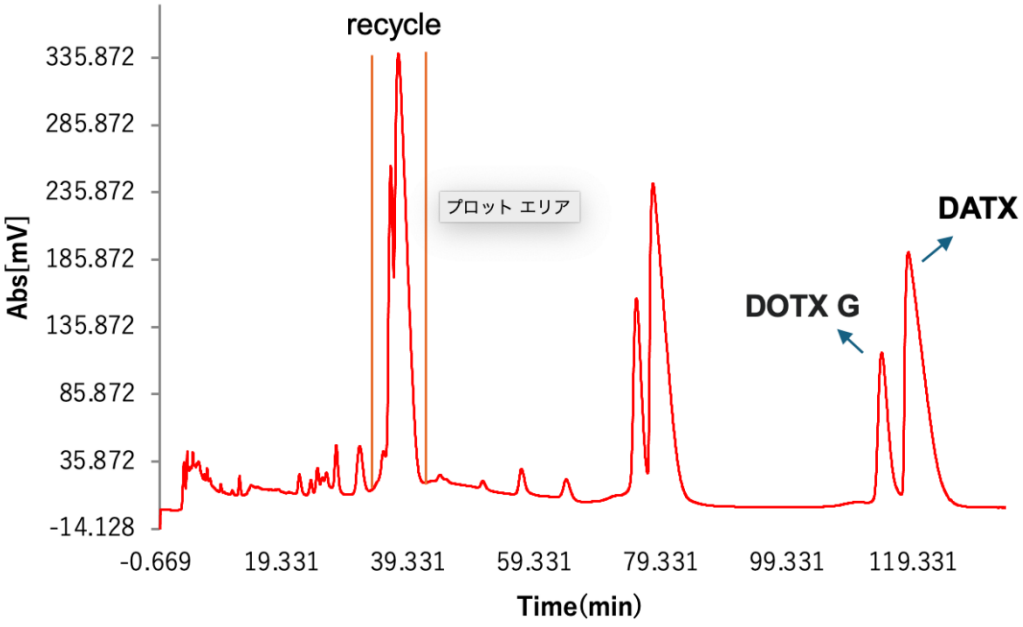

Figure 3.3-9 Recycle HPLC chromatogram of subfraction 4 containing OTX G and DATX.

Structure elucidation

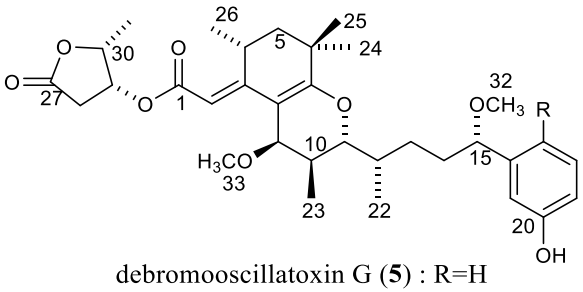

debromooscillatoxin G (**5**) : R=H
oscillatoxin G (**6**) : R=Br

Figure 3.3-10 Structures of DOTX G and OTX G.

Debromooscillatoxin G (**5**) was obtained as a white amorphous solid. Its molecular formula of $C_{33}H_{46}O_8$ with 11 degrees of unsaturation was deduced from a prominent $[M+H]^+$ peak at *m/z* 571.3288 (calcd. for $C_{33}H_{47}O_8$: *m/z* 571.3265). The molecular formula and ^1H NMR spectrum suggested that **5** was a debromo analog of oscillatoxin G (**6**). [30]

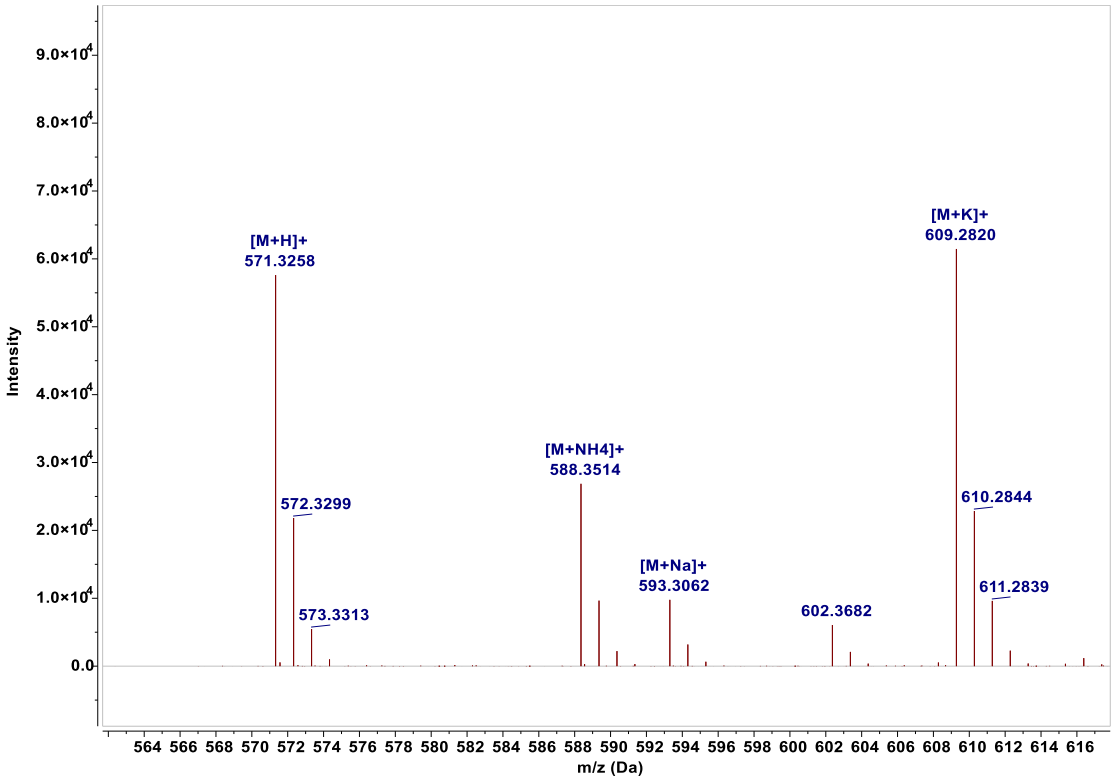

Figure 3.3-11 MS spectrum of DOTX G.

The ^{1}H NMR spectrum uncovered the presence of a 1,3-disubstituted aromatic ring (δ_H 7.15, 6.80, 6.77 and 6.73), four singlet methyls (δ_H 3.43, 3.16, 1.25, and 1.04), and four doublet methyls (δ_H 1.31, 1.18, 1.03, and 0.84). The ^{13}C NMR, and HSQC spectra of **5** revealed the presence of 33 carbons, including two ester carbons (δ_C 175.1 and 166.4), three quaternary olefinic carbons (δ_C 167.6, 165.4, 106.9),aromatic carbons (δ_C 158.5, 145.4, 130.1, 118.7, 115.2, 114.2), one olefinic methine (δ_C 104.8), five oxygenated methine carbons (δ_C 84.8, 79.8, 78.2, 75.5, and 71.1), two methoxy carbons (δ_C 58.4, 56.6), three aliphatic methine carbons (δ_C 35.5, 34.0, and 29.3) five methylene carbons (δ_C 42.9, 37.2, 36.7, 31.1, and 30.3) and six methyl carbons (δ_C 31.2, 28.2, 22.4, 14.5, 13.6, 12.76) (Table 3.3-2).

The COSY correlations from H-9 to H-15 and HMBC correlations of H_3-32/C-15, and H-15 (δ_H 4.07)/C-17 and C-21 confirmed the existence of the phenol side chain that is identical to the corresponding portion in debromooscillatoxins.[44]

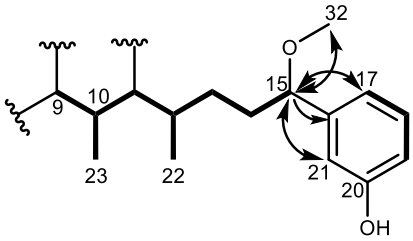

Figure 3.3-12 COSY and HMBC correlations of phenol side chain.

The presence of γ-lactone ring was deduced from the ^{1}H-^{1}H COSY correlations of H_2-28/H-29/ H-30/H_3-31 combined with the HMBC correlations from H_2-28 and H-29 to C-27(δ_C 174.7), where C-27 and C-30 were possibly connected by an ester bond based on the chemical shift of H-30 (δ_H 4.82). The γ-lactone ring was connected to C-1 through an ester linkage between C-1 and C-29, which was strongly supported by HMBC correlation from H29 (δ_H 5.50) to C-1 (δ_C 166.4)

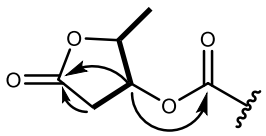

Figure 3.3-13 COSY and HMBC correlations of γ-lactone ring.

The COSY correlations of H_3-26/H-4/H-5 together with HMBC correlations of H-2 (δ_H 5.71)/C-1, H-2/C-3, C-4, and C-26 depicted the partial structure of from C-1 to C-5. The HMBC correlations of H3-24/H2-5, H3-25/H2-5 and H2-5/C6 (δC 35.3) indicated C-5 is connected to a quaternary carbon C-6 substituted with a pair of gem-dimethyl groups (C-24 and C-25). Meanwhile, HMBC correlations from H3-24, H3-25, and H2-5 to C-7 (δC 167.2) suggested a bond between C-6 and quaternary olefinic carbon C-7. Therefore, the two partial structures have been established as Figure.3.3-14.

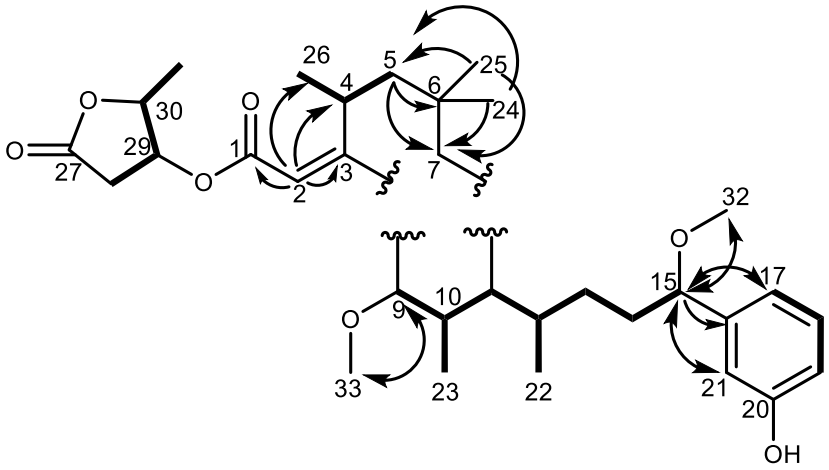

Figure 3.3-14 Two partial structures deduced from COSY and HMBC correlations.

According to these partial structures and the molecular formula $C_{33}H_{47}O_8$, there are two oxygen atoms left in **5** that are unattributed. One of these oxygen atoms was surely assign to a methoxy group based on the singlet proton signal at δ_H 3.43. The HMBC correlation from this methoxy to H-9 (δ_H 3.87) confirmed the position of methoxy group on C-9. Therefore, an oxabicyclic alkene feature has to be existed in **5** to complete the 11 degrees of unsaturation.

The HMBC correlations from H-9 to C-8 (δC 106.9), C-7 (δC 167.6), and C-3 (δC 165.4) suggested that C-3 and C-7 was connected through C-8 with the C9-C15 fragment, completing the closure of ring A. Moreover**,** the chemical shift of H-11(δ_H 4.03) and C-7 (δ_C 167.2) and the HMBC correlation from H-11 to C-7 confirmed that C-7, a quaternary olefinic carbon was connected with and C-11 by an ether bond. Overall, the planar structure of **5** with key COSY and HMBC correlations was established as Figure.3.3-15.

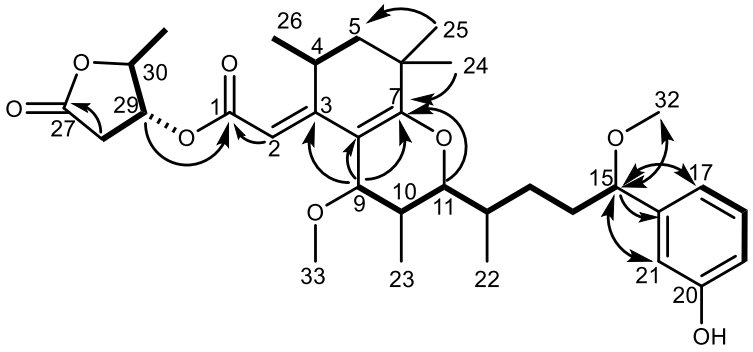

Figure 3.3-15 planar structure of DOTX G with key COSY and HMBC correlations.

Table 3.3-2 NMR data for DOTX G in Acetone-d6

debromooscillatoxin G		
^{1}H (600 MHz) and ^{13}C NMR (150 MHz) Acetone-d6 (δ in ppm, J in Hz)		
No	δ H (J in Hz)	δ C, type
1		166.38, qC
2	5.71, s	104.78, CH
3		165.42, qC
4	3.99, m	29.31, CH
5a	1.61, dd (13.9, 2.7)	42.95, CH_2
5b	1.74, d (5.8)	
6		35.25, qC
7		167.62, qC
8		106.89, qC
9	3.86, d (2.6)	75.47, CH
10	1.80, m	35.51, CH
11	4.03, dd (11.6, 2.0)	78.18, CH
12		34.02, CH
13a	1.52, ddd (13.0, 9.2, 6.1)	31.1, CH_2
13b	1.58, m	
14a	1.68, ddd (18.6, 11.4, 5.5)	
14b	1.80, m	36.74, CH_2
15	4.07, dd (7.3, 5.7)	84.84, CH
16		145.41, qC
17	6.77, d (7.5)	118.65, CH
18	7.15, t (7.7)	130.11 ,CH
19	6.73, dd (8.1, 2.4)	115.18, CH
20		158.48, qC
21	6.80, t (2.0)	111.45, CH
22	0.84, d (6.8)	12.86, CH_3
23	1.03, d (6.7)	13.63, CH_3
24	1.25, s	28.23, CH_3
25	1.04, s	31.16, CH_3
26	1.18 d, (7.2)	22.38, CH_3
27		175.14, qC
28a	2.49, brd (18.0)	37.24, CH_2
28b	3.07, dd (18.0, 6.1)	
29	5.50, dd (5.3, 4.8)	71.13, CH
30	4.82, qd (6.5, 4.0)	79.75, CH
31	1.31 d, (6.5)	14.5, CH_3
32	3.16, s	56.62, CH_3
33	3.43, s	58.44, CH_3
20-OH	8.28	

The NOESY experiments and vicinal coupling constants were utilized to establish the relative configuration of 5. The small coupling constants of H-5b (5.8 Hz) and H-5a (13.9, 2.7 Hz) indicated that H-4 was oriented equatorially. The *E* configuration of the double bond between C2 and C3 was deduced from the NOESY correlation of H-2/H-9. The large coupling constant $^{3}J_{H10\text{-}H11}$ (11.6 Hz) suggested that both H-10 and H-11 were axial protons, and the small coupling constant $^{3}J_{H9\text{-}H10}$ (2.6 Hz) of indicated that H-9 was oriented equatorially. The configurations of stereocenter C-29 and C-30 in the γ-lactone moiety were determined to be *R* by comparing the proton chemical shifts and coupling constants from H-28 to H-31 of debromooscillatoxin G with those of 30-methyloscillatoxin D. The proton coupling constants of H-28b/H-29 (6.1 Hz), and H-29/H-30 (4.0 Hz) in debromooscillatoxin G was agreed with those in 30-methyloscillatoxin D. Thus, the structure of debromooscillatoxin G was established as Figure 3.3-10.[29]

Debromooscillatoxin G

^{1}H NMR (600 MHz, acetone) δ 7.15 (t, *J* = 7.7 Hz, 1H, 18), 6.80 (t, *J* = 2.0 Hz, 1H, 21), 6.77 (d, *J* = 7.5 Hz, 1H, 17), 6.73 (dd, *J* = 8.1, 2.4 Hz, 1H, 19), 5.71 (s, 1H, 2), 5.50 (dd, *J* = 5.3, 4.8 Hz, 1H, 29), 4.82 (qd, *J* = 6.5, 4.0 Hz, 1H, 30), 4.07 (dd, *J* = 7.3, 5.7 Hz, 1H, 15), 4.03 (dd, *J* = 11.6, 2.0 Hz, 1H, 11), 4.01 – 3.98 (m, 0H, 4), 3.86 (d, *J* = 2.6 Hz, 1H, 9), 3.43 (s, 3H, 33), 3.16 (s, 3H, 32), 3.07 (dd, *J* = 18.0, 6.1 Hz, 1H, 28), 2.53 – 2.45 (m, 1H, 28), 1.87 – 1.75 (m, 3H), 1.74 (d, *J* = 5.8 Hz, 1H), 1.68 (ddd, *J* = 18.6, 11.4, 5.5 Hz, 1H), 1.61 (dd, *J* = 13.9, 2.7 Hz, 1H, 5), 1.52 (ddd, *J* = 13.0, 9.2, 6.1 Hz, 1H), 1.31 (d, *J* = 6.5 Hz, 3H, 31), 1.25 (s, 3H), 1.18 (d, *J* = 7.2 Hz, 3H, 26), 1.03 (d, *J* = 6.7 Hz, 6H), 0.84 (d, *J* = 6.8 Hz, 3H, 22).

^{13}C NMR (150 MHz, acetone) δ 175.14 (27), 167.62 (7), 166.38 (1), 165.42 (3), 158.47 (20), 145.41 (16), 130.11 (18), 118.65 (17), 115.18 (19), 114.15 (21), 106.90 (8), 104.78 (2), 84.84 (15), 79.75 (30), 78.18 (11), 75.47 (9), 71.13 (29), 58.44, 56.62 (32), 42.94 (5), 37.23 (28), 36.74 (14), 35.51 (10), 35.25 (6), 34.03 (12), 31.16 (25), 31.10 (13), 29.31 (4), 28.23 (24), 22.38 (26), 14.50 (31), 13.63 (23), 12.76 (22).

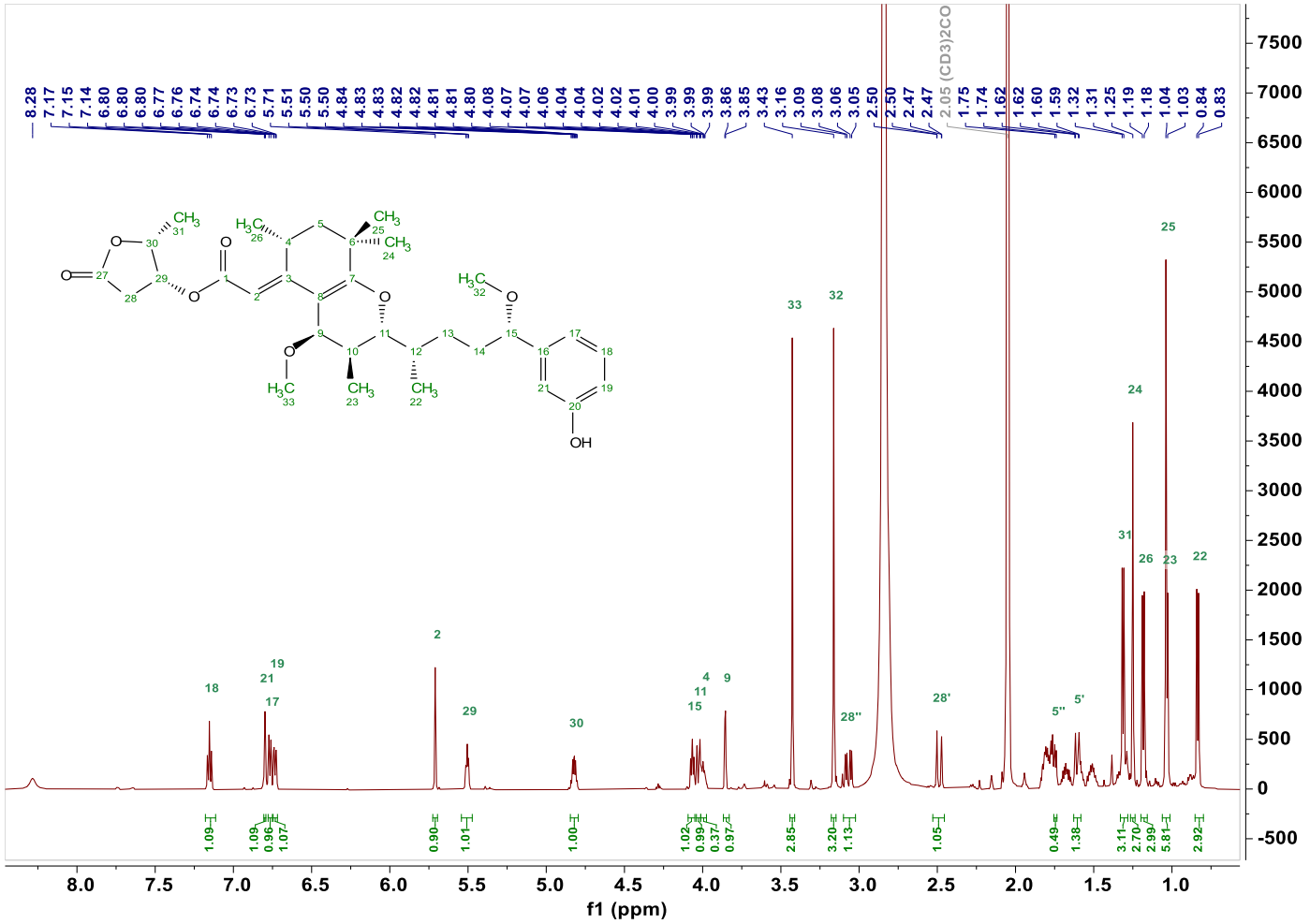

Figure 3.3-16 ^{1}H NMR spectrum of DOTX G with signals assignment.

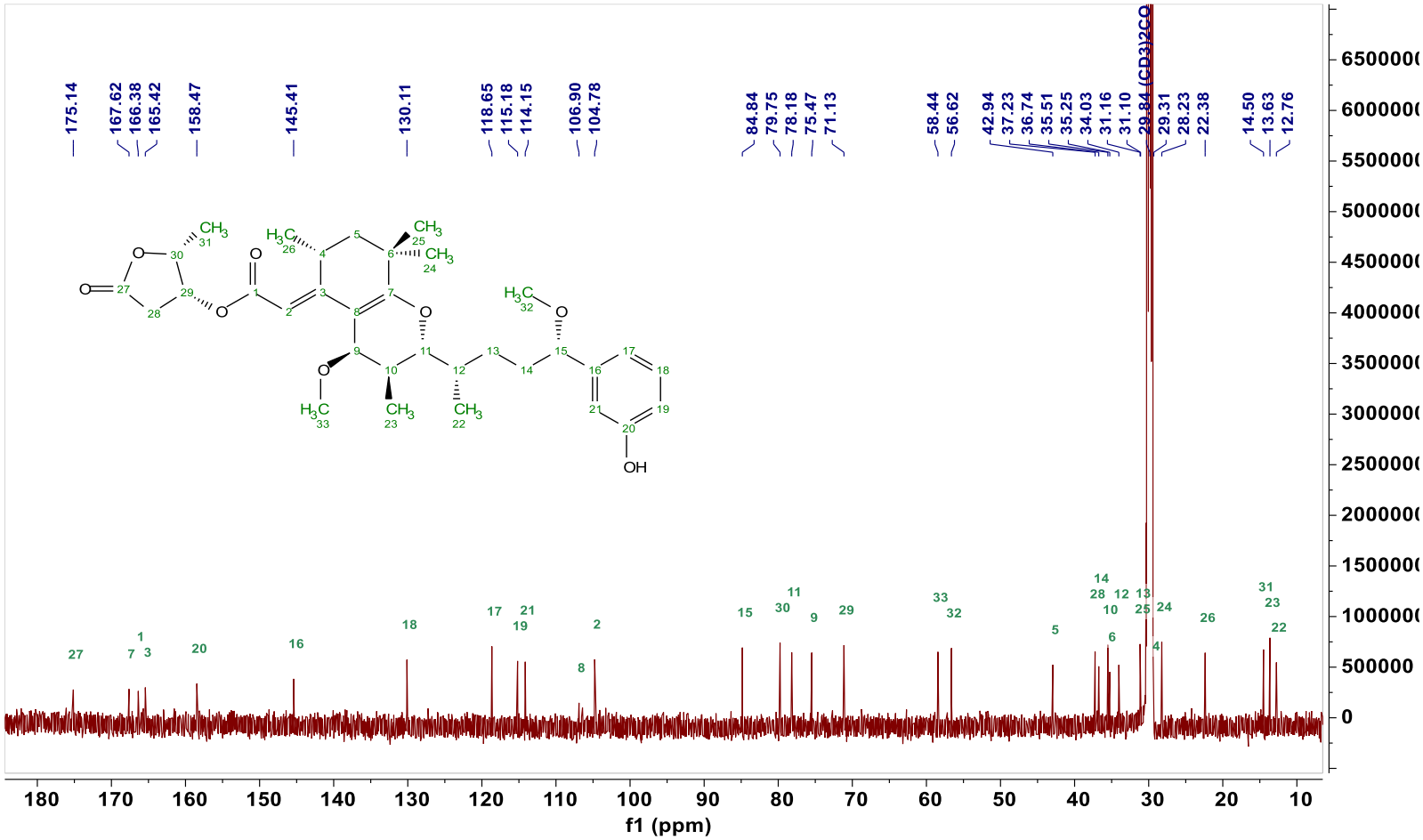

Figure 3.3-17 ^{13}C NMR spectrum of DOTX G with signals assignment.

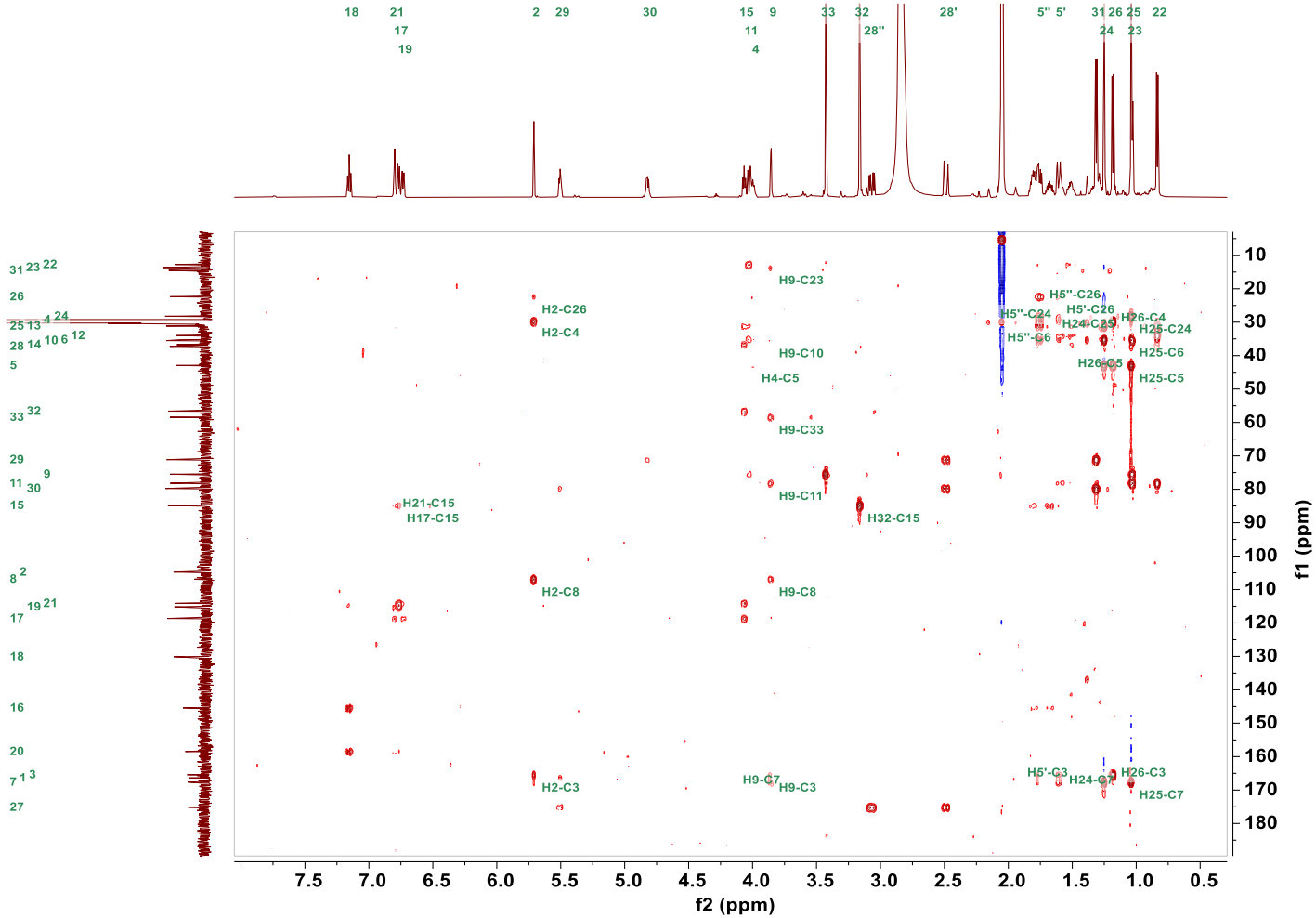

Figure 3.3-18 HMBC spectrum of DOTX G with signals assignment.

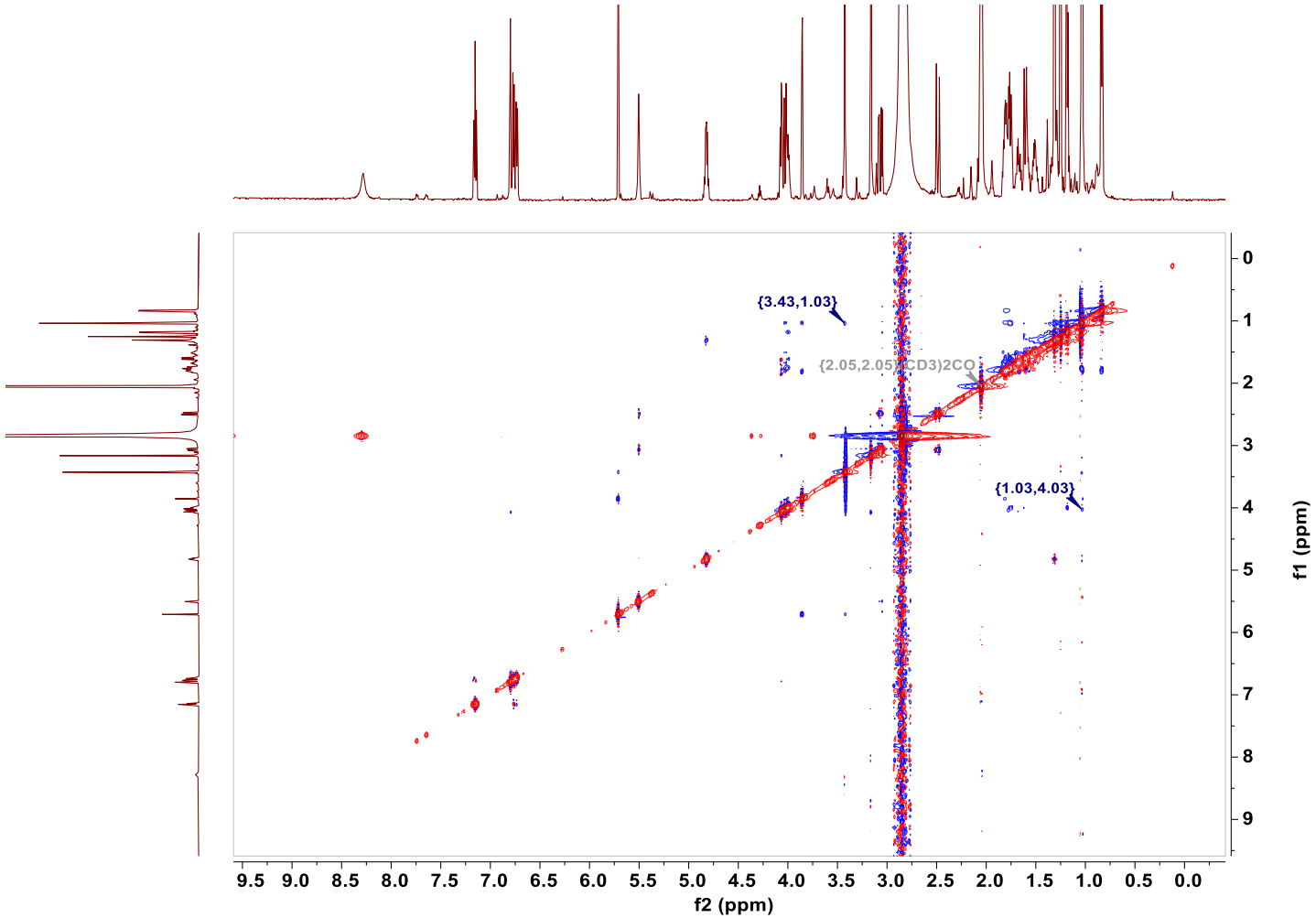

Figure 3.3-19 NOESY spectrum of DOTX G.

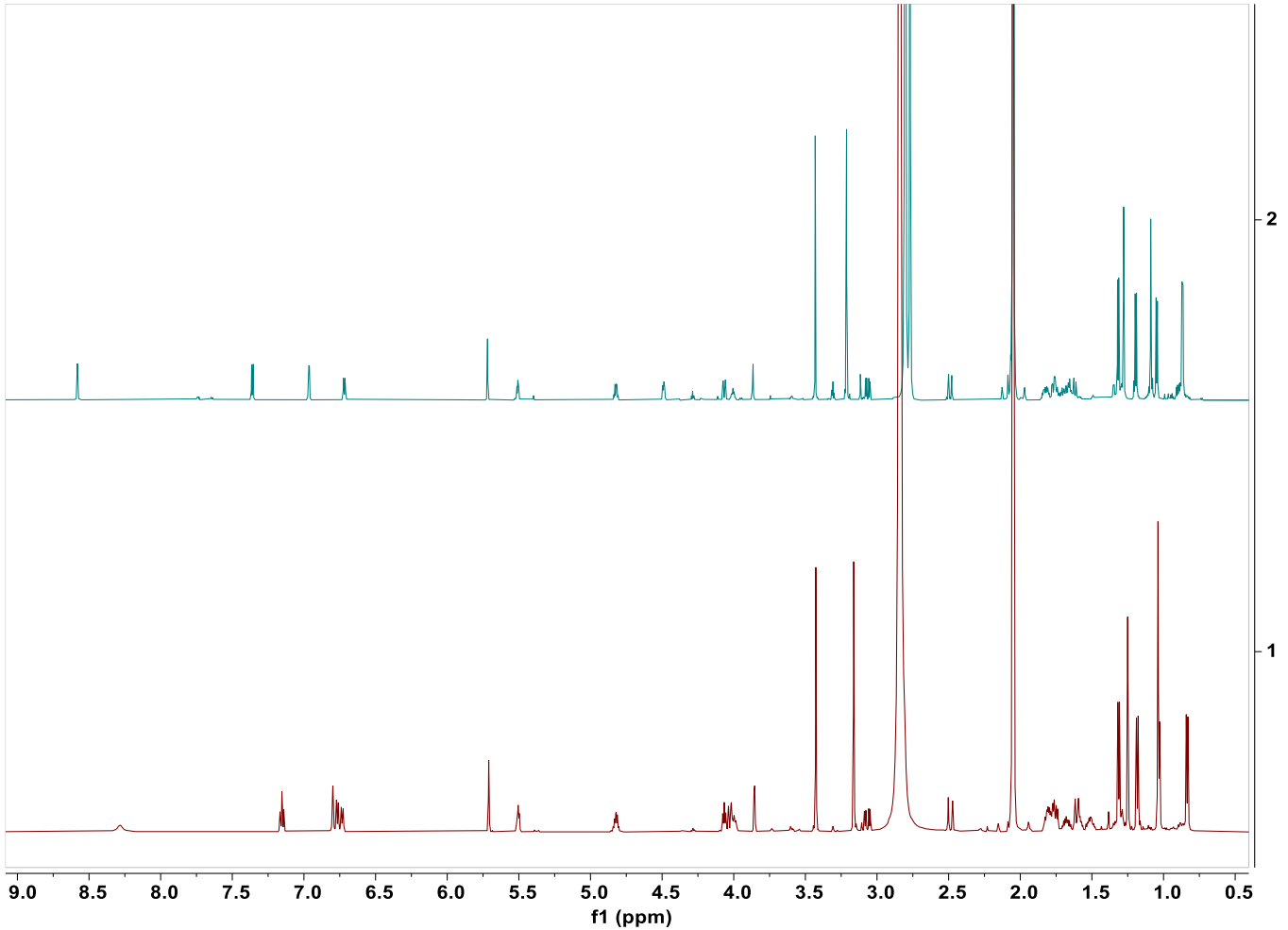

Figure 3.3-20 Comparison of ^{1}H NMR spectra of DOTX G and OTX G.

3.4 Putative biosynthetic pathways of ATXs

Overall, 24 ATX-related compounds were isolated from the Okinawan cyanobacterium *O. hirsuta* by our laboratory, of which 14 were novel. These isolated ATXs can be categorized into three groups based on the structures of rings A and B: acetal spiro ether ring, spiro ether ring, and fused ether ring (Figure 3.4-1). Furthermore, a common polyketide intermediate in ATXs biosynthesis was deduced. From this intermediate, three potential biosynthetic pathways were proposed according to the formation of the ring system (Figure 3.4-2).

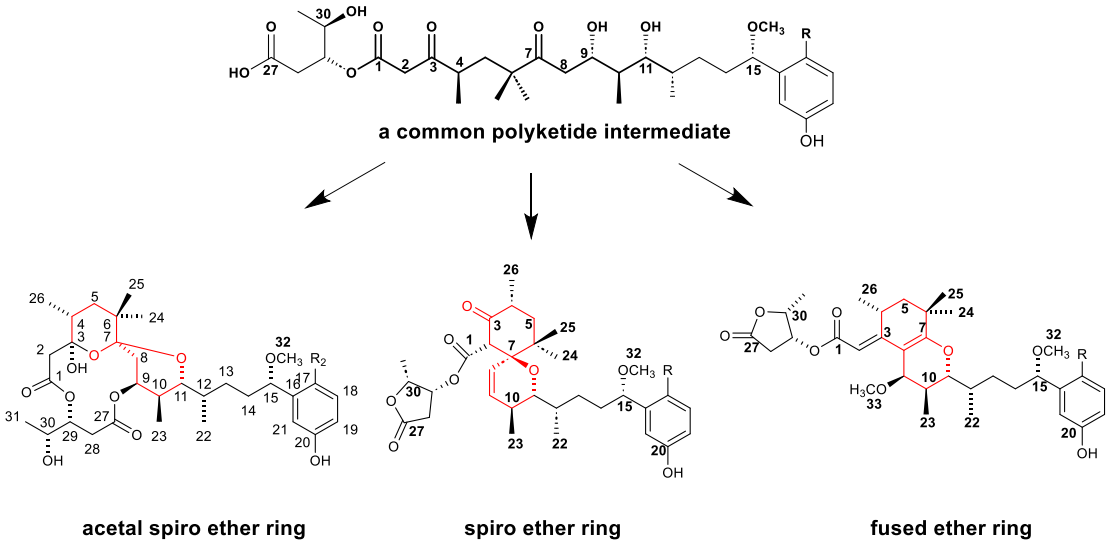

Figure 3.4-1 A common polyketide intermediate of ATXs.

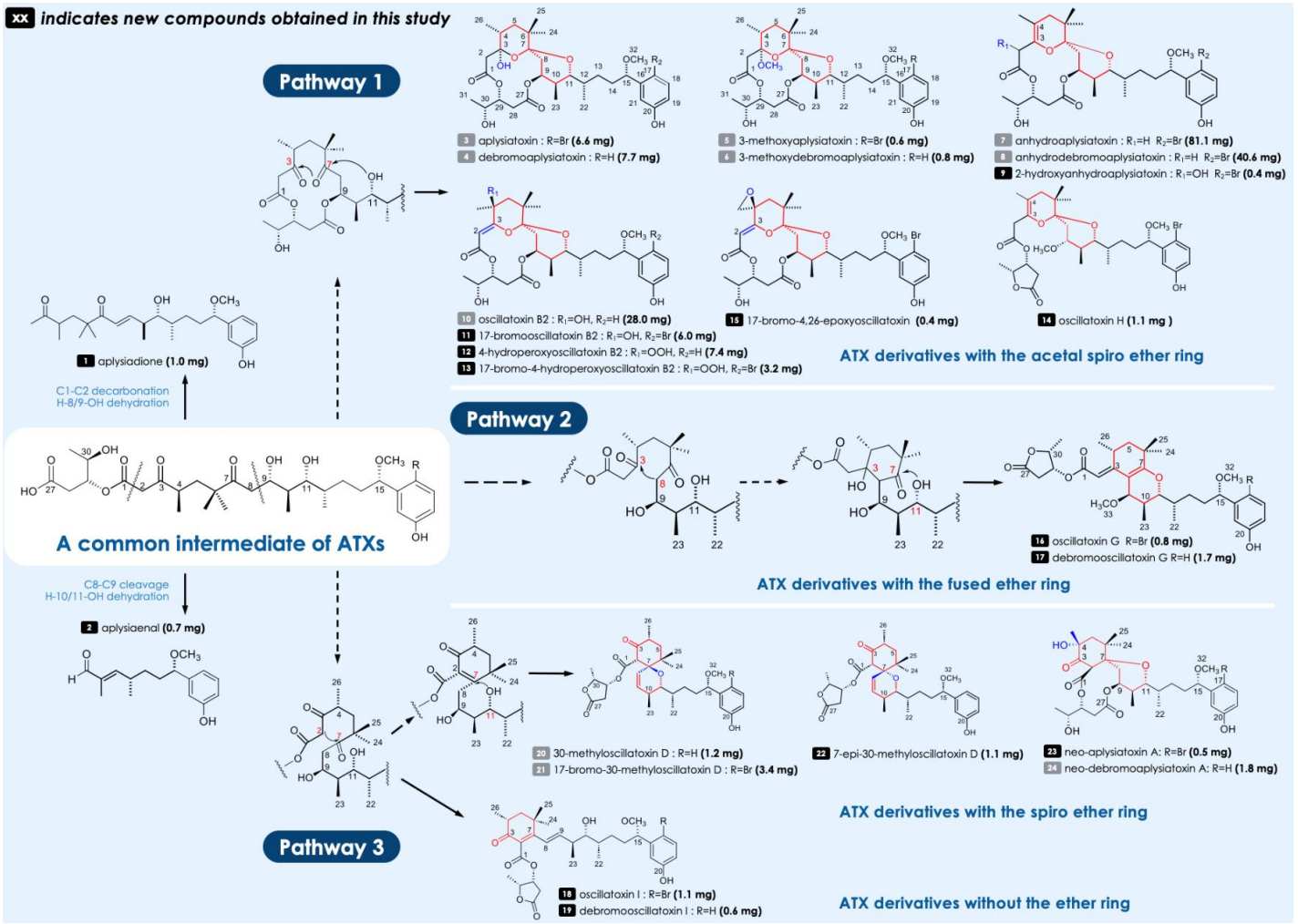

Figure 3.4-2 ATXs from the cyanobacterium *O.hirsuta* and proposed three biosynthetic pathways.

3.5 Biological activities of ATXs

Aplysiatoxins (ATXs), a class of dermatotoxins, exhibit potent pro-inflammatory effects. Consequently, exposure to these toxins can induce inflammation, resulting severe redness, swelling, and bleeding of the skin. They are identified as causative agents for severe skin irritation, known as Swimmer's itch and some food poisoning. [11,45]

Moreover, in 1977, DATX was discovered to possess anti-leukemic properties in mice with P-388 lymphocytic leukemia, sparking a significant increase in research on the effects of ATXs on tumors.[46] ATXs were then found to promote tumor growth by directly binding to and activating protein kinase C (PKC).[47] However, the regulation of PKC activity has recently been recognized as an important therapeutic approach for various cancers. Therefore, structure-activity studies on ATX derivatives have been carried out, leading to the development of a simplified synthetic analog of DATX, named aplog-1.[48] This compound shows antineoplastic activity with minimal tumor-promoting and pro-inflammatory properties. In addition, Kv1.5 ion channel inhibitory activities and Anti-Chikungunya viral activities have been uncovered recently.[49]

In the present study, the cytotoxicity against mouse L1210 leukemia cells and the growth-inhibitory activity toward the marine diatom *Nitzschia amabilis* were evaluated for the isolated ATXs.[50-51]

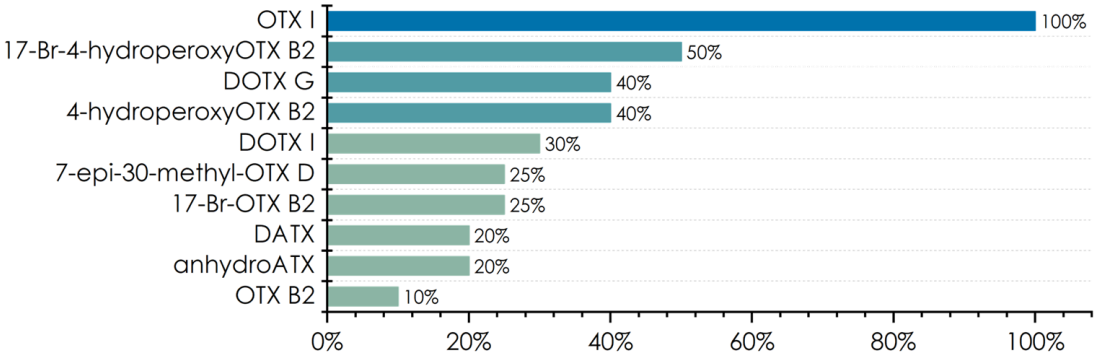

Figure 3.5-1 Cytotoxicity of isolated ATXs against mouse L1210 leukemia cells at 10 µg/mL.

*ATX-related compounds not shown in this figure were not cytotoxic at this concentration.

Among the isolated ATX analogs, OTX I (IC_{50} =4.6 µg/mL) showed the strongest cytotoxicity against L1210. This result is consistent with the findings that simplified analogs of DATX are more anti-proliferative against several cancer cell lines (HBC4, MDA-MB-231, SNB-78, HCC2998, NCI–H460, A549, LOX-IMVI, and St-4) *in vitro* through PKC activation. However, in terms of the IC_{50} value, even OTX I only showed moderate cytotoxicity against L1210. Overall, ATXs exhibited weak cytotoxicity, indicating the lack of correlation between cytotoxicity and the ability to bind to and activate PKC as reported by K. Irie and coworkers. Consequently, the use of cytotoxicity alone is not comprehensive enough for toxicity evaluation of ATXs.

Although, the diatom growth inhibition tests displayed slightly higher sensitivity to ATXs, the obtained results were almost similar to those of the cytotoxicity test.[30]

Chapter 4. *N*-Desmethylmajusculamide B, a Lipopeptide from the Okinawan Cyanobacterium *Okeania hirsuta*

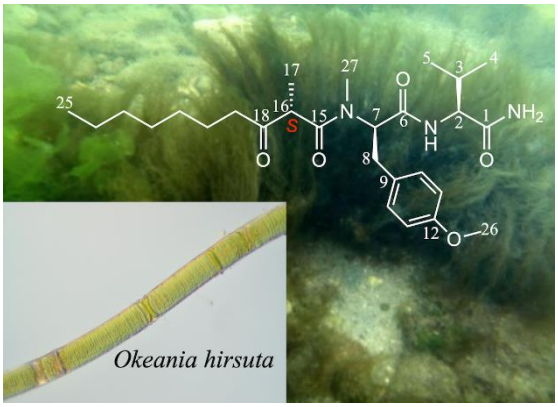

A new lipopeptide, *N*-desmethylmajusculamide B (**7**), was isolated from the Okinawan cyanobacterium *Okeania hirsuta* along with two known compounds majusculamide A (**8**) and majusculamide B (**9**).[52] The planar structure of **7** was elucidated by a detailed analysis of MS and NMR spectra. The absolute configurations of the amino acid residues were determined using Marfey's analysis. The configuration of C-16 in the α-methyl-β-keto-decanoyl moiety was determined unambiguously to be *S* by conducting a semi-synthesis of *N*-desmethylmajusculamide B from **9**. The cytotoxicity against mouse L1210 leukemia cells was evaluated for majusculamides (**7**-**9**).

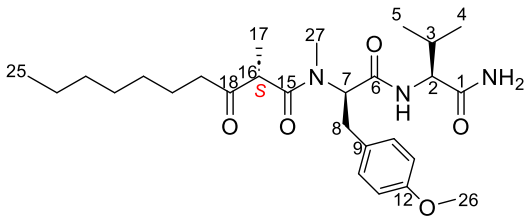

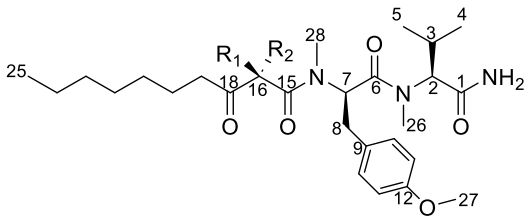

Figure 4-1 Structures of majusculamides isolated from *Okeania hirsuta*.

4.1 Isolation

Subfraction 7 (183 mg) was separated by HPLC [column, Cosmosil 5C_{18}-AR-II (φ 10 × 250 mm); flow rate, 2.0 mL/min; detection at 210 nm; solvent 75% MeOH] to obtain *N*-desmethylmajusculamide B (**7**, 1.3 mg), majusculamide A (**8**, 3.8 mg), and majusculamide B (**9**, 52.1 mg).

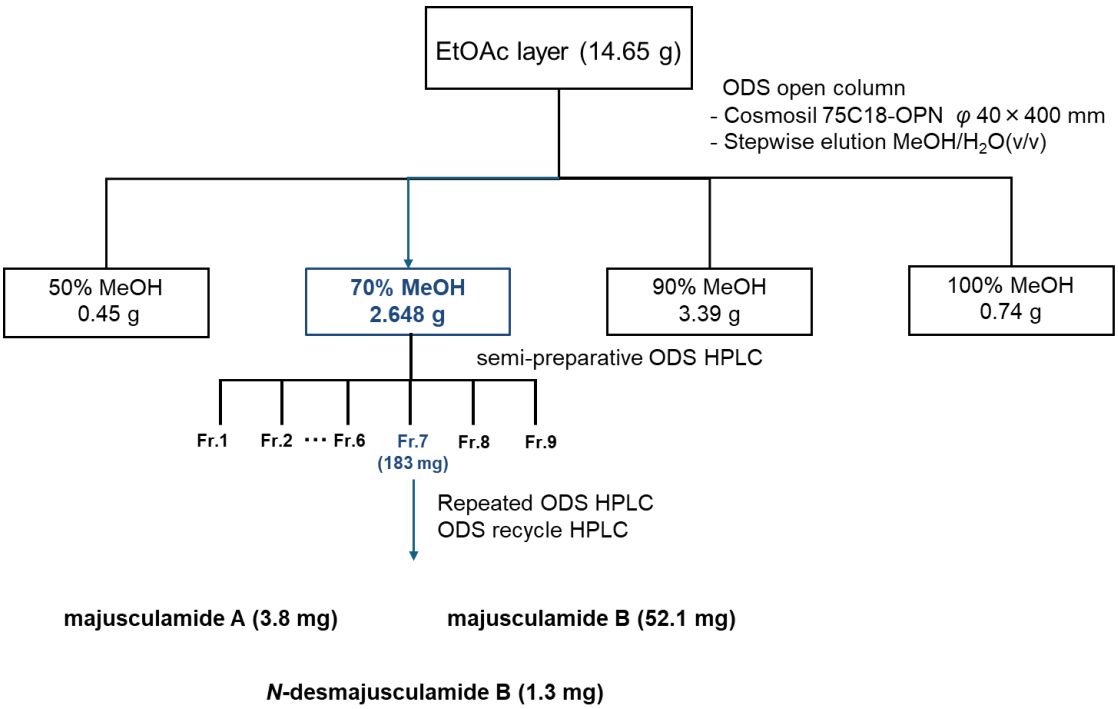

Scheme 4-1. Isolation of majusculamides from 70% MeOH fraction of EtOAc layer.

4.2 structure elucidation

Majusculamide A and majusculamide B

Majusculamides A and B, as the major lipophilic constituents of cyanobacteria *Lyngbya majusculamide* Gomont collected at Kahala Beach, Oahu, Hawaii, were first isolated and structurally characterized by Moore et al in 1977.[53] Since then, these two epimeric lipodipeptides have been discovered in several other cyanobacteria species as well.

In this study, majusculamide A (**8**) and majusculamide B (**9**) were obtained as white amorphous solid. Both compounds have the molecular formula $C_{28}H_{45}N_3O_5$, as confirmed by HRESIMS. The structural elucidation of **8** and **9** was carried out by comparing the NMR data and specific rotations with their synthetic counterparts.[54] The NMR spectra of **8** and **9** measured in $CDCl_3$ exhibited two interconverting conformers with an NMR signal ratio of 5:2, which can be attributed to the presence of tertiary amide moieties. A comprehensive analysis of the two-dimensional NMR spectra, particularly the HMBC and HSQC-TOCSY spectra, accomplished the complete assignment of **8** and **9** including their conformers. To the best of our knowledge, this was the first time completely assign the NMR spectra of majusculamides A and B with their rotamers. According to the assignment, it is possible to distinguish majusculamides A and B quickly via proton chemical shifts of H_3-17 and H_2-19.

Table 4.2-1 Detailed NMR spectral data for majusculamide A (**8**) in $CDCl_3$

No.	δ_H[a] (J in Hz)	δ_H[b](J in Hz)	δ_C[a]	δ_C[b]	type
1			171.94	172.65	qC
2	4.53, d (10.8)	3.71, d (10.8)	62.66	63.91	CH
3	2.21, m	2.28, m	25.64	27.82	CH
4	0.59[c], d (6.6)	0.84[c], d (6.6)	18.54[d]	18.80[d]	CH_3
5	0.97[c], d (6.6)	0.97[c], d (6.6)	20.08[d]	18.93[d]	CH_3
6			171.71	172.19	qC
7	5.71, dd (7.8, 7.8)	5.64, dd (9.5, 6.2)	54.50	55.89	CH
8a	2.89, dd (14.1, 7.6)	3.02, m	34.82	35.09	CH_2
8b	3.16, dd (14.1, 7.6)				CH_2
9			128.36	128.55	qC
10	7.13, d (8.6)	7.07, d (8.6)	130.32	130.52	CH
11	6.80, d (8.6)		114.12	113.97	CH
12			158.72		qC
13	6.80, d (8.6)		114.12	113.97	CH
14	7.13, d (8.6)	7.07, d (8.6)	130.32	130.52	CH
15			171.34	169.45	qC
16	3.58, q (7.0)	3.44, q (7.0)	51.45	50.84	CH
17	1.22, d (7.1)	0.94, d (7.1)	13.57	13.61	CH_3
18			207.07	206.86	qC
19a	2.35, m		40.24	40.71	CH_2
19b	2.40, m				CH_2
20	1.51, m		23.65	23.53	CH_2
21	1.23, m		29.22	28.91	CH_2
22	1.23, m		29.25	29.26	CH_2
23	1.23, m		31.79		CH_2
24	1.27, m		22.74		CH_2
25	0.87, dd (7.1, 7.1)		14.21	14.19	CH_3
26 -NCH_3	2.90, s	3.07, s	30.85	29.80	CH_3
27 -OCH_3	3.76, s		55.43		CH_3
28 -NCH_3	3.00, s	2.93, s	31.33	31.03	CH_3
NH_2	6.17, brs				
	5.19, brs				

[a] Major conformer. [b] Minor conformer. [cd] Interchangeable

Table 4.2-2 Detailed NMR spectral data for majusculamide A (**8**) in $CDCl_3$

No.	$\delta_H{}^a$ (J in Hz)	$\delta_H{}^b$(J in Hz)	$\delta_C{}^a$	$\delta_C{}^b$	type
1			171.94	172.65	qC
2	4.53, d (10.8)	3.71, d (10.8)	62.66	63.91	CH
3	2.21, m	2.28, m	25.64	27.82	CH
4	0.59[c], d (6.6)	0.84[c], d (6.6)	18.54[d]	18.80[d]	CH_3
5	0.97[c], d (6.6)	0.97[c], d (6.6)	20.08[d]	18.93[d]	CH_3
6			171.71	172.19	qC
7	5.71, dd (7.8, 7.8)	5.64, dd (9.5, 6.2)	54.50	55.89	CH
8a	2.89, dd (14.1, 7.6)	3.02, m	34.82	35.09	CH_2
8b	3.16, dd (14.1, 7.6)				CH_2
9			128.36	128.55	qC
10	7.13, d (8.6)	7.07, d (8.6)	130.32	130.52	CH
11	6.80, d (8.6)		114.12	113.97	CH
12			158.72		qC
13	6.80, d (8.6)		114.12	113.97	CH
14	7.13, d (8.6)	7.07, d (8.6)	130.32	130.52	CH
15			171.34	169.45	qC
16	3.58, q (7.0)	3.44, q (7.0)	51.45	50.84	CH
17	1.22, d (7.1)	0.94, d (7.1)	13.57	13.61	CH_3
18			207.07	206.86	qC
19a	2.35, m		40.24	40.71	CH_2
19b	2.40, m				CH_2
20	1.51, m		23.65	23.53	CH_2
21	1.23, m		29.22	28.91	CH_2
22	1.23, m		29.25	29.26	CH_2
23	1.23, m		31.79		CH_2
24	1.27, m		22.74		CH_2
25	0.87, dd (7.1, 7.1)		14.21	14.19	CH_3
26 -NCH_3	2.90, s	3.07, s	30.85	29.80	CH_3
27 -OCH_3	3.76, s		55.43		CH_3
28 -NCH_3	3.00, s	2.93, s	31.33	31.03	CH_3
NH_2	6.17, brs				
	5.19, brs				

[a] Major conformer. [b] Minor conformer. [cd] Interchangeable

N-desmethylajusculamide B

N-Desmethylmajusculamide B (**7**) was obtained as a white amorphous solid ($[\alpha]_D^{23}$ = +19.8 (c 0.61, EtOH)). Its molecular formula was determined to be $C_{27}H_{43}N_3O_5$ based on a prominent $[M+H]^+$ ion peak at *m/z* 490.3254 (calcd. for $C_{27}H_{44}N_3O_5$: 490.3281), which is 14 mass units (CH_2) less than that of the major ions in **8** and **9**. Moreover, the ^{1}H NMR spectra of **7** and **9** were similar, and both included signals for a terminal NH_2, a para-substituted anisole ring, and a linear alkyl group. However, **7** presented only one *N*-methyl proton signal at δ_H 2.80, whereas **9** had two *N*-methyl proton signals at δ_H 2.91 and δ_H 3.02. Combined with the lower molecular weight of **7** than that of **3**, it can be readily inferred that **7** is an *N*-demethylation analog of **9**. Interestingly, the NMR spectra of **7** measured in $CDCl_3$ presented only a very small proportion of the conformer (Figures S7-S8), which was different from those of **8** and **9**. The *N*-methyl proton signal in **7** was assigned to an *N,O*-dimethyltyrosine moiety based on the HMBC correlations from H_3-27 (δ_H 2.80) to C-7 and C-15 amide. The COSY correlations from H_3-4, H_3-5 to H-3, H-3 to H-2, and H-2 to an NH proton at δ_H 6.76, along with the HMBC correlations of an NH proton to C-1, C-2, and C-3, clearly indicated that **7** contained a valine residue instead of an *N*-methylvaline. Furthermore, the HMBC correlations from H-16 to C-15, C-18, and H_3-17 to C-15, C-18, combined with six aliphatic methylene groups observed in ^{13}C and HSQC NMR spectra, suggested the presence of an α-methyl-β-keto-decanoyl moiety in **7**. The planar structure of **7** and the key COSY and HMBC correlations were established as Figure 4-2-1.

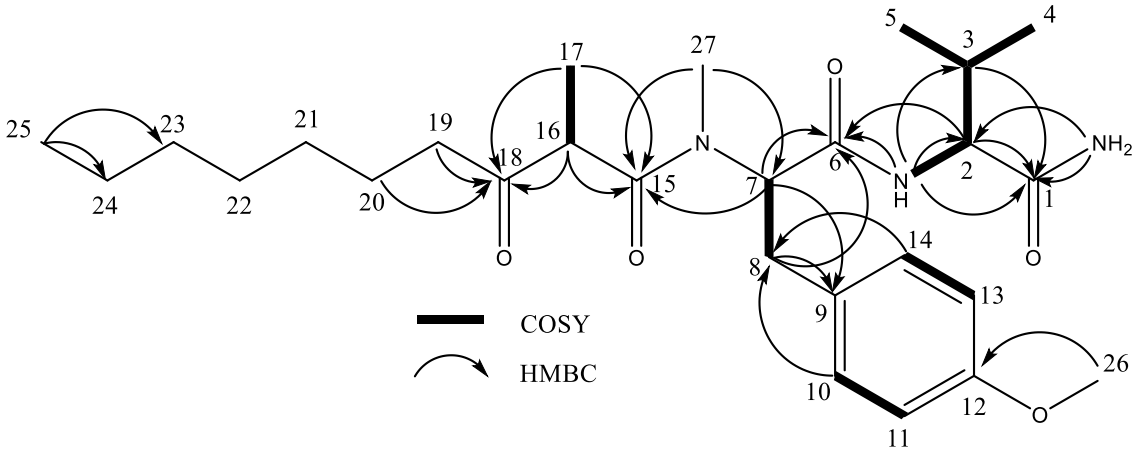

Figure 4.2-1 Key COSY and HMBC correlations of *N*-desmethylmajusculamide B

Table 4.2-3 NMR data for *N*-desmethylmajusculamide B (**7**) in $CDCl_3$.

No.	δ H[a] (*J* in Hz)	δ C[b], type
1		173.6, qC
2	4.25, dd (8.6, 5.5)	58.9, CH
3	2.29, m	29.8, CH
4	0.88, d (6.9)	19.5[c], CH_3
5	0.88, d (6.9)	17.6[c], CH_3
6		170.4, qC
7	5.43, dd (9.3, 7.1)	57.7, CH
8a	2.90, dd (14.7, 9.3)	32.8, CH_2
8b	3.36, dd (14.8, 7.1)	32.8, CH_2
9		128.8, qC
10	7.11, d (8.6)	129.9, CH
11	6.80, d (8.6)	114.1, CH
12		158.5, qC
13	6.80, d (8.6)	114.1, CH
14	7.11, d (8.6)	129.9, CH
15		172.3, qC
16	3.61, q (7.1, 7.1, 7.1)	51.0, CH
17	1.32, d (7.1)	13.7, CH_3
18		209.2, qC
19a	2.47, dd (7.4, 7.4)	40.5, CH_2
19b	2.50, dd (7.4, 7.4)	40.5, CH_2
20	1.54, m	23.7, CH_2
21	1.25, m	29.2, CH_2
22	1.25, m	29.2, CH_2
23	1.24, m	31.8, CH_2
24	1.28, m	22.7, CH_2
25	0.87, dd (7.3, 7.3)	14.2, CH_2
26-OCH_3	3.77, s	55.4, CH_3
27-NCH_3	2.80, s	31.3, CH_3
NH	6.76, d (8.6)	
NH_2	6.42, brs 5.35, brs	

[a]Measured at 800 MHz. [b]Measured at 200 MHz. [c]These carbon are interchangeable.

The absolute configurations of the two amino acid residues in **7** were determined using Marfey's method.[55] Following acid hydrolysis, the hydrolysate of **7** was derivatized using 1-fluoro-2,4-dinitrophenyl-5-L-leucinamide (L-FDLA, Marfey's reagent) and compared with valine and *N*,*O*-dimethyltyrosine standards that were similarly derivatized using L-FDLA. The *N*,*O*-dimethyltyrosine standard was synthesized by the methylation of commercially available Boc-protected tyrosine following a literature procedure.[56] These analyses revealed that **7** contained L-valine and *N*,*O*-dimethyl-D-tyrosine .

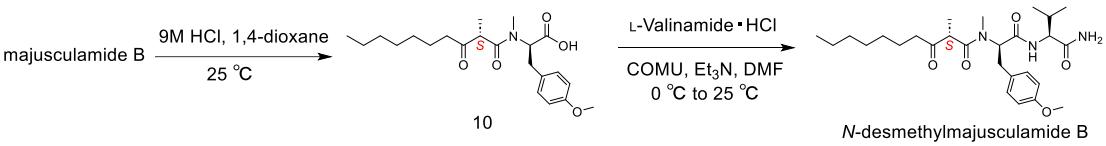

Scheme 4-2. Semi-synthesis of *N*-desmethylmajusculamide B from majusculamide B.

With regard to the fatty acid moiety, the observed NOESY correlation of H-16 with the *N*-methyl group (H_3-27) indicated the C–H bond at the α position (C-16) was on the same plane of the amide (C-15) in **7**. This stereostructure was also supported by the X-ray crystal structure of **9** as reported in the previous literature.[54] In this conformation, the methyl group (C-17) of the decanoyl group in **8** was positioned on the same side as the phenyl group of *N*,*O*-dimethyltyrosine, whereas that in **9** was positioned in the opposite direction. Therefore, the difference in the chemical shift of H_3-17 between **8** and **9** is possibly attributed to the anisotropic effect of the phenyl group in the adjacent tyrosine. The chemical shift of the H_3-17 methyl group (δ_H 1.32) in **7** was close to that of **9** (δ_H 1.28) rather than **8** (δ_H 1.22), suggesting **7** may have S configuration at C-16. This hypothesis was further confirmed by conducting a semi-synthesis of *N*-desmethylmajusculamide B from **9** (Scheme 4-2). Acid hydrolysis of **9** under mild conditions (9M HCl, 25 °C) followed by HPLC purification afforded a partial hydrolysate **10**. Compound **10** was then condensed with a commercially available L-valinamide hydrochloride using (1-cyano-2-ethoxy-2-oxoethylidenaminooxy) dimethylamino-morpholino-carbenium hexafluorophosphate (COMU), resulting in *N*-desmethylmajusculamide B with a 26% yield.[57] The ^{1}H NMR spectrum of the synthesized *N*-desmethylmajusclamide B was

consistent with that of the natural product. Consequently, the configuration of C-16 was unambiguously determined to be *S* for **7**. These results led us to establish the absolute configurations of **7** as shown in Figure 4-1.

The presence of *N*-desmethylmajusculamide A in the original sample was also considered. LC-MS was performed in both positive and negative modes for the EtOAc extract of *O. hirsuta*. However, only one signal corresponding to $C_{27}H_{43}N_3O_5$, *N*-desmethylmajusculamide B (**7)**, could be detected. Additionally, 3.8 mg of majusculamide A (**8)** and 52.1 mg of majusculamide B (**9)** were obtained simultaneously, which revealed that **9** was more abundant than **8** in this sample. Consequently, even if *N*-desmethylmajusculamide A was present in the *O. hirsuta* sample, the amount might be too small to be detected.

4.3 Biological activities

The cytotoxicity of isolated compounds against mouse L1210 leukemia cells was evaluated using WST-8 assay. The IC_{50} value of majusculamide A (**8**) was determined to be 34 μM. On the other hand, *N*-desmethylmajusculamide B (**7**) and majusculamide B (**9**) showed only 41% and 43% inhibition of cell growth at up to 100 μM, respectively. In addition, the growth-inhibitory activity toward the marine diatom *Nitzschia amabilis* was also conducted for the majusculamides (**7**-**9**). As a result, neither **7**, **8**, nor **9** showed growth-inhibitory activity at 10 μM.

In the cytotoxicity test, *N*-desmethylmajusculamide B (**7**) and majusculamide B (**9**) showed similar activities, which were clearly weaker than majusculamide A (**8**). From the perspective of the structure–activity relationship, the presence of a methyl group on *N*-methylvaline in majusculamides appears to be less important for their bioactivities. Furthermore, it was reported that **8** had a more significant effect in promoting osteoblast differentiation compared to **9** in MC3T3-E1 cells.[58] However, **9** exhibited more toxic to larvae of the barnacle, *Amphibalanus amphitrite* than **8** in the cyprid settlement assay.[59] It is intriguing to note that **8** and **9**, two epimers that differ only in their configuration at C-16, display remarkably distinct activities in various biological experiments, including the present study.

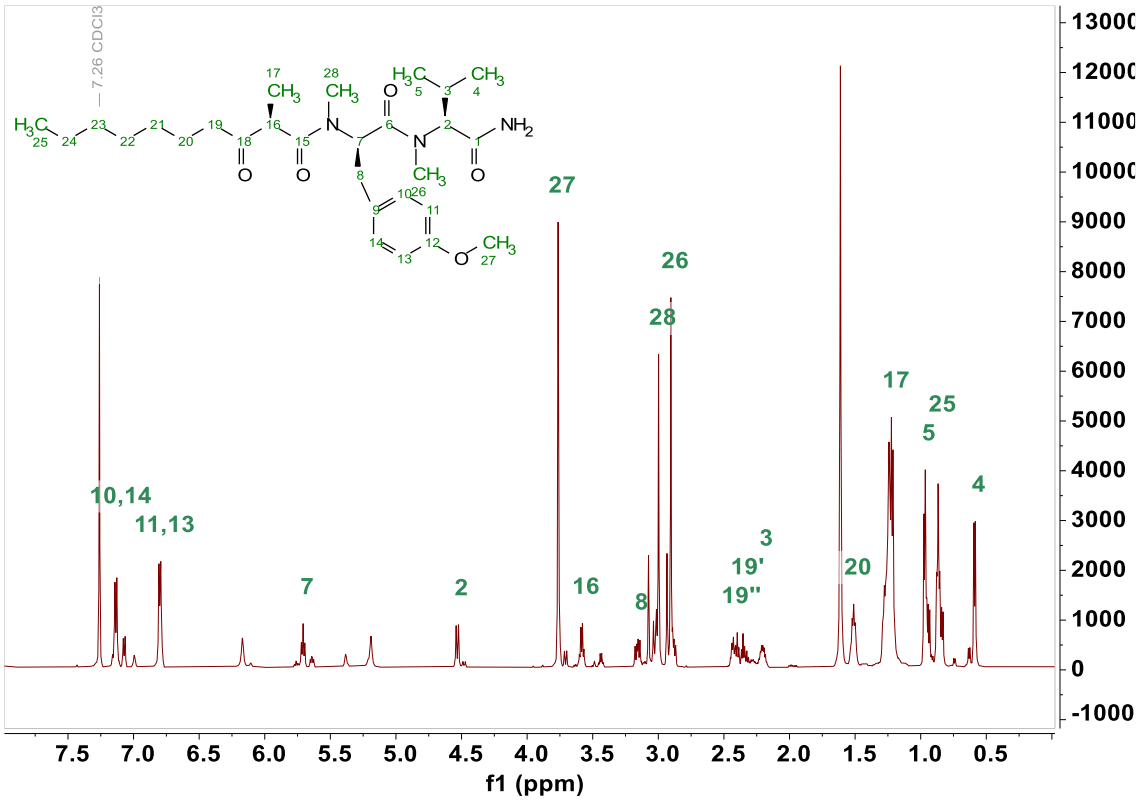

Figure 4.3-1 ^{1}H NMR (600 MHz, $CDCl_3$) spectrum of majusculamide A (**8**)

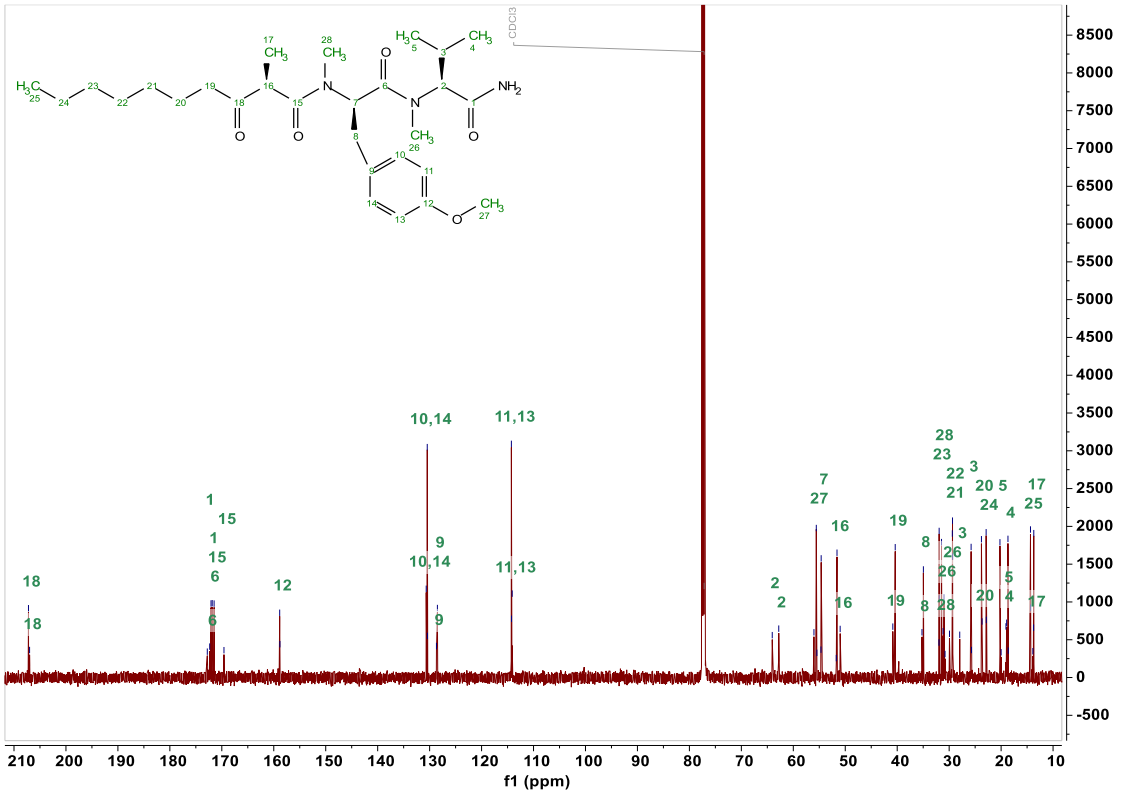

Figure 4.3-2 ^{13}C NMR (150 MHz, $CDCl_3$) spectrum of majusculamide A (**8**)

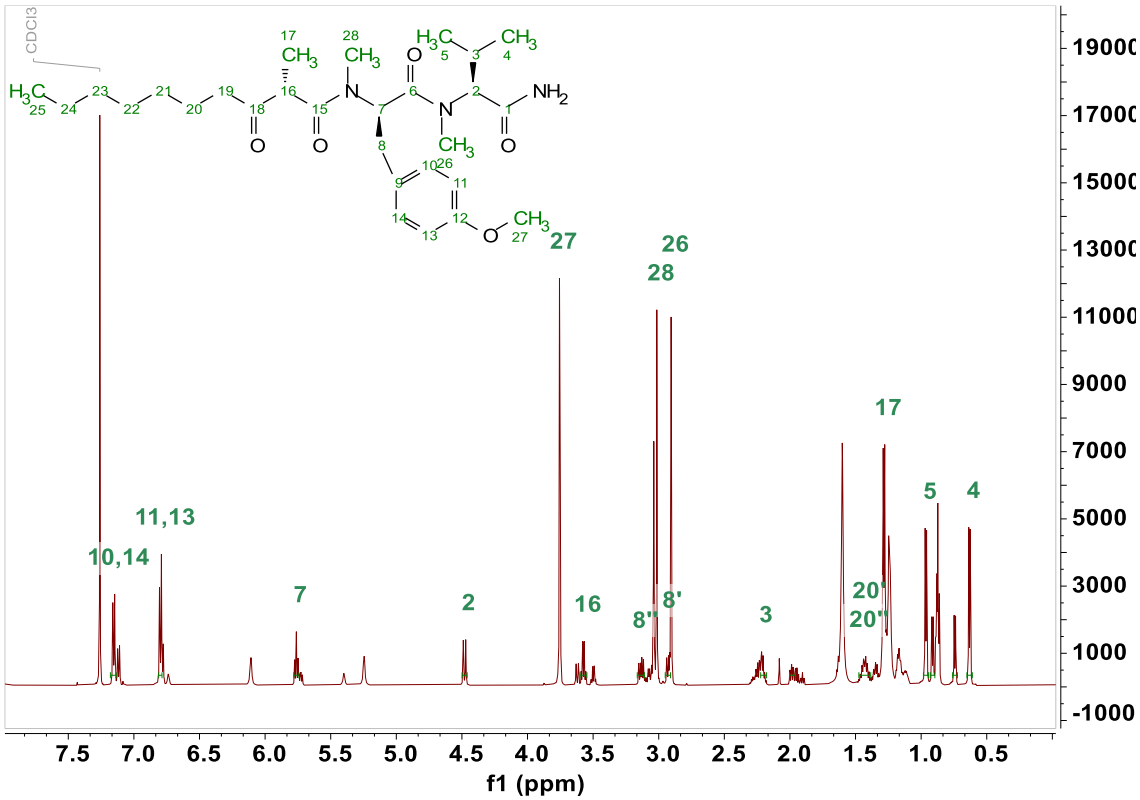

Figure 4.3-3 ^{1}H NMR (600 MHz, $CDCl_3$) spectrum of majusculamide B (**9**)

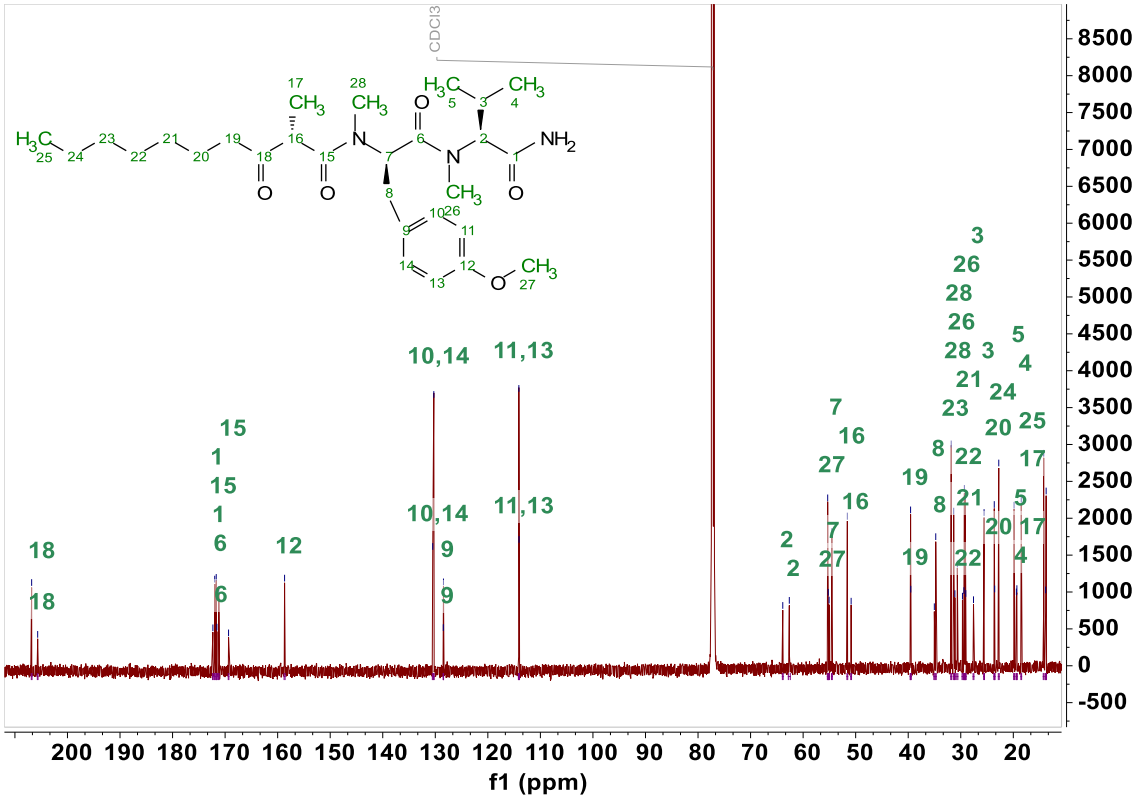

Figure 4.3-4 ^{13}C NMR (150 MHz, $CDCl_3$) spectrum of majusculamide B (**9**)

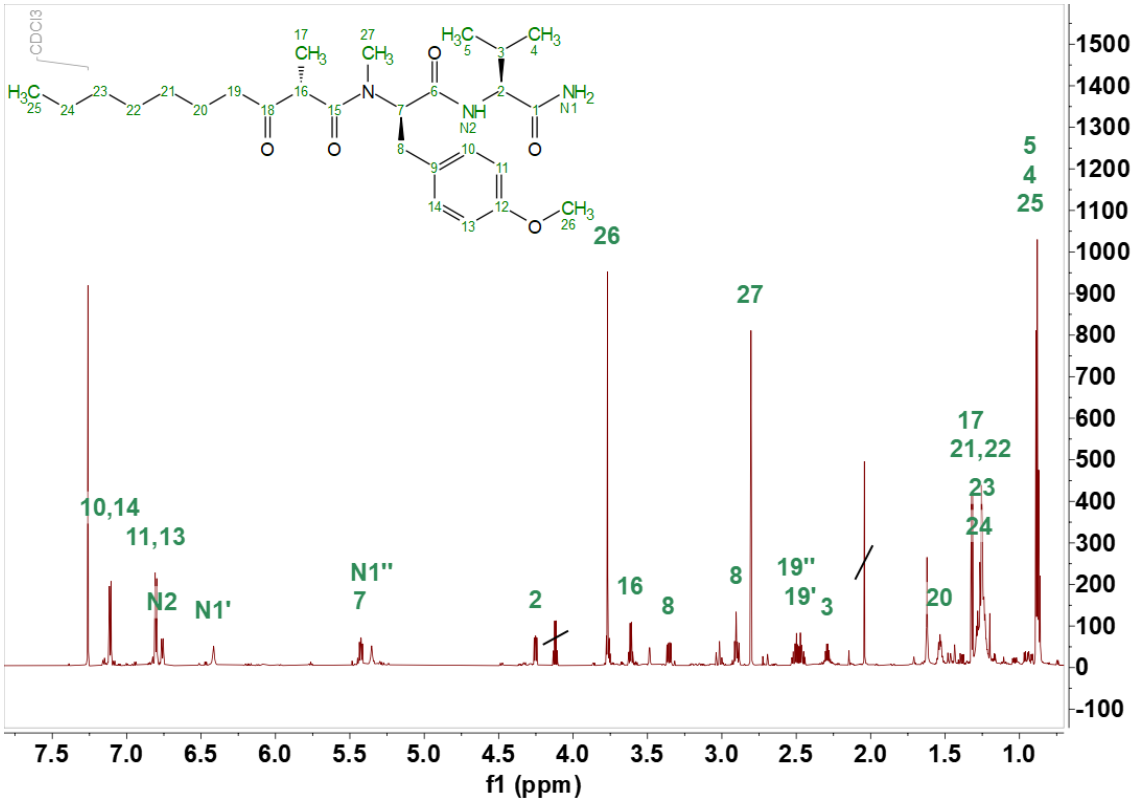

Figure 4.3-5 ^{1}H NMR (800 MHz, $CDCl_3$) spectrum of *N*-desmethylmajusculamide B (**7**)

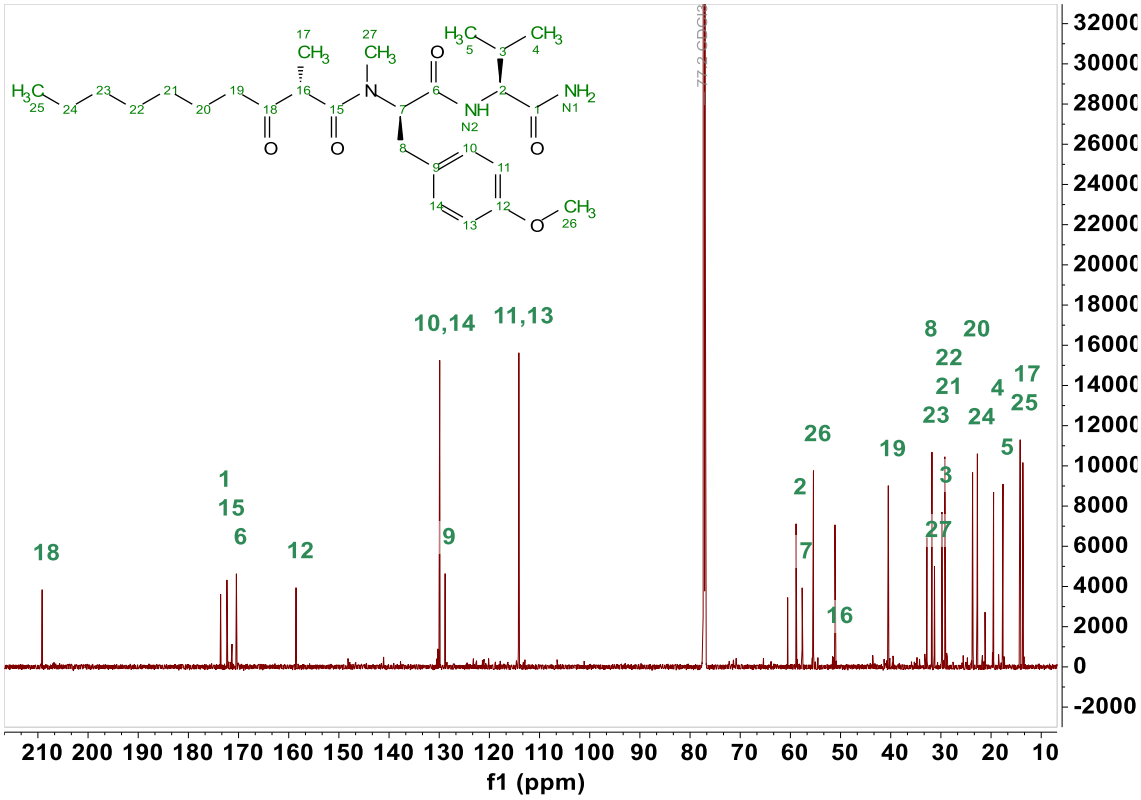

Figure 4.3-6 ^{13}C NMR (200 MHz, $CDCl_3$) spectrum of *N*-desmethylmajusculamide B (**7**)

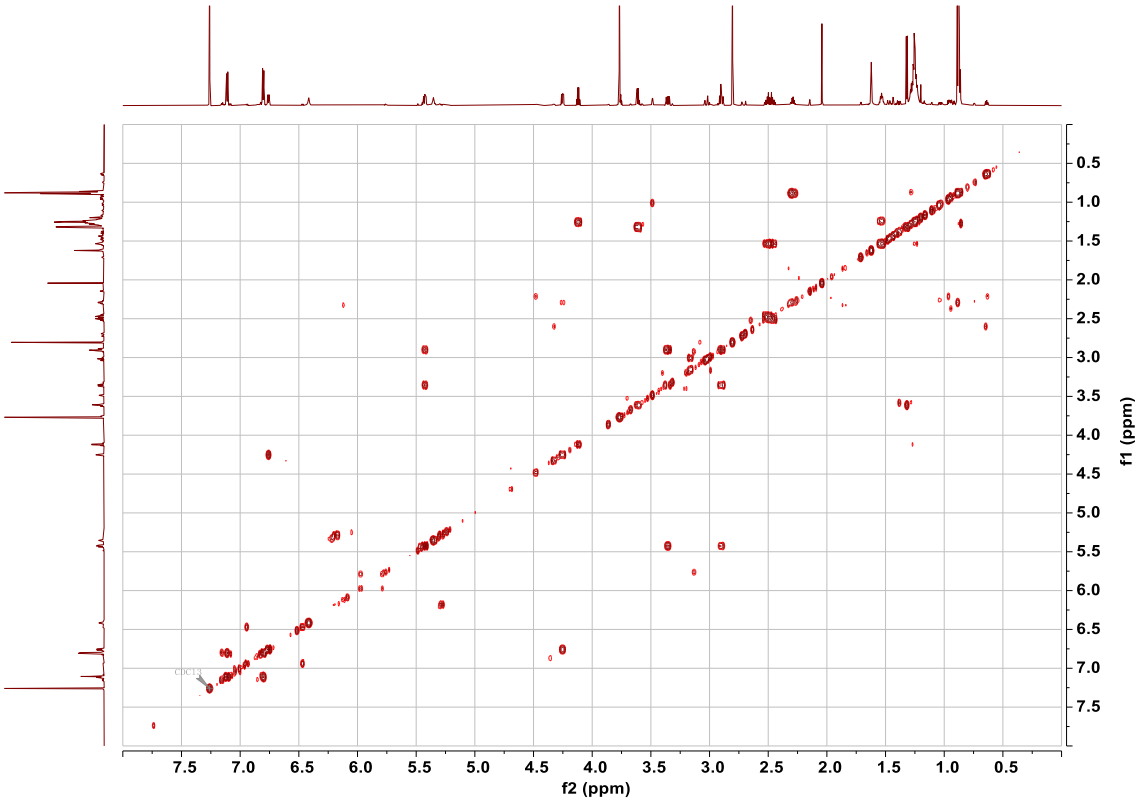

Figure 4.3-7 COSY spectrum (800 MHz, $CDCl_3$) of *N*-desmethylmajusculamide B (**7**)

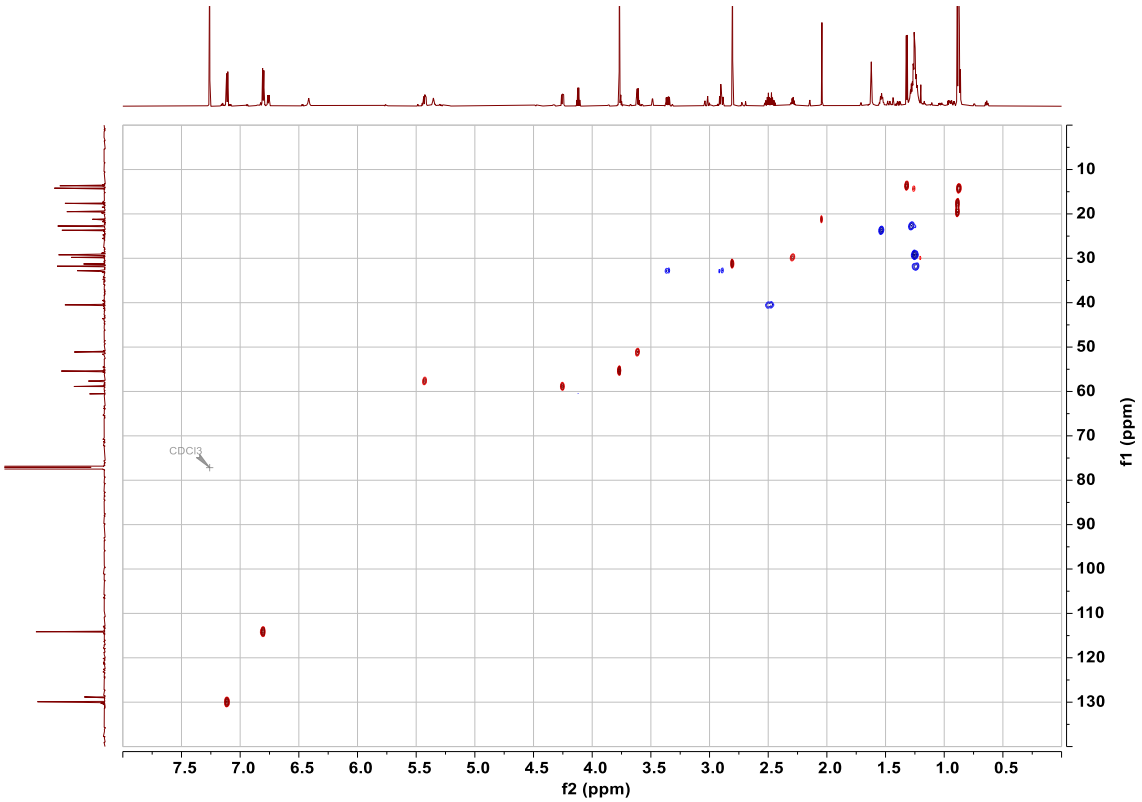

Figure 4.3-8 HSQC (800 MHz, $CDCl_3$) spectrum of *N*-desmethylmajusculamide B (**7**)

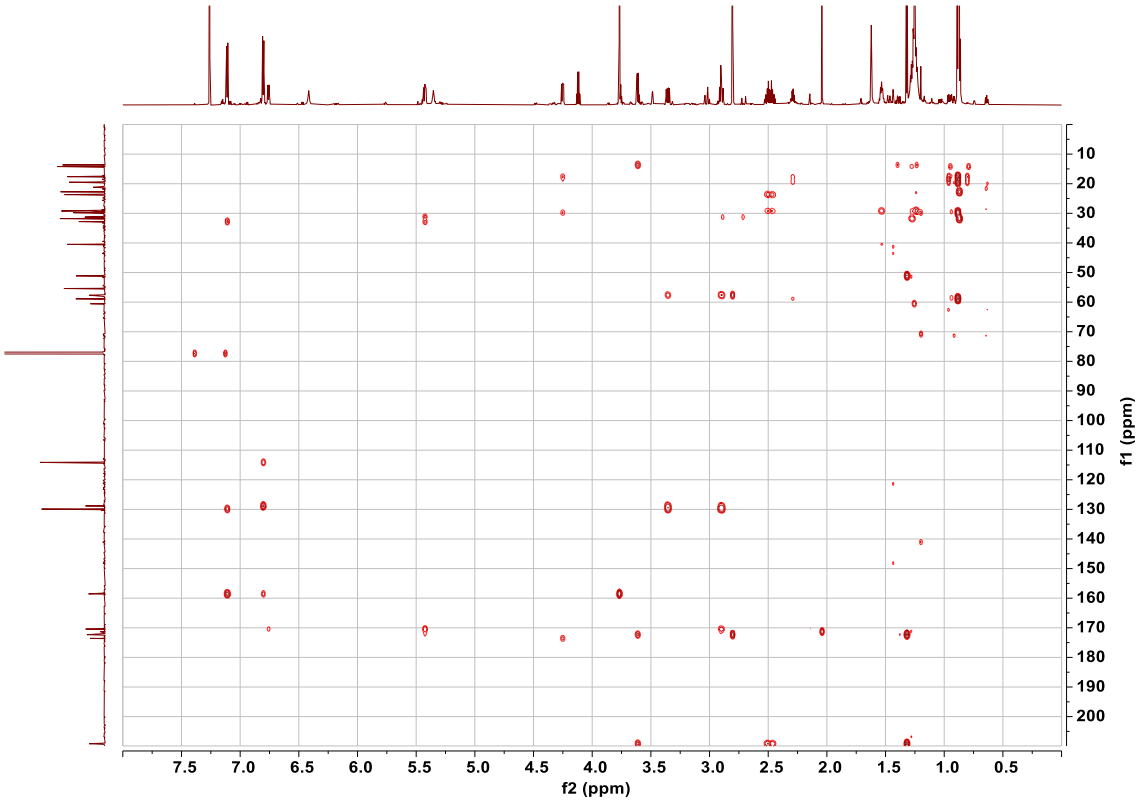

Figure 4.3-9 HMBC (800 MHz, $CDCl_3$) spectrum of *N*-desmethylmajusculamide B (**7**)

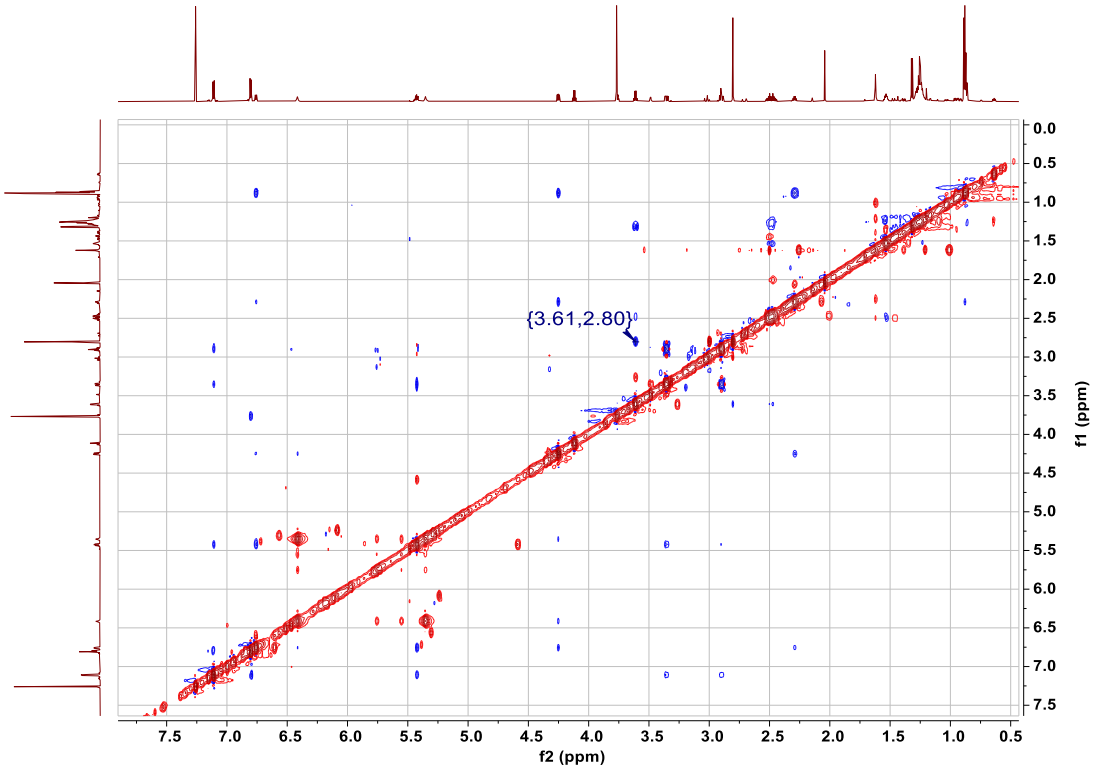

Figure 4.3-10 NOESY (800 MHz, $CDCl_3$) spectrum of *N*-desmethylmajusculamide B (**7**)

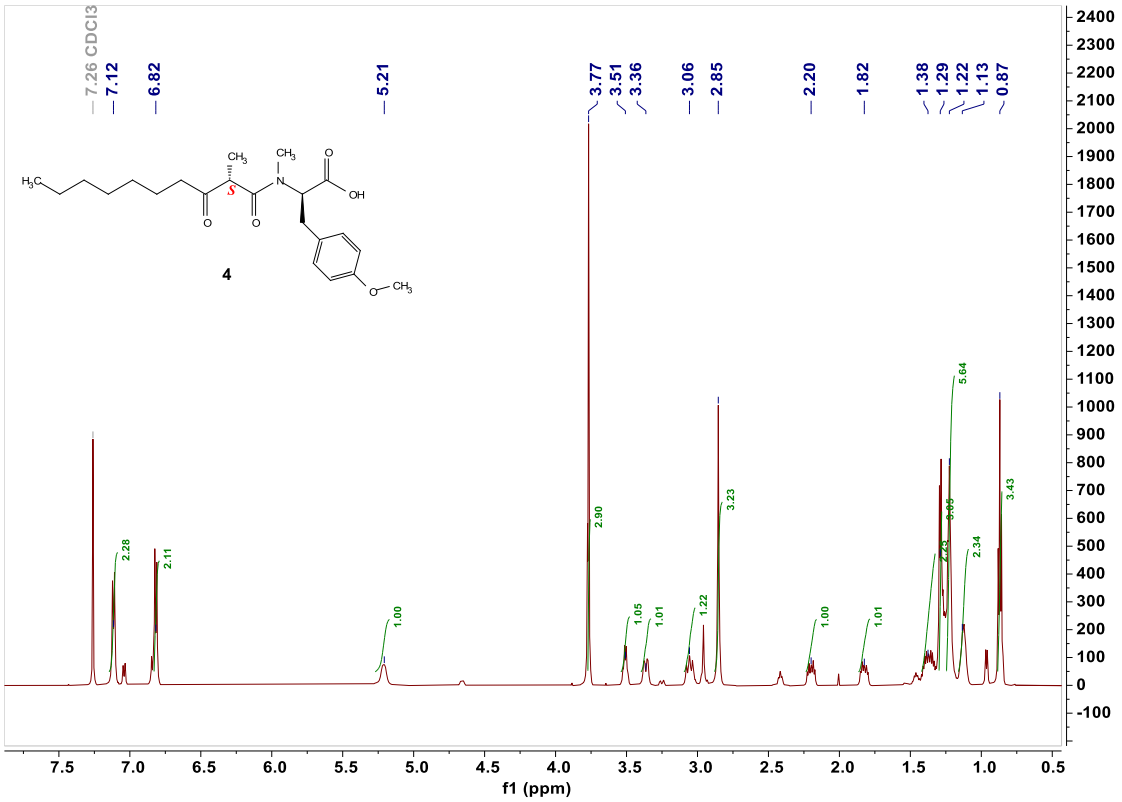

Figure 4.3-11 ^{1}H NMR (600 MHz, $CDCl_3$) spectrum of **10**

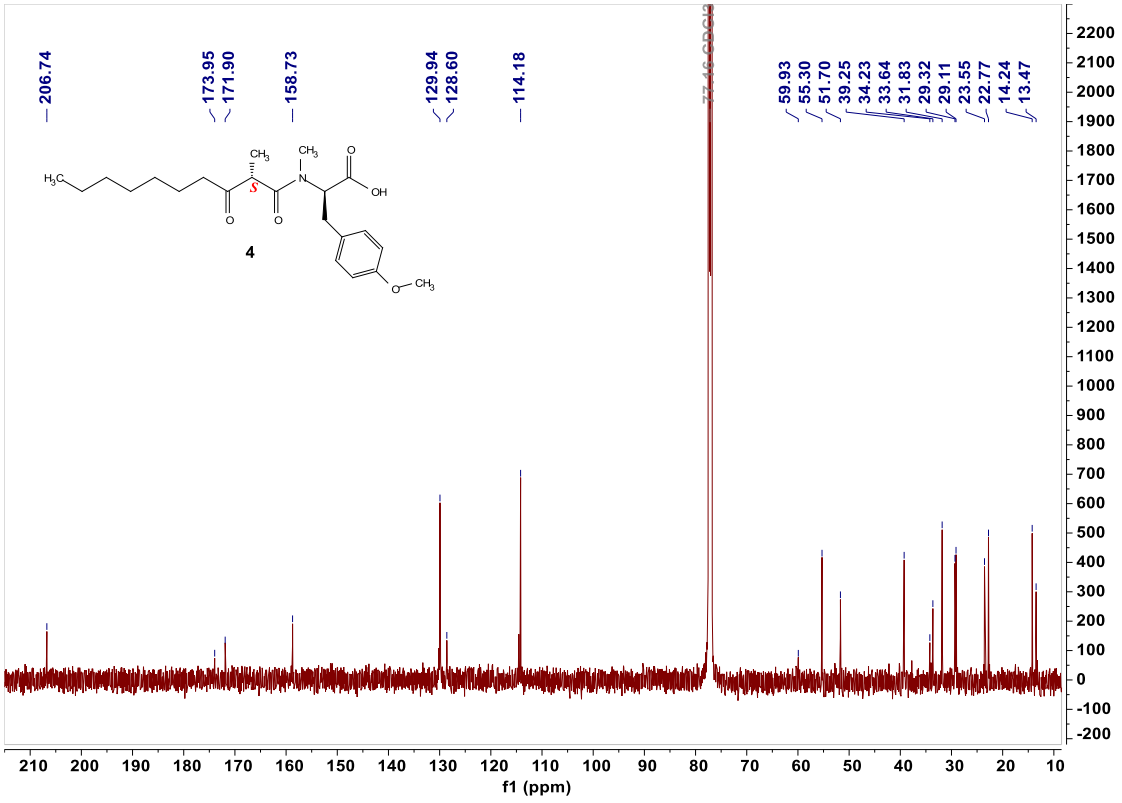

Figure 4.3-12 ^{13}C NMR (150 MHz, $CDCl_3$) spectrum of **10**

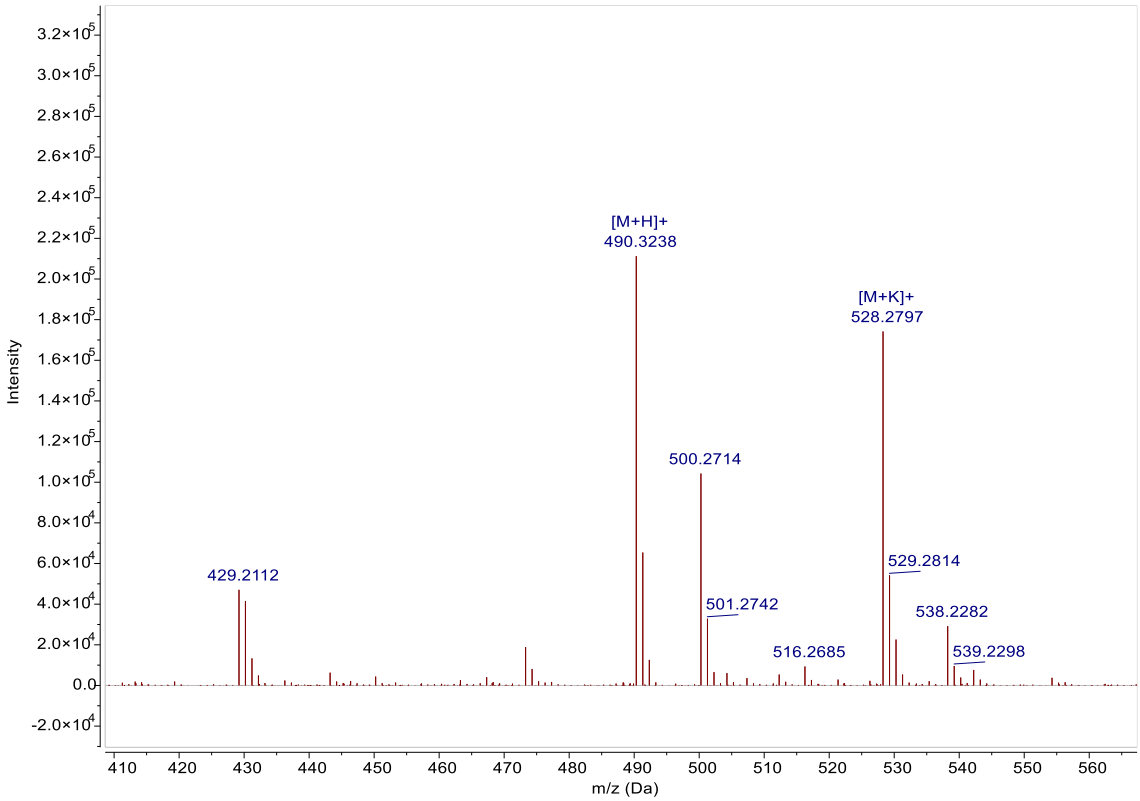

Figure 4.3-13 HR-ESI-MS spectrum of synthesized *N*-desmethylmajusculamide B in positive

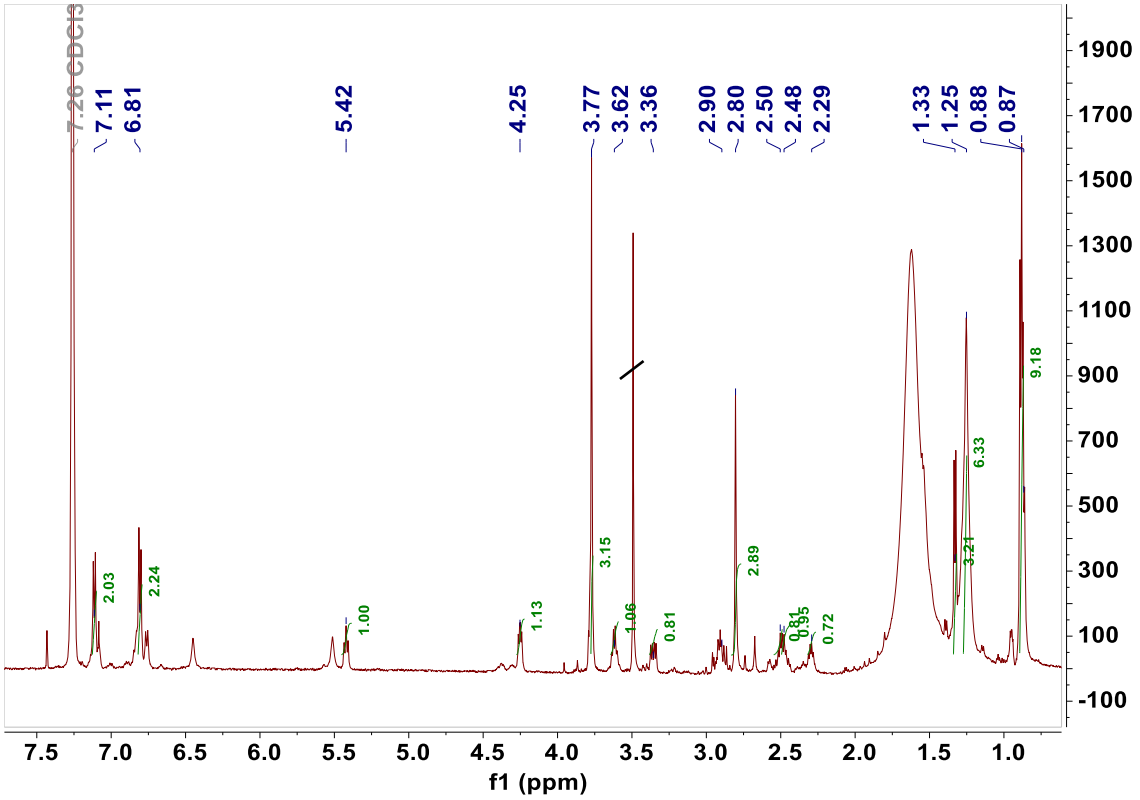

Figure 4.3-14 ^{1}H NMR (600 MHz, $CDCl_3$) spectrum of synthesized *N*-desmethylmajusculamide B

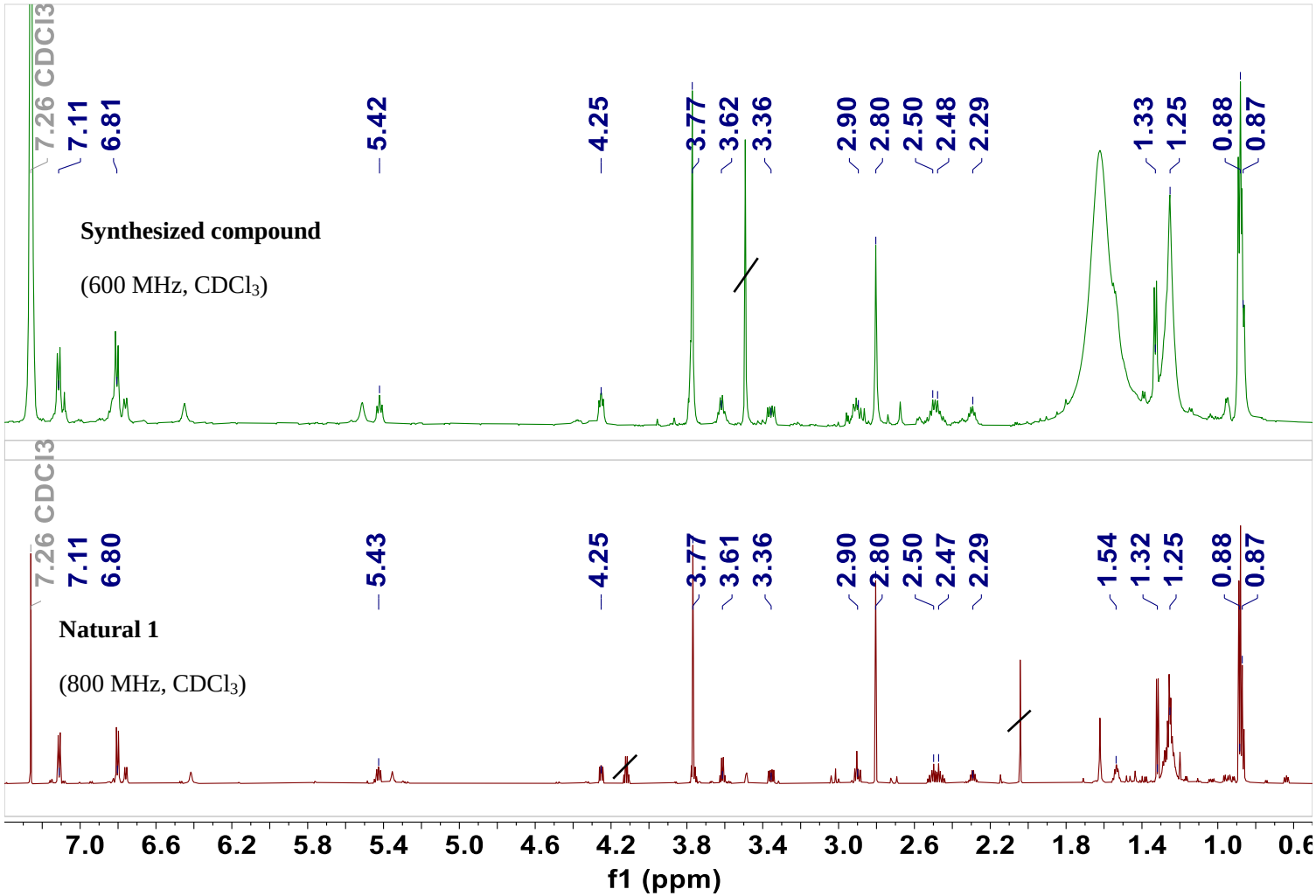

Figure 4.3-15 Comparison of ^{1}H NMR spectra of the synthesized *N*-desmethylmajusculamide B and natural

Analyses of the absolute configurations of amino acids in **7**

Analysis of authentic Val-L-DLA: column, TSKgel ODS-120H (5 μm, φ4.6 × 150 mm); flow rate, 1.0 mL/min; temperature 40 °C; detection at 340 nm; solvent system (a) MeCN/H_2O acidified with 0.1% HCOOH, 35 min linear gradient elution from 20% to 55% MeCN.

t_R(min): L-FDLA (23.2), authentic L-Val-L-DLA (23.2), authentic D-Val-L-DLA (29.3)

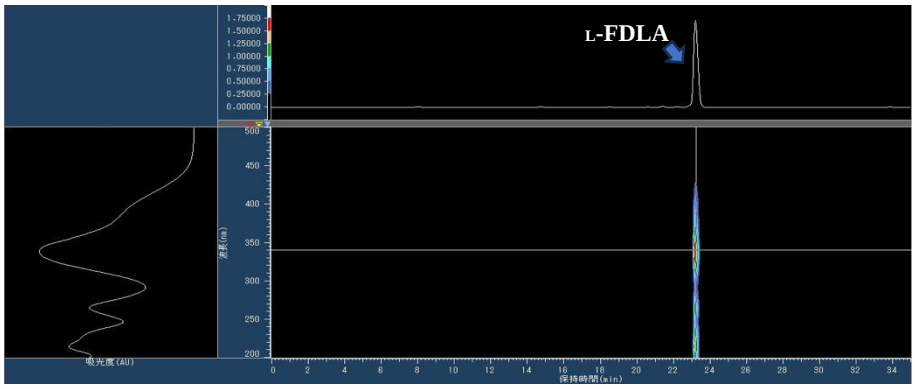

L-FDLA

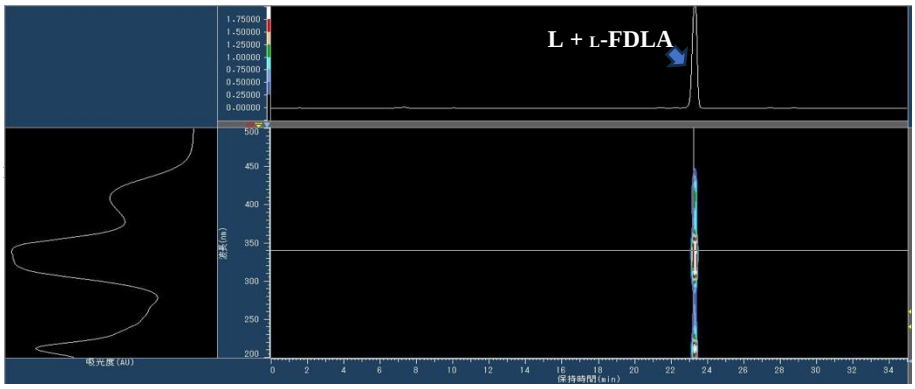

Authentic L-Val-L-DLA

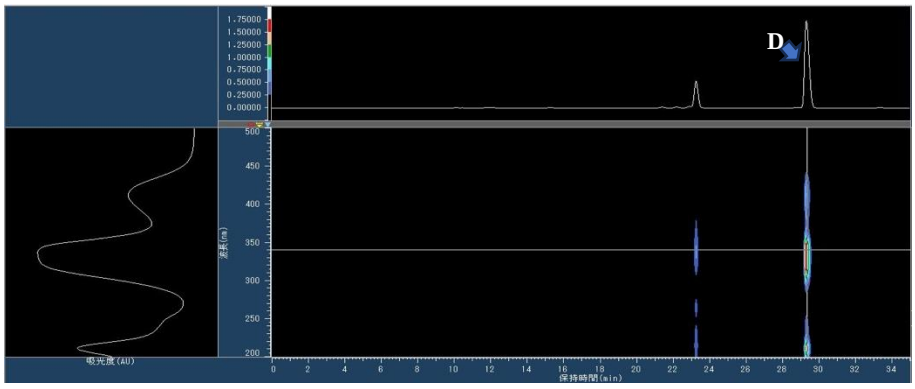

Authentic D-Val-L-DLA

Figure 4.3-16 Analysis of authentic Val-L-DLA

The experiments revealed that L-Val-L-DLA could not be separated from L-FDLA with solvent system (a). Therefore, the analysis of Val-L-DLA derived from the hydrolysate of **7** was performed with another solvent system (b).

Analysis of Val-L-DLA prepared from the hydrolysate of **7**: **7** did not contain D-Val as written in the **Experimental** section of the paper. With regard to L-Val, further analysis for peak at 23.2 min was carried out with the following conditions.

Conditions: column, TSKgel ODS-120H (5 μm, φ4.6 × 150 mm); flow rate, 1.0 mL/min; temperature 40 °C; detection at 340 nm; solvent MeCN/H_2O acidified with 0.1% HCOOH, 30 min isocratic elution with 35% MeCN.

t_R(min): L-FDLA (25.2), authentic L-Val-L-DLA: (26.2),

Val-L-DLA prepared from the hydrolysate of **7**: (26.2).

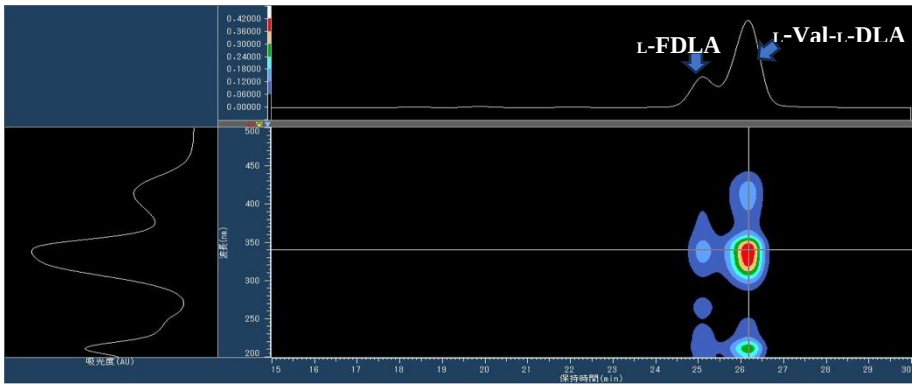

Authentic L-Val-L-DLA

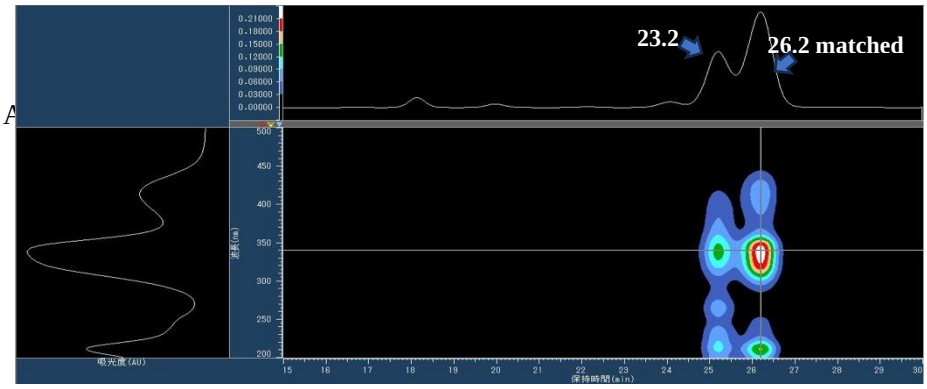

Val-L-DLA prepared from the hydrolysate of **7**

Figure 4.3-17 Analysis of Val-L-DLA prepared from the hydrolysate of **7**

The retention time of Val-L-DLA prepared from the hydrolysate of **7** was identical with that of authentic L-Val-L-DLA.

Analysis of DLA derivative of *N*,*O*-dimethyl-Tyr residue in **7**: column, TSKgel ODS-120H (5 μm, φ4.6 × 150 mm); flow rate, 1.0 mL/min; temperature 40 °C; detection at 340 nm; solvent system (b) MeCN/H_2O acidified with 0.1% HCOOH, 35 min linear gradient elution from 20% to 55% MeCN. t_R(min): synthesized *N*,*O*-dimethyl-L-Tyr-L-DLA: (26.9), synthesized *N*,*O*-dimethyl-D-Tyr-L-DLA: (28.1),*N*,*O*-dimethyl-Tyr-L-DLA prepared from the hydrolysate of **7**: (28.1).

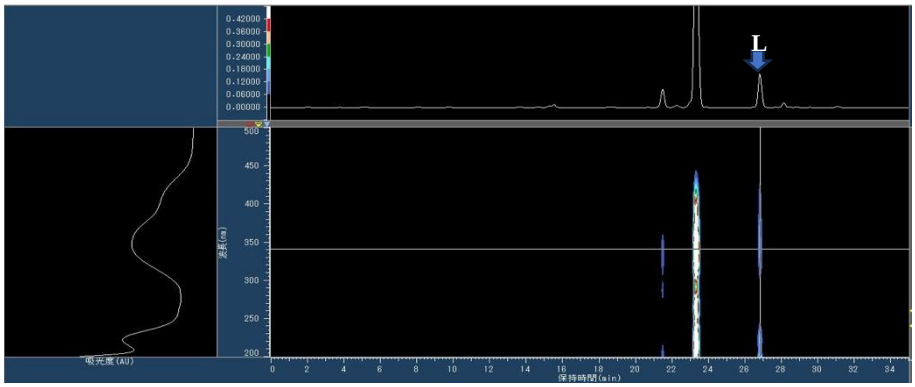

Synthesized *N*,*O*-dimethyl-L-Tyr-L-DLA.

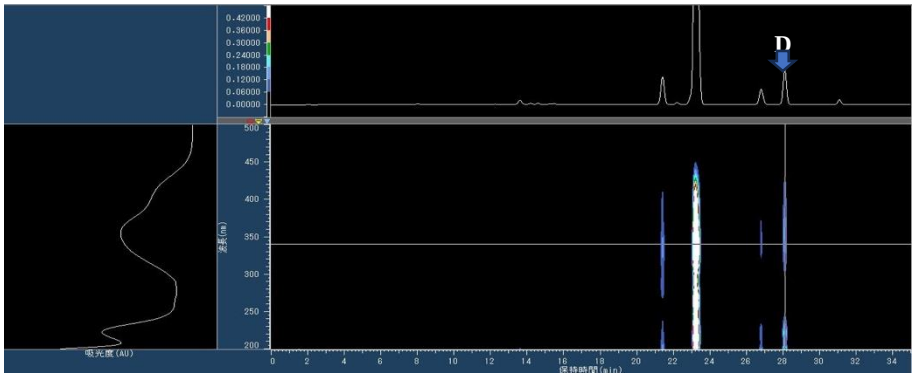

Synthesized *N*,*O*-dimethyl-D-Tyr-L-DLA.

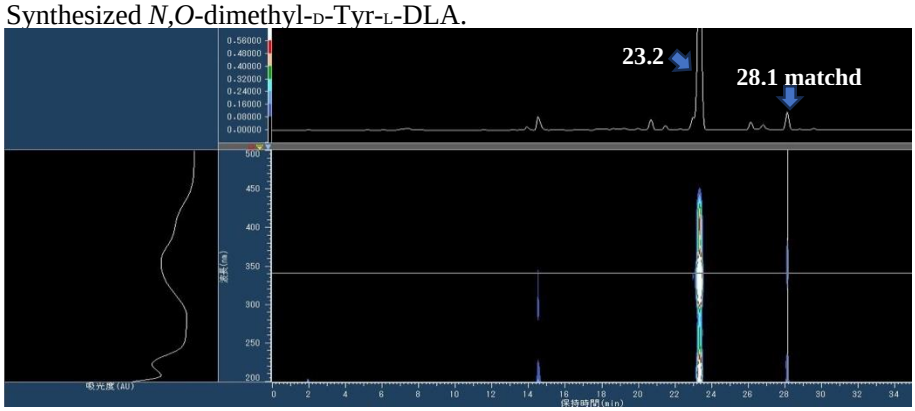

N,*O*-dimethyl-Tyr-L-DLA prepared from the hydrolysate of **7**

Figure 4.3-18 Analysis of *N*,*O*-dimethyl-Tyr-L-DLA prepared from the hydrolysate of **7**

The retention time of *N*,*O*-dimethyl-Tyr-L-DLA prepared from the hydrolysate of **7** was identical with synthesized *N*,*O*-dimethyl-D-Tyr-L-DLA.

Conclusion

Filamentous benthic marine cyanobacteria from the tropics have been a prolific source of structurally unique bioactive secondary metabolites. Among them, Cyanobacteria ascribed to the genus *Lyngbya* were recognized as a potential therapeutic gold mine, rich in structurally diverse and highly bioactive natural products. However, recent phylogenetic analyses have led to the taxonomy revision on this genus, resulting in the establishment of six new cyanobacterial genera from the *Lyngbya* including genera *Dapis*, *Limnoraphis*, *Moorena* (previously *Moorea*), *Microseira* and *Okeania*.

In July 2010, a massive outbreak of toxic filamentous cyanobacteria occurred in Okinawa prefecture. The predominant species in this sample was later identified as *Okeania hirsuta* by an analysis of the 16S rRNA sequence. Because of this cyanobacterial boom, we were able to collect a large number of samples, nearly 20 kg, and conduct a comprehensive investigation of the bioactive components in them. Throughout our extensive exploration on this *O. hirsuta*, the primary toxic constituents were uncovered as aplysiatoxin (ATX)-related compounds. Furthermore, a variety of secondary metabolites belonging to different class have been discovered, highlighting the exceptional biosynthetic capability of this sample. Regarding this remarkable biosynthetic ability and the substantial quantity of the sample obtained, we attempted to analyze and characterize the trace components from unpurified subfractions of this sample, including side fractions, aiming to discover structurally novel and bioactive compounds. In addition, the biosynthetic gene cluster and pathway for ATX remain unknown. We are eager to find more new natural analogs and ATX-related compounds in this sample to gain insights into their biosynthetic mechanisms.

In this study, the ethyl acetate extracts of this *O. hirusuta* sample afford a number of ATX derivatives, including a new compound debromooscillatoxin G. Overall, 24 ATX-related compounds were isolated from the Okinawan cyanobacterium *O. hirsuta* by our laboratory. Based on the structures of these isolated compounds, a common polyketide intermediate was deduced. From this intermediate, three potential biosynthetic pathways were proposed according to the formation of the ring system.

Besides ATX-related compounds, a new lipopeptide, *N*-desmethylmajusculamide B, together with two known compounds majusculamide A and majusculamide B, was isolated from the cyanobacterium *Okeania hirsuta* from Okinawa, Japan. The absolute configurations of the amino acid residues were determined using Marfey's method. Furthermore, a semi-synthesis of *N*-desmethylmajusculamide B from majusculamide B was conducted to establish the absolute configuration of C-16 as *S*. In the cytotoxicity test against mouse L1210 leukemia cells, the activities of *N*-desmethylmajusculamide B and majusculamide B were almost identical. In terms of structure-activity relationship, the presence of a methyl group on *N*-methylvaline in majusculamides appears to be less important for their bioactivities. In addition, the cytotoxicity of majusculamide A was more potent than those of *N*-desmethylmajusculamide B and majusculamide B. In this regard, the configuration of the C-16 position was shown to have a significant impact on biological activity.

In summary, this study demonstrates that marine cyanobacteria are suitable sources for the discovery of trace compounds with novel chemical structures and biological properties. Meanwhile, the quantity of sample is very crucial in such explorations.

Acknowledgements (謝辞)

During these years in Japan in the field of marine natural product chemistry, I have been encouraged by many people. Here I would like to thank the people who have made the research in this thesis possible in many ways.

まずは、留学生であった著者を修士課程から博士課程まで受け入れてくださいました永井宏史教授に厚く御礼申し上げます。最初の頃は、日本語さえ上手く話せなかった著者に対して、永井先生は常に話しかけてくださり、心が温まりました。日々の研究においては、著者の疑問や意見を親身に聞いてくださり、沢山のご助言と暖かい励ましを頂いたおかげで、著者は天然物研究の醍醐味を味わうことができ、研究観を大きく広げる契機となりました。

日本での 6 年以上にわたる学びの中で、永井先生から受けた指導は学術研究にとどまらず、物事に対する厳密ながらも柔軟なアプローチも著者に深い影響を与えました。この影響は、著者の物事に対する見方、問題解決のロジック、困難に向き合う姿勢など多方面に及んでいます。この 6 年以上の歳月は、著者にとって人格と価値観の形成に重要な役割を果たしました。キャリアプランにおいても、永井先生はご自身の経験を基に、研究者になるために必要な素質、能力、そしてそれに伴う苦労と奮闘について教えてくださいました。これにより、著者は未来への不安と戸惑いから抜け出し、現状分析をした上で、手元の仕事に集中し一歩一歩着実な足取りで進むことができるようになりました。

この成長の旅路で、こんなに賢明な先生と出会い、そして指導が得られたことを大変幸運に思います。

次は、神尾道也先生から受けた丁寧なご指導に感謝申し上げます。神尾先生の研究に対する熱意、丁寧な姿勢、迅速かつ効率的な仕事ぶりは、常に著者の学びの手本となっています。そして、研究環境の整備に対する先生のご尽力に最大の敬意を表します。さらに、神尾先生はいつも生徒たちの気持ちや生活状況に気遣いをしてくださり、留学生としてとても暖かいと感じています。そのおかげで、健康で快適な気持ちで研究に打ち込むことが出来ました。

天然物化学(物取り)でもっとも難しいかつ重要な構造決定において、ご指導いただきました東京大学大学院理学系研究科　佐竹真幸先生に心より感謝申し上げます。特にNMR 解析および化学反応において、最も専門的かつ熱心なご指導をいただき、研究の遂行にとって不可欠でした。実験や論文作成の際に、質問などをいつもタイムリーに答えてくださり、さらに、お忙しい中何度も足を運んでくださったことに本当に感謝いたします。また、佐竹先生からの励ましは、著者がNMR に興味を持ち、研究を続けるモチベーションにもなっています。

日々の研究の中に、MS 測定と分析において、細やかな支援をしてくださいました水産技術研究所　内田肇様に心から感謝申し上げます。*N*-desmethyl 体の論文のリバイス段階で、水産研究所に何度もお邪魔し、加水分解物の成分解析に関していろいろ手伝ってくださいました。そのおかげで、ついに化合物の半合成を完成させることができ、論文の出版につながりました。その時、内田様のご支援がなければ、著者は博士号を取得することができません。厚く御礼申し上げます。

新規化合物を追い求め、共に切磋琢磨した永井研の皆様に感謝申し上げます。日本での最初の 2 年間に色々お世話になった安盛里実氏、肖越云氏、廣川友氏、林和孝氏に心より感謝いたします。そして、修士課程に進学し共に長い時間を過ごしたラン藻班の神田菜緒氏、西野陽香氏、川邊稜也氏は、優秀な後輩として日々の討論や成果に刺激を受けると共に、研究を行う上で大きなモチベーションになりました。厚く御礼申し上げます。

上海海洋大学で卒業した後、日本で学ぶ機会を与えてくださいました東京海洋大学婁小波教授に心より感謝申し上げます。来日後、日常生活とキャリア形成に関して、婁先生から沢山の助言を頂きました。特に、日本に来たばかりの頃、「日本語をしっかり学ぶように」というアドバイスを今でも心から感謝しています。そのアドバイスに従って努力したおかげで、だんだん日本社会に馴染めるようになりました。

研究を行うにあたり、長谷川留学生奨学財団に採用頂き、金銭面での援助を頂きました。また、本研究の一部は東京海洋大学創発的海洋研究・産業人材育成支援プロジェクト(JST SPRING JPMJSP2147)の助成を受けたものであり、 関係者の皆様に厚く御礼申し上げます。

最後、博士課程の間にそばで共に成長し、支えてくれた彼女　朱一葦に感謝いたします。日本に留学することを快諾し、離れた地から常に金銭面・精神面で支え、いついかなるときも全力で応援してくださいました父 章正禧、母　章霄敏、兄　章博文に心から感謝いたします。

2024年3月　章　博韜

References

(1) Whitton, B. A.; Potts, M. The Ecology of Cyanobacteria: Their Diversity in Time and Space; Springer Science & Business Media, **2007**.

(2) Charpy, L.; Casareto, B. E.; Langlade, M.-J.; Suzuki, Y. Cyanobacteria in Coral Reef Ecosystems: A Review. *Journal of Marine Sciences* **2012**, *2012*.

(3) Tidgewell, K.; Clark, B. R.; Gerwick, W. H. The Natural Products Chemistry of Cyanobacteria. *Comprehensive Natural Products II*; Elsevier, **2010**; pp 141–188.

(4) Osborne, N. J. T.; Webb, P. M.; Shaw, G. R. The Toxins of *Lyngbya Majuscula* and Their Human and Ecological Health Effects. *Environment International* **2001**, *27* (5), 381–392.

(5) Paerl, H. W.; Paul, V. J. Climate Change: Links to Global Expansion of Harmful Cyanobacteria. *Water Research* **2012**, *46* (5), 1349–1363.

(6) Nawaz, T.; Gu, L.; Fahad, S.; Saud, S.; Jiang, Z.; Hassan, S.; Harrison, M. T.; Liu, K.; Khan, M. A.; Liu, H.; El-Kahtany, K.; Wu, C.; Zhu, M.; Zhou, R. A Comprehensive Review of the Therapeutic Potential of Cyanobacterial Marine Bioactives: Unveiling the Hidden Treasures of the Sea. *Food and Energy Security* **2023**, *12* (5), e495.

(7) Kang, H. K.; Choi, M.-C.; Seo, C. H.; Park, Y. Therapeutic Properties and Biological Benefits of Marine-Derived Anticancer Peptides. *International Journal of Molecular Sciences* **2018**, *19* (3), 919.

(8) the International Natural Product Sciences Taskforce; Atanasov, A. G.; Zotchev, S. B.; Dirsch, V. M.; Supuran, C. T. Natural Products in Drug Discovery: Advances and Opportunities. *Nat Rev Drug Discov* **2021**, *20* (3), 200–216.

(9) Richard E. Moore (1933−2007). *J. Nat. Prod.* **2010**, *73* (3), 301–302.

(10) Kato, Y.; Scheuer, P. APLYSIATOXIN AND DEBROMOAPLYSIATOXIN, CONSTITUENTS OF THE MARINE MOLLUSK STYLOCHEILUS LONGICAUDA. *J. Am. Chem. Soc.* **1974**, *96*(7), 2245-2246.

(11) Mynderse, J. S.; Moore, R. E. Toxins from Blue-Green Algae: Structures of Oscillatoxin A and Three Related Bromine-Containing Toxins. *J. Org. Chem.* **1978**, *43* (11), 2301–2303.

(12) Pettit, G. R.; Kamano, Y.; Herald, C. L.; Tuinman, A. A.; Boettner, F. E.; Kizu, H.; Schmidt, J. M.; Baczynskyj, L.; Tomer, K. B.; Bontems, R. J. The isolation and structure of a remarkable marine animal antineoplastic constituent: dolastatin 10. *J. Am. Chem. Soc.*109(22), 6883-6885.

(13) Luesch, H.; Moore, R. E.; Paul, V. J.; Mooberry, S. L.; Corbett, T. H. Isolation of Dolastatin 10 from the Marine Cyanobacterium Symploca Species VP642 and Total Stereochemistry and Biological Evaluation of Its Analogue Symplostatin 1. *J. Nat. Prod.* **2001**, *64* (7), 907–910.

(14) Gerwick, W. H.; Proteau, P. J.; Nagle, D. G.; Hamel, E.; Blokhin, A.; Slate, D. L. Structure of Curacin A, a Novel Antimitotic, Antiproliferative and Brine Shrimp Toxic Natural Product from the Marine Cyanobacterium *Lyngbya majuscula*. *J. Org. Chem.* **1994**,59(6), 1243-1245.

(15) Total Structure Determination of Apratoxin A, a Potent Novel Cytotoxin from the Marine Cyanobacterium *Lyngbya majuscula*. *J. Am. Chem. Soc*. **2001**, 123(23), 5418-5423.

(16) Taori, K.; Paul, V. J.; Luesch, H. Structure and Activity of Largazole, a Potent Antiproliferative Agent from the Floridian Marine Cyanobacterium Symploca sp. *J. Am. Chem. Soc.* **2008**, *130* (6), 1806–1807.

(17) Morita, M.; Ogawa, H.; Ohno, O.; Yamori, T.; Suenaga, K.; Toyoshima, C. Biselyngbyasides, Cytotoxic Marine Macrolides, Are Novel and Potent Inhibitors of the Ca^{2+} Pumps with a Unique Mode of Binding. *FEBS Letters* **2015**, *589* (13), 1406–1411.

(18) Kurisawa, N.; Iwasaki, A.; Teranuma, K.; Toyoshima, C.; Hashimoto, M.; Suenaga, K. Structure Determination, Total Synthesis, and Biological Activity of Iezoside, a Highly Potent Ca^{2+}-ATPase Inhibitor from the Marine Cyanobacterium *Leptochromothrix Valpauliae*. *J. Am. Chem. Soc.* **2022**, 144(24), 11019-11032.

(19) Underestimated biodiversity as a major explanation for the perceived rich secondary metabolite capacity of the cyanobacterial genus *Lyngbya*. **2011** *Environmental Microbiology*, *13*(6), 1601-1610.

(20) Cyanobacterial Taxonomy: Current Problems and Prospects for the Integration of Traditional and Molecular Approaches. *Algae*, **2006**, 21 (4), 349–375.

(21) Engene, N.; Gunasekera, S. P.; Gerwick, W. H.; Paul, V. J. Phylogenetic Inferences Reveal a Large Extent of Novel Biodiversity in Chemically Rich Tropical Marine Cyanobacteria. *Applied and Environmental Microbiology* **2013**, *79* (6), 1882–1888.

(22) Youssef, D. T., Mufti, S. J., Badiab, A. A., & Shaala, L. A. Anti-Infective Secondary Metabolites of the Marine Cyanobacterium *Lyngbya* Morphotype between 1979 and 2022. **2022** *Marine Drugs* 20.12 (2022): 768.

(23) Engene, N.; Paul, V. J.; Byrum, T.; Gerwick, W. H.; Thor, A.; Ellisman, M. H. Five Chemically Rich Species of Tropical Marine Cyanobacteria of the Genus *Okeania* Gen. Nov. (Oscillatoriales, Cyanoprokaryota). *J. Phycol.* **2013**, *49* (6), 1095–1106.

(24) Cardellina, J. H.; Dalietos, D.; Marner, F.-J.; Mynderse, J. S.; Moore, R. E. (−)-*Trans*-7(S)-Methoxytetradec-4-Enoic Acid and Related Amides from the Marine Cyanophyte *Lyngbya Majuscula*. *Phytochemistry* **1978**, *17* (12), 2091–2095.

(25) Ainslie, R. D.; Jr, J. J. B.; Kuniyoshi, M.; Moore, R. E.; Mynderse, J. S. *Structure of malyngamide C*. *J. Org. Chem.* **1985**, *50*(16), 2859-2862.

(26) Hermitamides A and B, Toxic Malyngamide-Type Natural Products from the Marine Cyanobacterium *Lyngbya majuscula*. *J. Nat. Prod.* **2001**, 63(7), 952-955.

(27)沖縄県衛生研究所神谷大二郎ら (**2011**) 「平成 22~23 年度ハブクラゲ等危害防止事業報告書」pp 18-20.

(28) Kanda, N.; Zhang, B.-T.; Shinjo, A.; Kamiya, M.; Nagai, H.; Uchida, H.; Araki, Y.; Nishikawa, T.; Satake, M. 7- *Epi* -30-Methyloscillatoxin D From an Okinawan Cyanobacterium *Okeania Hirsuta*. *Natural Product Communications* **2023**, *18* (5), 1934578X2311737.

(29) Nagai, H.; Iguchi, K.; Satake, M.; Nishio, Y.; Zhang, B.-T.; Kawashima, K.; Uchida, H. Debromooscillatoxins G and I from the Cyanobacterium Moorea Producens. *Heterocycles* **2021**, *102* (7), 1287.

(30) Nagai, H.; Watanabe, M.; Sato, S.; Kawaguchi, M.; Xiao, Y.-Y.; Hayashi, K.; Watanabe, R.; Uchida, H.; Satake, M. New Aplysiatoxin Derivatives from the Okinawan Cyanobacterium *Moorea Producens*. *Tetrahedron.* **2019**, 75(17), 2486-2494.

(31) Nagai, H.; Sato, S.; Iida, K.; Hayashi, K.; Kawaguchi, M.; Uchida, H.; Satake, M. Oscillatoxin I: A New Aplysiatoxin Derivative, from a Marine Cyanobacterium. *Toxins* **2019**, 11(6), 366.

(32) Jiang, W.; Bu, Y.-Y.; Kawaguchi, M.; Osada, H.; Fukuoka, M.; Uchida, H.; Watanabe, R.; Suzuki, T.; Nagai, H. Five New Indole Derivatives from the Cyanobacterium Moorea Producens. *Phytochemistry Letters.* **2017**, 22, 163–166.

(33) Kawaguchi, M.; Satake, M.; Zhang, B.-T.; Xiao, Y.-Y.; Fukuoka, M.; Uchida, H.; Nagai, H. Neo-Aplysiatoxin Isolated from Okinawan Cyanobacterium *Moorea Producens. Molecules*. **2020**, *25* (3), 457.

(34) Satake, M.; Iguchi, K.; Watanabe, R.; Uchida, H.; Nagai, H. Aplysiadione and Aplysiaenal: Truncated Biosynthetic Intermediates of Aplysiatoxins from a Cyanobacterium. *Results in Chemistry*. **2021**, 3, 100206.

(35) The structure of tetrodotoxin. *Pure and Applied Chemistry*. **1964**, 9(1), 49-74.

(36) Tetrodotoxin Blockage of Sodium Conductance Increase in Lobster Giant Axons. *The Journal of general physiology*. **1964**, 47(5), 965-974.

(37) Schantz, E. J., Ghazarossian, V. E., Schnoes, H. K., Strong, F. M., Springer, J. P., Pezzanite, J. O., & Clardy, J. Structure of saxitoxin. *J. Am. Chem. Soc.* **1975**, 97(5), 1238-1239.

(38) Moore, R. E., & Bartolini, G. Structure of palytoxin. *J. Am. Chem. Soc.* **1981**, *103*(9), 2491-2494.

(39) Murata, M., Legrand, A. M., Ishibashi, Y., & Yasumoto, T. Structures of ciguatoxin and its congener. *J. Am. Chem. Soc.* **1989**, *111*(24), 8929-8931.

(40) Kato, Y.; Scheuer, P. J. The Aplysiatoxins. *Pure and Applied Chemistry* **1975**, *41* (1–2), 1–14.

(41) Entzeroth, M.; Blackman, A. J.; Mynderse, J. S.; Moore, R. E. Structures and Stereochemistries of Oscillatoxin B, 31-Noroscillatoxin B, Oscillatoxin D, and 30-Methyloscillatoxin D. *J. Org. Chem.* **1985**, *50* (8), 1255–1259.

(42) Araki, Y.; Hanaki, Y.; Kita, M.; Hayakawa, K.; Irie, K.; Nokura, Y.; Nakazaki, A.; Nishikawa, T. Total Synthesis and Biological Evaluation of Oscillatoxins D, E, and F. *Bioscience, Biotechnology, and Biochemistry* **2021**, *85* (6), 1371–1382.

(43) Tang, Y.-H.; Wu, J.; Fan, T.-T.; Zhang, H.-H.; Gong, X.-X.; Cao, Z.-Y.; Zhang, J.; Lin, H.-W.; Han, B.-N. Chemical and Biological Study of Aplysiatoxin Derivatives Showing Inhibition of Potassium Channel Kv1.5. *RSC Adv.* **2019**, *9* (14), 7594–7600.

(44) Entzeroth, M.; Blackman, A.; Mynderse, J. S.; Moore, R. Structures and Stereochemistries of Oscillatoxin B, 31-Noroscillatoxin B, Oscillatoxin D, and 30-Methyloscillatoxin D. *Journal of Organic Chemistry* **1985**, *50*, 1255–1259.

(45) Nagai, H.; Yasumoto, T.; Hokama, Y. Aplysiatoxin and Debromoaplysiatoxin as the Causative Agents of a Red Alga Gracilaria Coronopifolia Poisoning in Hawaii. *Toxicon*, **1996**, *34 7*, 753–761.

(46) Mynderse, J. S.; Moore, R.; Kashiwagi, M.; Norton, T. Antileukemia Activity in the Osillatoriaceae: Isolation of Debromoaplysiatoxin from *Lyngbya*. *Science*, **1977**, *196 4289*, 538–540.

(47) Nakamura, H.; Kishi, Y.; Pajarest, M. A.; Randott, R. R. Structural Basis of Protein Kinase C Activation by Tumor Promoters. *Proceedings of the National Academy of Sciences of the United States of America* **1989**, *86 24*, 9672–9676.

(48) Nakagawa, Y.; Yanagita, R. C.; Hamada, N.; Murakami, A.; Takahashi, H.; Saito, N.; Nagai, H.; Irie, K. A Simple Analogue of Tumor-Promoting Aplysiatoxin Is an Antineoplastic Agent Rather than a Tumor Promoter: Development of a Synthetically Accessible Protein Kinase C Activator with Bryostatin-like Activity. *Journal of the American Chemical Society* **2009**, *131 22*, 7573–7579.

(49) Han, B.-N.; Liang, T.-T.; Keen, L. J.; Fan, T.-T.; Zhang, X.-D.; Xu, L.; Zhao, Q.; Wang, S.-P.; Lin, H.-W. Two Marine Cyanobacterial Aplysiatoxin Polyketides, Neo-Debromoaplysiatoxin A and B, with K^+ Channel Inhibition Activity. *Org. Lett.* **2018**, *20* (3), 578–581.

(50) Jiang, W.; Akagi, T.; Suzuki, H.; Takimoto, A.; Nagai, H. A New Diatom Growth Inhibition Assay Using the XTT Colorimetric Method. *Comparative Biochemistry and Physiology Part C: Toxicology & Pharmacology* **2016**, *185–186*, 13–19.

(51) Kawabata, T.; Lindsay, D. J.; Kitamura, M.; Konishi, S.; Nishikawa, J.; Nishida, S.; Kamio, M.; Nagai, H. Evaluation of the Bioactivities of Water-Soluble Extracts from Twelve Deep-Sea Jellyfish Species. *Fish Sci* **2013**, *79* (3), 487–494.

(52) Zhang, B.-T.; Nishino, H.; Kawabe, R.; Kamio, M.; Watanabe, R.; Uchida, H.; Satake, M.; Nagai, H. *N*-Desmethylmajusculamide B, a Lipopeptide Isolated from the Okinawan Cyanobacterium Okeania Hirsuta. *Bioscience, Biotechnology, and Biochemistry* **2024**, zbae015.

(53) Marner, F.-J.; Moore, R. E.; Hirotsu, K.; Clardy, J. Majusculamides A and B, Two Epimeric Lipodipeptides from *Lyngbya Majuscula Gomont. J. Org. Chem.* **1977**, *42* (17), 2815–2819.

(54) Nakajima, D.; Sueyoshi, K.; Orihara, K.; Teruya, T.; Yokoshima, S. Synthesis of Majusculamides A and B. *Synlett* **2019**, *30* (08), 924–927.

(55) Marfey P. Determination of D-amino acids. II. Use of a bifunctional reagent, 1, 5-difluoro-2, 4-dinitrobenzene. *Carlsberg Res Commun*. **1984**;49:591-6.

(56) Boger, D. L.; Yohannes, D. Studies on the Total Synthesis of Bouvardin and Deoxybouvardin: Cyclic Hexapeptide Cyclization Studies and Preparation of Key Partial Structures. *J. Org. Chem.* **1988**, *53* (3), 487–499.

(57) El-Faham, A.; Funosas, R. S.; Prohens, R.; Albericio, F. COMU: A Safer and More Effective Replacement for Benzotriazole-Based Uronium Coupling Reagents. *Chemistry – A European Journal* **2009**, *15* (37), 9404–9416.

(58) Natsume, N.; Ozaki, K.; Nakajima, D.; Yokoshima, S.; Teruya, T. Structure–Activity Relationship Study of Majusculamides A and B and Their Analogues on Osteogenic Activity. *J. Nat. Prod.* **2020**, *83* (8), 2477–2482.

(59) Tan, L. T.; Goh, B. P. L.; Tripathi, A.; Lim, M. G.; Dickinson, G. H.; Lee, S. S. C.; Teo, S. L. M. Natural Antifoulants from the Marine Cyanobacterium *Lyngbya Majuscula*. *Biofouling* **2010**, *26* (6), 685–695.